

ABSTRACT

KIM, HEY-SANG. Capillary Phenomena in Textiles with Continuous Microfluidic Flow (Under the direction of Dr. Stephen Michielsen and Dr. Emiel DenHartog).

Wicking phenomena in fabrics are driven by capillary action, which is affected by the fiber parameters, yarn structures and liquid properties. By developing a better wicking performance fabric, we can improve physiological comfort by removing liquid from the sweating source through capillary channels as well as faster evaporation. Even though the liquid transport in the void space between fibers within a yarn (or in-between yarns) is known to be the most critical phenomenon in fabric wicking, typical wicking test methods, such as vertical wicking test and gravimetric absorbency testing, cannot explain the role that yarn-level wicking plays within the fabric. For this reason, we developed a new method called '*Single-pore Wicking Evolution Apparatus for Textiles (SWEAT)*' test to investigate liquid transport in fabrics based on within-yarn and yarn-to-yarn transfer wicking. This SWEAT test was conducted by supplying continuous liquid flow to a single yarn within the fabric. In order to mimic human sweating phenomenon, this SWEAT test method avoided the flooding liquid stage by controlling flow rate to be similar to a single sweat gland and by choosing a similar diameter of liquid source to sweat gland pore size. By controlling liquid flow rate, we evaluated wicking phenomena of fabrics with image analysis for quantitative measurement. We have successfully measured directional wicking rates and individual yarn wicking performance, which has not yet been explained in this area. Additionally, we found liquid movement in knit fabrics follows the time-wicking length superposition principle: liquid wicks within a single yarn initially, subsequently it spills over to adjacent yarns through contact points, but the wicking rate in adjacent yarns is identical to the initial course yarn. Furthermore, we found that the graph of the sum of the total wicking lengths of all yarns of a fabric follows a "one minus an exponential of time" curve trendline which takes into consideration the

liquid rates of feeding, storage, and evaporation. The experimental graph finally reaches a plateau stage without further increase of the wicked area because the supplied liquid flow amount matches the evaporation amount from the wetting area. A better understanding of wicking performance with this SWEAT test method promises to provide a predictive model of wicking performance fabrics and should result in a large contribution to textile industry including sportswear, military apparel and textile printing.

© Copyright 2019 by Hey-sang Kim

All Rights Reserved

Capillary Phenomena in Textiles with Continuous Microfluidic Flow

by
Hey-sang Kim

A dissertation submitted to the Graduate Faculty of
North Carolina State University
in partial fulfillment of the
requirements for the degree of
Doctor of Philosophy

Fiber and Polymer Science

Raleigh, North Carolina
2019

APPROVED BY:

Dr. Stephen Michielsen
Co-Chair of Advisory Committee

Dr. Emiel DenHartog
Co-Chair of Advisory Committee

Dr. Warren Jasper

Dr. Andre West

Dr. Chau-Wai Wong

BIOGRAPHY

Hey-sang Kim was born in Daejeon, South Korea, July 1st 1988. She moved to Seoul and started her college career at the Department of Clothing and Textiles at Seoul National University in 2008. After summer internship on the Business Development team at Pfizer Korea in her senior year, she decided to build up strong knowledge of her undergraduate research field of textiles. Her interest in multi-functional textiles led her to pursue Master program in Textile Science at Seoul National University and current PhD program in Fiber and Polymer Science at the Wilson College of Textiles at NC State University. Hey-sang started doctoral program in fall 2016 with Provost's Fellowship and joined Dr. Stephen Michielsen's research group as a Research Assistance where she investigated capillary phenomena of textile substrates with a new wicking measurement system.

ACKNOWLEDGMENTS

First and foremost, I would like to express my gratitude to my two advisors, Dr. Stephen Michielsen and Dr. Emiel DenHartog for their assistance and encouragement in helping me to complete my doctoral degrees. Specifically, Dr. Michielsen provided me an opportunity to start my graduate research in his group with a collaboration project funded by the U.S. Special Operation Command (USSOCOM) and continue my research through another collaborative project with Dr. DenHartog funded by Eastman Chemical Company. Thanks to two awesome advisors' support, I was able to learn a lot in many ways, attend several domestic and international conferences, and receive grants and awards within three and a half years of PhD journey.

I would like to extend my thanks to all of the members of my committee; Dr. Warren Jasper, Dr. Andre West, and Dr. Chau-Wai Wong. I also want to thank my former and current lab mates, and my friends. I thank all of everyone who contributed to my studies across the campus and their support especially people at the Eastman Chemical Company.

Last but not the least, I would like to thank my mother and my father for their continuous support and belief in me.

TABLE OF CONTENTS

LIST OF TABLES	vi
LIST OF FIGURES	vii
Chapter 1: Introduction	1
Chapter 2: Research Outline	5
Chapter 3: Overview of Capillary Phenomena in Porous Media	
3.1 Wetting and Wicking	7
3.1.1. Wetting.....	7
3.1.2. Wicking and Capillary Force	8
3.2. Wicking in Porous Media	21
3.2.1. In-plane Wicking	21
3.2.2. Trans-planar Wicking (Through-thickness wicking).....	25
3.2.3. Yarn-level Wicking.....	27
3.2.4. Between Two Plates.....	36
3.2.5. Saturation-level	41
3.2.6. Effect of Wicking Properties on Physiological Comfort	46
3.2.7. Limitations of Current Textile Wicking Test Methods.....	51
Chapter 4: New Wicking Measurement System to Mimic Human Sweating Phenomena with Continuous Microfluidic Flow	
4.1. Needs for a New Wicking Measurement System	57
4.2. Introduction.....	58
4.3. Experimental Section	62
4.3.1. Fabric Substrates.....	62
4.3.2. Dye Solution for Wicking Length Indicator	63
4.3.3. Vertical Wicking Test.....	63
4.3.4. Droplet Wicking Test.....	64
4.3.5. New Measurement System: Single-pore Wicking Evolution Apparatus for Textiles (SWEAT) Test.....	64
4.3.6. Wicking Performance Measurements	65
4.4. Results and Discussions.....	67
4.4.1. Preparation of Wicking Indicator with Dye Solution	67
4.4.2. Wicking Performance from Vertical Wicking Test	70
4.4.3. Wicking Performance from Droplet Wicking Test.....	72
4.4.4. Wicking Performance of New Measurement System, SWEAT Test (Single-pore Wicking Evolution Apparatus for Textiles)	76
4.5. Conclusions.....	84
Chapter 5: Time-wicking Length Superposition for Textiles	
5.1. Abstract	86
5.2. Introduction.....	87
5.3. Experimental Section	88
5.3.1. Fabric Substrates.....	88

5.3.2. Upward–horizontal–downward Wicking Test.....	90
5.3.3. Droplet Wicking Test.....	91
5.3.4. Single–pore Wicking Evolution Apparatus for Textiles (SWEAT) test	92
5.4. Results and Discussions.....	93
5.4.1. Time-wicking Length Superposition.....	95
5.5. Conclusions.....	103
Chapter 6: New Textile Wicking Theory	
6.1. Wicking Performance in Fabrics	105
6.2. SWEAT Theory of Wicking in Textiles	106
6.3. Experimental Analysis Based on the SWEAT Theory of Wicking in Textiles.....	110
6.4. Supplementary Information	116
Chapter 7: Conclusions and Future Work	120
REFERENCES	123

LIST OF TABLES

Table 3-1. Wicking performance-related equations and their assumptions.....	53
Table 3-2. Limitations of typical fabric wicking test methods.	54
Table 4-1. Wicking performance comparison between the usage of infinite reservoir and droplet.	58
Table 4-2. Surface tension of dye indicator solutions including deionized water (DI), rose bengal dye (0.2, 0.4 and 0.6 wt%), brilliant blue G (BBG), and brilliant blue R(BBR).....	69
Table 4-3. Wicking performance comparison from dropping liquid (4 μ l) on the cotton–polyethylene, and the polyester–polyethylene blended interlock fabrics by picking hydrophilic or hydrophobic yarns independently.....	75
Table 4-4. Characteristic comparison between human sweat gland pore and testing methods, including the vertical wicking test (AATCC 197), the moisture management test (MMT, AATCC 195) and the SWEAT (Single–pore Wicking Evolution Apparatus for Textiles) test with a needle.....	76
Table 4-5. Wicking performance comparison from the SWEAT (flow rate: 50 nanoliter/min) on the cotton–polyethylene, and the polyester–polyethylene blended interlock fabrics by picking hydrophilic or hydrophobic yarns independently.	80
Table 4-6. Wicking performance comparison between the SWEAT test (flow rate: 50 nanoliter/min) and the droplet wicking test (1.5, 2, 3, and 4 μ l).....	83
Table 5-1. Wicking length comparison over time from the Upward-horizontal-downward wicking test on polyester interlock knit fabrics, including the EASTMAN flat yarn fabric and a commercial textured yarn fabric for 7, 15, 30, and 100 min (unit: cm, [the range] : the range of wicking length of ≥ 4 times repeated tests at the certain time).....	94
Table 6-1. The trendline from the three-times repeated wicking performance test of EASTMAN single jersey knit fabric. $f(t)$ is the sum of wicking length function depending on time (unit: micrometer), and $[a, b]$ is the time range from a to b (unit: min).....	112
Table 6-2. Comparison between the calculated- and the actual-wetting area at a plateau stage from the three-times repeated wicking performance test of EASTMAN single jersey knit fabric. $[a, b]$ is the time range from a to b (unit: min). The calculated wetted area was obtained from equation 6-14.....	113

LIST OF FIGURES

Figure 3-1.	Water droplets on flat solid surface (left), Wenzel state (middle), and Cassie–Baxter state (right)	8
Figure 3-2.	(a) The free body diagram of half a droplet, and (b) The capillary rise in a narrow cylindrical tube	10
Figure 3-3.	The hydrostatic pressure drop between points B and A offsets the Laplace under pressure at point A	12
Figure 3-4.	A general example of water-air-glass system depending on the radius of channel	13
Figure 3-5.	(a) Film of water between two glass plates and (b) calculation of the vertical curvature	15
Figure 3-6.	(a) Penetration of a small drop into a capillary. (b) the final equilibrium situation for $\theta_a < 90^\circ$. (c) the final equilibrium situation for $\theta_a > 90^\circ$	18
Figure 3-7.	(a) Stages of drop penetration into a thin porous medium. (b) “phase diagram” for penetration of a drop into a thin porous medium	18
Figure 3-8.	Kinetics of penetration into paper from an infinite liquid reservoir, the theoretical prediction of the radical capillary model, a limited liquid reservoir, and a drop.	19
Figure 3-9.	(a) Horizontal–downward wicking data, wicking length vs. time, and (b) horizontal wicking data, wicking length vs. the square root of time, for a single knit fabric at upward wicking heights (h) of 1.5, 2.5, 3.5, and 4.5 cm, corresponding to saturations of 0.87, 0.78, 0.74, and 0.69, respectively.....	23
Figure 3-10.	Manual method for measuring wicking area (left). (a) Results of the morphological segmentation technique and (b) the region merging technique ...	24
Figure 3-11.	Entry of a liquid into a fabric pore: (a) liquid surface just before contact with the pore; (b) when liquid surface is contacting the pore, the angle between liquid and solid surface becomes $\theta_a = 180^\circ$; (c) not possible with convex meniscus; (d) allowable mode of liquid entry.....	26
Figure 3-12.	(a) Effect of twist on yarn diameter, and (b) the effect of twist level on yarn wicking performance of continuous filament yarns.....	30
Figure 3-13.	Effect of (a) twist, (b) cross-section, and (c) texturing on wicking height of yarns	31

Figure 3-14.	Effect of twist factor on (a) wicking time, (b) wicking height, and (c) relationship between equilibrium wicking height and percentage of floats and arcs for wet- and dry-textured yarns with and without spin finishing	33
Figure 3-15.	Schematic diagram for (a) a liquid bridge between identical parallel surface and definition of symbol and (b) an asymmetric liquid bridge between different parallel surfaces. The profile can be separated into a combination of two different symmetric half bridge	37
Figure 3-16.	Cross-sectional schematic of a liquid drop placed between two nonparallel plates	38
Figure 3-17.	(a) When $l_p/l_l > 5.1$, a water drop was at rest. (b) A water drop was initially at rest. And then when water was added to increase l_l , the drop started to move toward the apex edge, and finally filled the corner. (c) A water drop was initially at rest, and after water was added and the top plate was lifted up, and finally filled the corner. The scale bars represent 6 mm	39
Figure 3-18.	IM-to-SU and SU-to-IM resting mode transitions for (a) the Etched SAM and (b) Smooth SAM grooves as β changed. (c) Schematic diagram of a droplet in the stable IM mode depending on β (the cross sectional angle) and θ (the apparent contact angle of the groove inner wall) θ	41
Figure 3-19.	Schematic of fluid transport through a rectangular strip of porous material. Planes indicate positions of cross-sectional areas during transport of a perfectly wetting fluid in a porous material. (A) Cross-sectional areas for a strip of material with a single effective pore size show complete saturation behind the visible wetted front, L_1 . (B) The cross-sectional areas of a material with three different pore sizes show a position-dependent saturation behind the visible wetted front, L_1 . The wetted front positions for the two larger pore sizes, L_2 and L_3 , are also shown.....	42
Figure 3-20.	The microscopic configuration of liquid water in (a) hydrophilic and (b) hydrophobic porous media, and (c) the macroscopic water transport due to a saturation gradient.....	44
Figure 3-21.	(a) Schematic diagram of liquid-vapor interfacial configurations during transition from adsorption to capillary dominated imbibition in the unit cell: (a) Liquid films adsorbed on pore and slit walls and liquid held in corners due to capillary forces at low matric potentials, (b) spontaneous slit fill up (capillary condensation), (c) pore snap off, and (d) full unit cell	46
Figure 3-22.	(a) Schematic diagram of sweating guarded hot plate and (b) top view of measurement unit of sweating guarded hot plate.....	49

Figure 4-1.	(a) Interlock knit structure with a single course yarn layout in magenta color, repeating unit of (b) the cotton and polyethylene blended, and (c) the polyester and polyethylene blended interlock knit.	62
Figure 4-2.	SWEAT test experimental setup with top view scheme and actual captured image.	66
Figure 4-3.	Affinity investigation through wicking flow rate comparison among deionized water (DI), 0.6 wt% dye solutions of rose Bengal dye, brilliant blue G (BBG), and brilliant blue R(BBR). The captured picture shows wicking rate comparison, from left, deionized water, and two of the rose Bengal dye solutions	69
Figure 4-4.	Dye solution visibility on fabric substrates with 0.6 wt% of (a) rose Bengal, (b) brilliant blue G, and brilliant blue R	70
Figure 4-5.	The variation of wicking length within a strip as well as the degree of saturation based on color intensity is shown for the vertical wicking test results on the interlock knit fabrics after 30 min: (a) the wale direction, (b) the course direction of cotton and polyethylene blended fabric, (c) the wale and (d) the course direction of the polyester and polyethylene blended fabric. ...	72
Figure 4-6.	Wicking rate comparison of between the SWEAT test (50 nanoliter/min) and the droplet wicking (4 μ l) on the polyester–polyethylene blended interlock fabric. Wicking rate of the SWEAT test is obtained from four directions with the needle’s hole as a center (in the inserted picture on the top right) when a hydrophilic yarn picked from the polyester–polyethylene blended interlock fabric: course direction–right (red solid line) and –left (red dotted line), and wale direction– top (blue solid line), –bottom (blue dotted line). Wicking rate of dropping method is determined by the average rate of course direction and wale direction, respectively.	81
Figure 4-7.	(a) Individual yarn wicking performance within the polyester–polyethylene blended interlock fabric with the continuous flow rate through the SWEAT test (50 nanoliter/min) with the square root of time. (b) In the schematic of the interlock knit structure, ‘C(0)’ denotes the yarn picked by the needle of SWEAT system, and ‘C(1)’ is the closest adjacent yarn to C(0). After 120 min, the result of wicking performance is shown in (c).	82
Figure 5-1.	EASTMAN flat filament polyester yarns were knitted for a single jersey knit: (a) top view from microscope and (b) SEM image of the cross-section of course direction. Yellow circle in (b) and (e) displays individual yarn within a fabric. EASTMAN flat filament yarn has (c) a unique cross-sectional shape of EASTMAN flat filament yarn with 220 filaments per this yarn consist of 44 subunits (orange circle) with 5 filaments. Commercial textured polyester yarn was knitted for a single jersey knit: (d) top view and (e) SEM image of the	

	cross-section of course direction. A commercial polyester fabric has (f) the circular shaped filaments	89
Figure 5-2.	(a) Schematic of Upward–horizontal–downward (UHD) wicking test. From (b) the actual UHD wicking test setup in a glove box, wicking performance of a fabric strip is recorded from three video cameras for the views of (ci) upward (h), (cii) horizontal (H_L), and (ciii) downward (D_L) segment, respectively.	91
Figure 5-3.	Wicking performance comparison from the droplet wicking test (1 μ l) on the EASTMAN interlock knit fabric with flat filament yarns and a commercial PET interlock knit fabric.....	98
Figure 5-4.	Wicking performance comparison from the SWEAT test (continuous flow rate: 50nl/min) on the EASTMAN interlock knit fabric with flat filament yarns and a commercial PET interlock knit fabric.....	98
Figure 5-5.	Apparent wicking length of EASTMAN single jersey knit from the SWEAT test (continuous flow rate: 50nl/min): (a) apparent wicking length over time, (b) apparent wicking length over square root of time. And (c) shows the wicking length graph of each course yarn over square root of time ($L-\sqrt{t}$) overlap each other when the graph of each yarn's wicking is shifted to place all starting point at the wicking beginning point of the C(0) yarn in order to check the time-wicking length superposition principle	99
Figure 5-6.	Theoretical schematic illustration of liquid moving in yarn.....	100
Figure 5-7.	(a) Actual wicking length presents the yarn length considering textile structures, but apparent wicking length is the shortest distance from the wicking start point. (b) shows wicking performance based on actual wicking length over time. (c) shows that the contacting point of the interlock knit fabric and (d) the actual yarn-to-yarn transfer wicking happens through the connecting point in-between yarns. For the interlock knit fabric, every other column becomes getting wet due to the contact points.....	102
Figure 5-8.	Wicking performance comparison from the SWEAT test (continuous flow rate: 50nl/min) on a commercial textured PET single jersey, EASTMAN single jersey knit, and EASTMAN interlock knit fabrics.....	103
Figure 6-1.	(a) Average wicking length of individual yarn, including C(+n) and C(-n), separately, (b) the total actual wicking length of the apparent wicking length of C(n) with C(+n) and C(-n), and (c) the sum of the total wicking length of all yarns at the given time. (Fabric: EASTMAN single jersey knit with multi-filament flat yarn, Test #3 video code: SJK_B_1090).....	114

Figure 6-2.	Sum of the total wicking length of all yarn over time for the experimental data of the SWEAT test (blue line) and the fitted model (red line). (Fabric: EASTMAN single jersey knit with multi-filament flat yarn, Test #3 video code: SJK_B_1090).	115
Figure S6-1.	(a) Average wicking length of individual yarn, including C(+n) and C(-n), separately, (b) the total actual wicking length of the apparent wicking length of C(n) with C(+n) and C(-n), and (c) the sum of the total wicking length of all yarns at the given time. (Fabric: EASTMAN single jersey knit with multi-filament flat yarn, Test #2 video code: 0425_003)	116
Figure S6-2.	Sum of the total wicking length of all yarn over time for the experimental data of the SWEAT test (blue line) and the fitted model (red line). (Fabric: EASTMAN single jersey knit with multi-filament flat yarn, Test #2 video code: 0425_003).....	117
Figure S6-3.	(a) Average wicking length of individual yarn, including C(+n) and C(-n), separately, (b) the total actual wicking length of the apparent wicking length of C(n) with C(+n) and C(-n), and (c) the sum of the total wicking length of all yarns at the given time. (Fabric: EASTMAN single jersey knit with multi-filament flat yarn, Test #1 video code: 0425_002)	118
Figure S6-4.	Sum of the total wicking length of all yarn over time for the experimental data of the SWEAT test (blue line) and the fitted model (red line). (Fabric: EASTMAN single jersey knit with multi-filament flat yarn, Test #1 video code: 0425_002).....	119
Figure 7-1.	(a) Future experimental setup for overlapping effect and (b) future experimental setup for capillary bridge	122

CHAPTER 1. Introduction

Liquid movement in yarn is driven by capillary action, which is governed by the fiber parameters, yarn structure and liquid characteristics. For a better understanding of liquid transport mechanisms, knowledge of yarn structure based on fibers and fabric structure as well as their surface energies are critical. However, capillary action in porous media, particularly fibrous materials, is complicated by many additional factors, including void space between fibers (or in-between yarns), twist level, tension and contact with adjacent yarns, which all affect the wicking phenomena simultaneously.

For example, the diameter of a single yarn in knit fabric varies depending on the location. That means other yarn features such as twist level, tension and contact points with adjacent yarns are subject to change even within a single yarn. Furthermore, we need to consider not only liquid movement within a yarn but also yarn-transfer wicking since the liquid in a yarn can spill over to the adjacent yarns through their contact points. For those reasons, it seems to be almost impossible to anticipate wicking performance of textiles based on their structures and material properties.

Even though many models have been developed to understand capillary action in complex porous materials in various fields, there are only a few attempts in the textile field starting from plain woven fabrics [1, 2], which have relatively simple structures rather than knitted fabrics. However, much more research is still needed to develop an empirical model of fabrics to predict wicking performance.

Additionally, liquid transport in textile fabrics is one of the critical factors affecting physiological comfort. When we wear clothes, clothing creates a macro-environment between the skin and clothing. Depending on the ambient environment, macro-environment of the textile fabrics is generally hotter and more humid than the ambient environment. For this reason, clothing

generally represents a layer of insulation and imposes a barrier to heat transfer. Especially during exercise, however, textile fabrics can also hinder sweat evaporation from the skin and increase skin and core temperature. Furthermore, when clothing interferes with evaporation of sweat from the wet skin, the efficiency of body cooling is reduced [3]. The rate of water evaporation of sweat from the skin is dependent on the textile-related factors including wettability and permeability of the clothing, and the micro-environmental conditions such as temperature (depending on the ambient temperature and the metabolic heat produced during exercise), humidity, the air velocity, and skin-clothing-ambient air pressure [4]. In addition to the insulating properties in textile fabrics, the effect of clothing on evaporation of sweat is of critical concern because it affects thermal comfort [5]. Moreover, those various factors correlate with each other, and it is hard to investigate wicking performance in sweating circumstance considering the correlation effects.

Even though typical wicking performance test methods for textiles, such as vertical wicking test (AATCC 197 [6]) and the Moisture Management Test (AATCC 195 [7]), are simple and easy to compare between substrates, they cannot explain wicking mechanism in sweating circumstances. Those methods are conducted with infinite reservoir or limited but still large amount of liquid (i.e. liquid droplet) so those methods do not represent human perspiration circumstances with continuous microfluidic flow from sweat pores. Also, when we compare fabrics' wicking performance with those typical methods, sometimes the results were opposite between infinite reservoir and limited amount of liquid. That means we do not fully understand wicking mechanism in textiles yet, so many steps remain to find out how to improve wicking performance of textile substrates.

Therefore, first a better wicking performance test method must be developed, which mimics a sweating situation. Furthermore, in order to develop a better wicking performance fabric,

we need to identify the fundamental influences on liquid transport mechanisms and determine which parameters are most critical. When we drop a small amount of liquid on a fabric surface, the liquid droplet moves through capillary channels during the wicking phenomenon. Therefore, there are three categories to consider in terms of wicking in textile substrates: 1) within-a-yarn wicking based on the channels in-between fibers, 2) yarn-to-yarn transferring toward adjacent yarns, and 3) capillary bridge effect between skin and textiles. Although wicking mechanism of fabrics are directly derived from those three factors, there has only been a feeble attempt to understand each factor as well as the relationships among them.

In this study, we have attempted to develop a better wicking measurement system called SWEAT test to understand capillary channel relationships in textiles as well as to mimic sweating phenomenon starting from a single sweat pore. Because this measurement system supplied continuous microfluidic flow with the similar rate of a single sweat pore, we could investigate how the liquid flow moves within-a-yarn and through yarn-to-yarn transfer in a sweating situation. Also, we will measure the directional wicking rate of individual yarns and the wetting area changes over time with this new wicking measurement method in order to predict the wicking length of a yarn as well as when the liquid spills over from the yarn to adjacent yarns. Furthermore, wicking performance depends on the diameter of capillary channels and the surface energy of liquid and textile substrate. With the new measurement system, we should find out which factors are critical to capillary action of textiles and the relationship between factors. Those experimental results from a new measurement system will help us to understand the capillary mechanism in textile fabrics as well as to develop a predictive model based on void space in-between fibers and in-between yarns. This capillary action model should enable rapid textile product development because the

model should enable us to determine the ideal fiber- and yarn-level capillary channels to improve wicking performance.

CHAPTER 2. Research Outline

In order to understand wicking performance in textiles, generally the following keywords have been considered: 1) wetting vs. wicking, 2) in-plane vs. trans-planer wicking, 3) yarn-level vs. fabric-level wicking, 4) wicking between two plates to simulate sweating circumstance between skin and a fabric, 5) saturation level, 6) physiological comfort, and 7) wicking test methods. Those key factors will be reviewed in Chapter 3. Even though many studies have been performed for each keyword in textile field, it is still hard to determine conditions to fabricate the ideal type of wicking performance textiles under realistic human sweating circumstance.

In terms of typical wicking performance test methods for fabrics, because they use either infinite reservoir or limited but large amount of liquid (i.e. droplet), they have significant limitations to represent human sweating circumstance in which the activated sweat glands generate continuous liquid flow during exercise [8, 9]. For this reason, we developed a better measurement system, which releases continuous microfluidic flow to simulate liquid perspiration generated from a single sweat pore. If we can understand wicking mechanism of complicated capillary structures in textiles through our new test method, we might predict liquid movement of fabrics considering material properties and fabric structures, and we could control wicking performance depending on various applications by controlling major influence factors. For these reasons, our primary research goal in this study is to understand wicking performance of fabrics under realistic human sweating situations.

Firstly, precedent studies regarding wicking performance in fabrics will be introduced in Chapter 3 for overview of capillary phenomena in porous media. And then, a new measurement system will be proposed to simulate human sweating circumstances with continuous liquid flow considering human sweat rate and gland diameter in Chapter 4. With the new test method, liquid

transport performance will be analyzed through visual investigation based on within-a-yarn and yarn-to-yarn transfer wicking performance in Chapter 4 and 5. Additionally, we will discuss the wicking mechanism principles in textiles to explain how liquid moves in knitted fabrics based on our experimental data from our new measurement system in Chapter 5. In Chapter 6, we will introduce a new textile wicking theory from analyzing of the wicking performance data through the SWEAT test method.

CHAPTER 3. Overview of Capillary Phenomena in Porous Media

3.1. Wetting and Wicking

3.1.1. Wetting

Wetting and wicking phenomena in textiles is important to describe liquid transport in the capillary channels. While both wetting and wicking properties affect manufacturing processing as well as the overall wear comfort, there is a clear distinction between these two terms. Wetting is the initial process involved in liquid spreading on the solid substrate. Because a liquid that does not wet a substrate's surfaces cannot wick thorough a fabric, wetting is a prerequisite for wicking[10]. Since wettability of textiles is the potential of a surface to be wetted by liquid, the surface wettability (generally referred to as hydrophobicity and hydrophilicity) is determined by the balance of surface energy in the interface between air, liquid, and solid materials (fiber or fabric)[10]. Wettability is the initial behavior of a fabric, yarn, and fiber when brought into contact with a liquid. It also describes the interaction between the liquid and the substrate prior to the wicking phenomenon. Specifically, solid-liquid interface replaces solid-vapor interface during the wetting process. When a liquid is in contact with a flat solid surface and a vapor at the same time, the forces involved in equilibrium are described by the Young–Dupré equation[11]:

$$\gamma_{lv} \cos \theta = \gamma_{sv} - \gamma_{sl} \quad (3-1)$$

Here, θ is the static contact angle (CA) and γ_{lv} , γ_{sv} , and γ_{sl} are the interfacial tensions between the liquid and vapor phase (or the surface tension of the liquid phase), the solid and vapor phase (or the surface energy of the solid surface), and the solid and liquid phase, respectively. In Young's equation, the magnitude of θ is determined by the thermodynamic equilibrium of the surface free energy at the solid-liquid-vapor interfaces for flat surfaces.

When liquid wets a rough surface, there are two possible wetting status, Wenzel and Cassie-Baxter (**Figure 3-1**). In the Wenzel state, liquid fully wets every area of the rough surface. However, in the case of the Cassie-Baxter state, pockets of air are trapped during liquid wetting, forming a liquid-solid-air composite interface. Based on these theoretical models, many studies have tried to find the relationship between the contact line radius and contact angle considering experimental results [12-14].

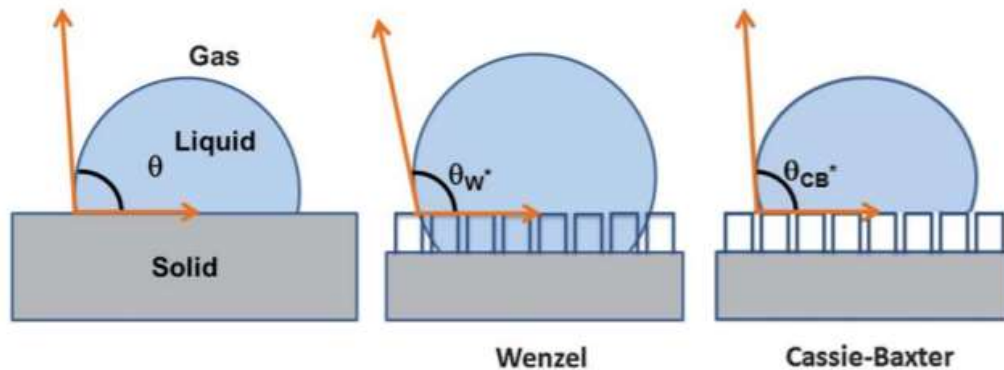


Figure 3-1. Water droplets on flat solid surface (left), Wenzel state (middle), and Cassie-Baxter state (right) [15, 16].

3.1.2. Wicking and Capillary Force

The liquid transport mechanism in which liquid is driven into a porous system by capillary forces is termed wicking. Wicking is a result of spontaneous wetting in a capillary system, i.e. capillary forces are caused by wetting. Wetting process is affected by the surface structure of the fibrous assembly i.e. fibers, yarn, and woven/nonwoven/knitted fabrics. For a liquid to move through a porous medium, wetting process of the material surfaces is essential before being transported through a capillary by means of capillary action.

Capillary motion is the ability of a liquid to flow through narrow spaces without the assistance of, or even in opposition to, external forces such as gravity. However, even though the

direction of both gravity and a capillary channel decides wicking rate and height, most of the studies have been done in vertical wicking mode by investigating the maximum wicking height in a cylindrical tube dipped vertically in an infinite reservoir. However, depending on the amount of liquid as well as the direction of gravity and capillary pressure, the wicking performance, including the wicking rate and the wicking area, is determined. Especially for wicking performance of textiles during exercise, the liquid source may simply be each sweat gland on the skin surface, so it is not an infinite reservoir but continuous microfluidic flow during exercise. Additionally, the value of capillary force should vary depending on the location on the skin, such as armpit, back and shoulder, due to the direction of capillary force and local flow rate.

Capillary phenomena, arising from the capillary force, depends upon the wetting characteristics of both liquid and solid substrate of a capillary channel. Specifically, capillary action occurs when the adhesion to the walls is stronger than the cohesive forces between the liquid molecules. Depending on the relative strength of cohesive and adhesive force, a fluid tends to be raised or suppressed in a vertical capillary tube. The curvature of the liquid inside the narrow capillary channel will lead to pressure difference with the relatively flat surface outside of the capillary channel. A pressure difference between air and liquid forms the curved interface, where the pressure at the concave side of the interface is greater depending on the radius of curvature and the surface tension of the fluid. Inside of the capillary channel, the liquid with surface tension (γ) attains an equilibrium of capillary forces. Specifically, the inertial force is the mass of the fluid in the capillary channel multiplied by its acceleration. And this inertial force is then equal to the sum of all the forces acting on the fluid as it rises in the channel through capillary action. The capillary force draws the fluid into the capillary channel, and viscous as well as gravitational forces work in opposition [17].

If we assume capillary action is derived from capillary force and surface tension only, the fluid rises inside the narrow channel to a height (h) until the surface tension forces balance the weight of the fluid. In a capillary tube whose diameter is small compared to the capillary length, the leading meniscus (within the tube) is a portion of a sphere. Considering a hemispherical meniscus (radius R) as shown in Figure 3-2 (a), a curved liquid–air interface indicates a pressure difference across the interface. The pressure difference, ΔP_{surf} at the interface, causes the liquid interface to rise in the capillary tube until the weight of the suspended column of fluid balances the capillary force. Equation (2) can be used to describe the rise of fluids in a capillary tube when the surface tension forces ($(2\pi R)\gamma$) balance the weight of the fluid ($\Delta P_{surf}(\pi R^2)$):

$$(2\pi R)\gamma = \Delta P_{surf}(\pi R^2)$$

$$\therefore \Delta P_{surf} = \frac{2\gamma}{R} = \frac{2\gamma}{\frac{r}{\cos \theta_E}} = \frac{2\gamma \cos \theta_E}{r} \quad (3-2)$$

where γ is surface tension, r is the tube radius, and then, the radius of curvature R becomes $\frac{r}{\cos \theta_E}$

(Figure 3-3).

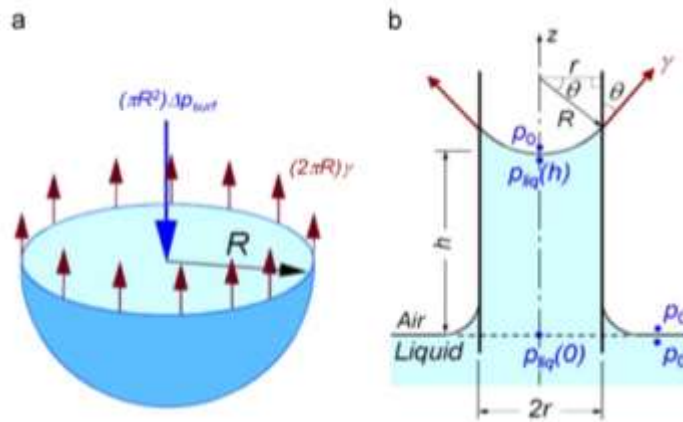


Figure 3-2. (a) The free body diagram of half a droplet[18, 19], and (b) the capillary rise in a narrow cylindrical tube [19, 20]. * R is a radius of curvature of a hemispherical meniscus.

Under the assumption of vertical capillary channel and infinite reservoir, most previous studies have focused on investigating the maximum wicking height at the equilibrium state. In order to get the value of wicking height, the capillary pressure P_c ($= \Delta P_{surf}$) is defined as the pressure difference across the interface, or the pressure difference between air (gas phase) P_a and water P_w (liquid phase) at a level with height of h from the top free surface of liquid as follows:

$$\Delta P_{surf} = P_g - P_l(h) = P_a - P_w(h) \quad (3-3)$$

For example, for hydrophobic materials the capillary pressure is negative ($P_w > P_a$) as their contact angle is larger than 90° .

In Figure 3-3, the pressure at point B (located at height h at $z = 0$) is P_a . The pressure difference between point A and B is purely hydrostatic so the point B is bearing the weight of a liquid column of height (h). Expressing the equilibrium of pressures gives:

$$P_a = P_l(0) = P_w(h) + P_h \quad (3-4)$$

$$P_h = \rho g h \quad (3-5)$$

$$\therefore \Delta P_{surf} = P_c = P_a - P_w(h) = \rho g h = \frac{2\gamma \cos \theta_E}{r} \quad (3-6)$$

where the capillary pressure is P_c and hydrostatic pressure is P_h . For vertical wicking, when a thin vertical tube is immersed in a liquid at one end, the liquid rises vertically inside the tube under the effect of capillary forces (Figure 3-3). Capillary forces cause the liquid to overcome the downward gravity forces and it makes the liquid rise upwards until hydrostatic pressure balances capillary pressure in equilibrium.

Eq. 3-6 derived from Eqs. 3-4 and 3-5 is Jurin's law. It explains that the equilibrium height can be expressed as

$$h = \frac{2\gamma \cos \theta_E}{\rho g r} \quad (3-7)$$

in which h is the liquid height, ρ is the liquid density (mass per unit volume), g is the gravitational acceleration, and r is the tube radius. The height reached by the liquid is inversely proportional to the radius of the tube. Also, rapid wicking through the capillary channels is mainly associated with larger diameter capillary channels. This property, usually referred to as Jurin's law, concluded that the liquid goes up in the tube if the surface energy of the dry wall is larger than that of the wetted wall by using the principle of minimum energy. Most previous studies of wicking in textiles have investigated the maximum wicking height based on Eq. 3-7 but it is not clear how to define the capillary channel radius in textiles considering the various ranges of channel size i.e. the distance between fibers or between yarns.

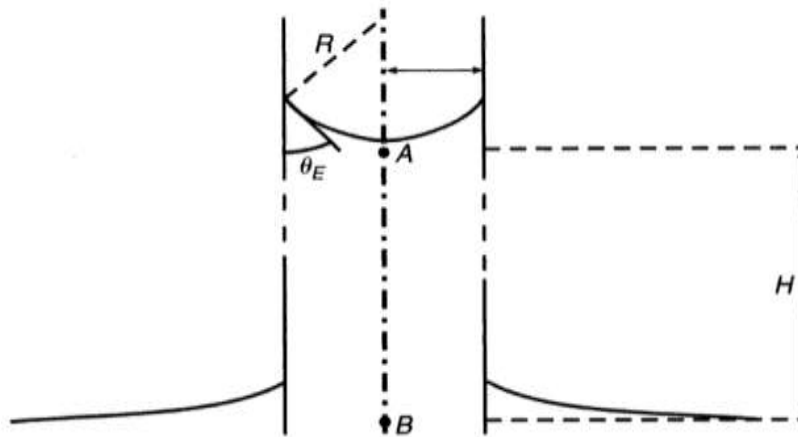


Figure 3-3. The hydrostatic pressure drop between points B and A offsets the Laplace pressure at point A.[21]

For the capillary phenomenon to occur, free energy has to be gained and the work of penetration has to be positive. In other words, when the interfacial energy of the fiber surface in

contact with vapor γ_{SV} exceeds the interfacial energy between the liquid and the fiber surface γ_{SL} , the capillary phenomenon occurs.

$$W_p = \gamma_{SV} - \gamma_{SL} \quad (3-8)$$

in which the work of penetration W_p is a measure of the energy required for capillary penetration. The liquid rises in a channel if $W_p > 0$. When the liquid rises in the channel, the system gains potential energy due to the elevation of a volume of liquid, and then loses capillary energy because of the reduction of the surface energy.

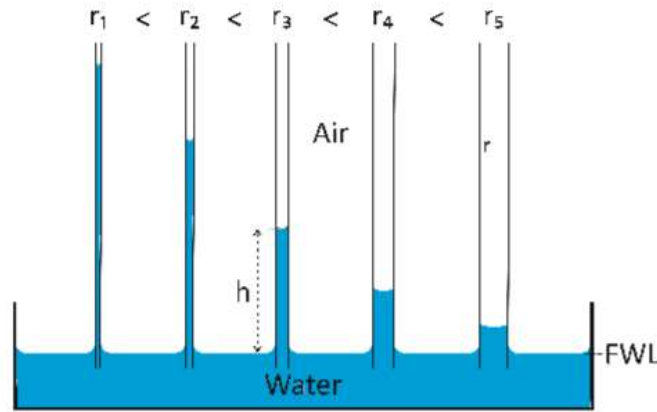


Figure 3-4. A general example of water-air-glass system depending on the radius of channel [22].

Moreover, a capillary bridge may form between two rigid bodies and is also governed by the interfacial curvature between the two phases. According to Laplace–Young equation [11, 23-26], the capillary pressure is:

$$\Delta P_{surf} = \gamma \left(\frac{1}{R_1} + \frac{1}{R_2} \right) \quad (3-9)$$

where γ is the surface tension, R_1 and R_2 are the principal radii of curvature of liquid surface in two planes. In the special case of a spherical surface, the liquid-gas interface has radius of curvature R and the two radii are identical (i.e. $R_1 = R_2$)

A liquid film placed between two parallel plates and that wets the plates makes them very adhesive, so it is difficult to separate the plates (Figure 3-5 (a)). In between two plates, it is observed that the meniscus of liquid has a round shape in order to minimize the free energy. Based on Laplace's law at the free interface, there is an equation for the vertical radius (R'_2) and the contact angle (θ_E) (Figure 3-3).

$$R'_2 \sin\left(\frac{\pi}{2} - \theta\right) = \frac{h}{2}$$

$$\therefore R'_2 = \frac{h}{2 \cos \theta} \quad (3-10)$$

From Laplace's law (Eq 3-9), the capillary pressure at the parallel plates is as follows:

$$\Delta P_{surf} = \gamma \left(\frac{1}{R'_1} + \frac{2 \cos \theta}{h} \right) \quad (3-11)$$

Because the horizontal radius (R'_1) is much larger than R'_2 ($\frac{1}{R'_1} \rightarrow 0$), the capillary pressure is approximately:

$$\Delta P_{surf} \approx \frac{2 \gamma \cos \theta}{h} \quad (3-12)$$

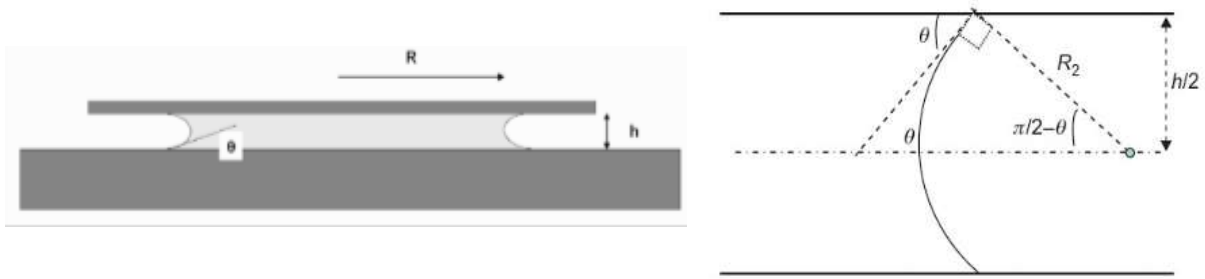


Figure 3-5. (a) Film of water between two glass plates and (b) calculation of the vertical curvature.

[27]

Additionally, the critical factor of wicking performance of fabrics is how fast liquid can move away from sweating source site. The wicking volume rate at which liquid moves through a porous channel is related to the driving force by Poiseuille’s law:

$$dV = \frac{\pi r^4}{8\eta h} \Delta P dt \quad (3-13)$$

where r = effective radius of the pore, η = liquid viscosity, x = distance within the pore, and ΔP = effective pressure gradient. Poiseuille’s law explained that at a given temperature, water flow through tubes in porous media is inversely proportional to the length of the tube and directly proportional to the pressure gradient and to the fourth power of the tube diameter. Based on Poiseuille’s law, we can anticipate the velocity of liquid flow under certain structural conditions in porous media.

The rate of liquid penetration through a capillary channel is Eq. 3-13 by assuming the steady-state flow and according to Poiseuille’s law expressing the balance between viscous forces and capillary and hydrostatic forces (neglecting inertial effect). The relationship between the liquid volume and height is given by:

$$dV = r^2 \pi dh \quad (3-14)$$

The difference between capillary P_c and hydrostatic pressure P_h allows calculating the pressure drop (ΔP).

$$\Delta P = \frac{2\gamma \cos \theta_E}{r} - \rho gh \quad (3-15)$$

By substitution of Eq. 3-14 and 3-15 to Eq. 3-13, the penetration rate is transformed into:

$$dV = r^2 \pi dh = \frac{\pi r^4}{8\eta h} \left(\frac{2\gamma \cos \theta_E}{r} - \rho gh \right) dt \quad (3-16)$$

$$\therefore \frac{dh}{dt} = \frac{r^2}{8\eta h} \left(\frac{2\gamma \cos \theta_E}{r} - \rho gh \right)$$

Assuming that the hydrostatic pressure can be neglected in case of flow under capillary pressure, Eq. 3-17 can be rewritten as follows:

$$h \frac{dh}{dt} = \frac{r \gamma \cos \theta_E}{4\eta} \quad (3-17)$$

The Lucas-Washburn equation is obtained after the integration of Eq. 3-17 with the initial condition ($h=0$ at $t=0$).

$$h^2 = \frac{r \gamma \cos \theta_E}{2\eta} t \quad (3-18)$$

The study by Marmur (1992) is quite interesting and his approach can apply to textile substrates because he investigated capillary penetration considering the thickness of porous media (Figure 3-7) as well as nonuniformity in the pore size distribution[28]. Figure 3-6 (a) shows the P_w (liquid phase) at a level with height of h (Eq. 3-9) will be changed to $\rho g l \sin \theta_a$ depending on the tilt angle, θ_a . Also, he investigated the relationship between the substrate thickness and surface

wettability to explain wicking phenomena as shown in Figure 3-6. Depending on the pore size, it has two competing effects: small pores imply high driving forces for penetration but has a lower penetration rate than big pores. That's because the increased driving force in small pore brings with it an increased viscous resistance. Consequently, the initial stages of penetration must be derived from a relatively rapid penetration through large pores. Furthermore, he explained that when the liquid reservoir is finite, the liquid may redistribute itself at later stages by flowing from the large pores into the small ones. That effect is called the redistribution.

Kissa (1981) found the kinetics of drop penetration into paper with the wetting area, A on time [29]:

$$A = \pi R^2 = kt^{0.3} \quad (3-19)$$

where k is a proportionality constant which depends on the properties of the paper and liquid. According to Lucas-Washburn equation (Eq. 3-18), unidirectional wetting into a paper strip from an infinite reservoir is proportional to time. With comparison results among infinite, limited liquid and a droplet, Marmur pointed out the penetration and displacement of small liquid reservoirs depends on the reservoirs curvature, and not only on the contact angle, as had been previously believed (Figure 3-8). Even though he could not find the exact reason for that, it would be very important for textile wicking performance test. Although a single sweat pore supplies microfluidic flow over times, typical vertical wicking method has been widely used.

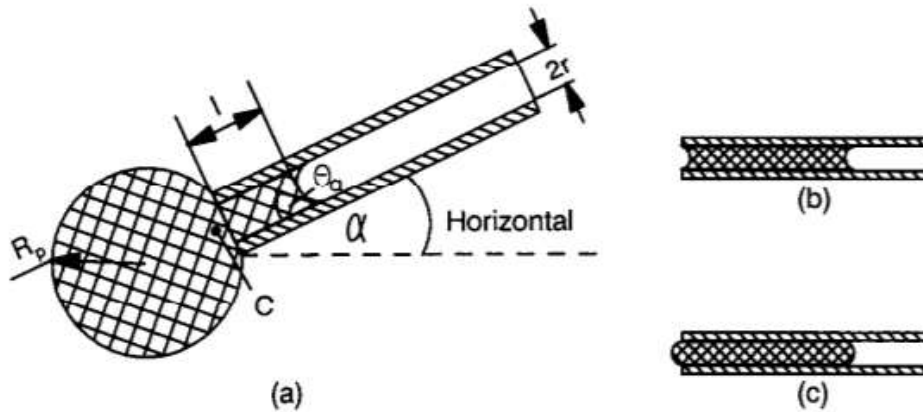


Figure 3-6. (a) Penetration of a small drop into a capillary. (b) the final equilibrium situation for $\theta_a < 90^\circ$. (c) the final equilibrium situation for $\theta_a > 90^\circ$ [28].

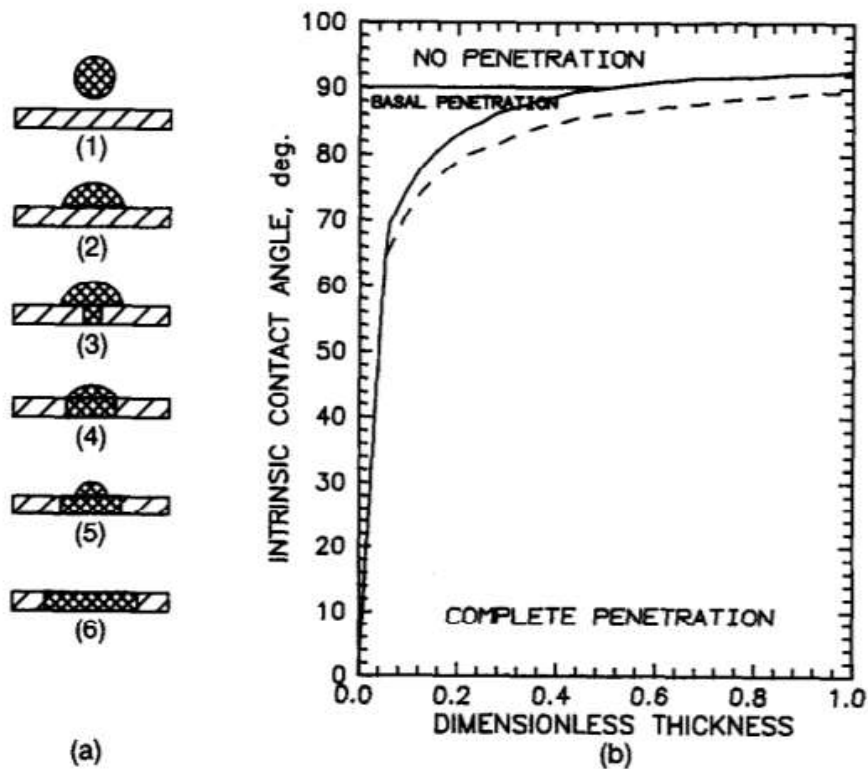


Figure 3-7. (a) Stages of drop penetration into a thin porous medium. (b) “phase diagram” for penetration of a drop into a thin porous medium [28].

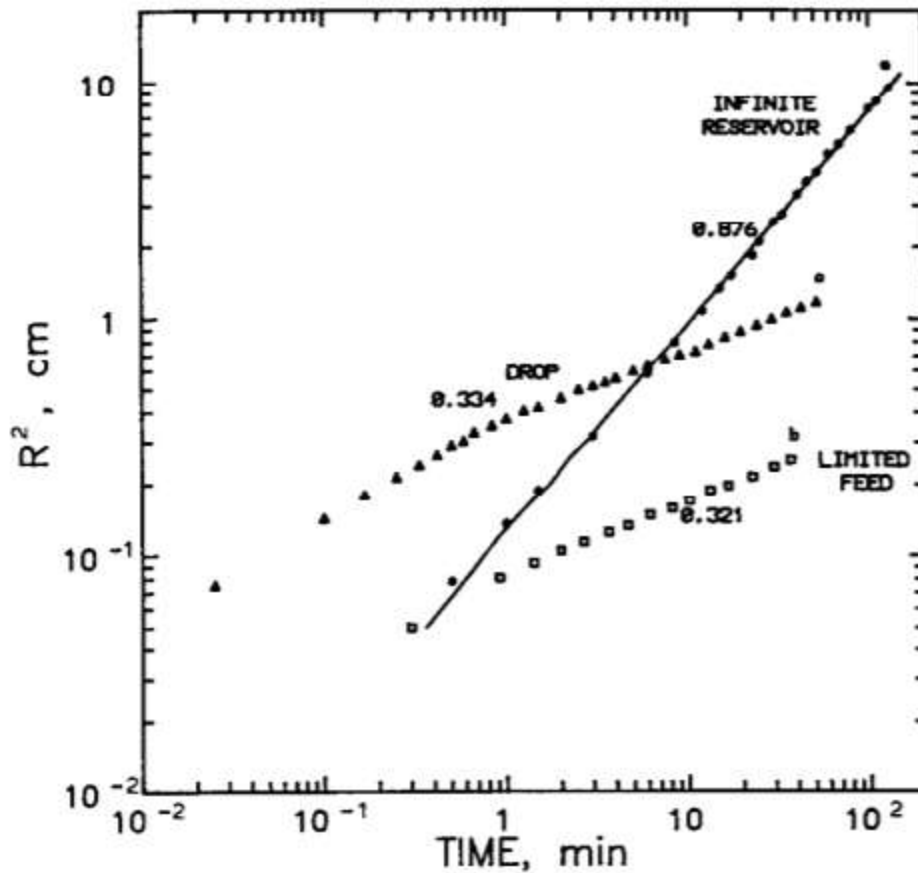


Figure 3-8. Kinetics of penetration into paper from an infinite liquid reservoir, the theoretical prediction of the radial capillary model, a limited liquid reservoir, and a drop [28].

Wicking in fabric substrates is caused by external forces or by capillary forces and the transport of a liquid into a capillary channel is generally referred to as in-between yarns and fibers. For example, when we shed sweat, capillary force is important in order to remove moisture away from textile fabrics. The transport of liquid has been one of the popular subjects in previous studies with various fabric types, but most studies have focused on which factors affect the vertical wicking height. Specifically, previous studies in the textile field have been conducted as focusing on the relationship between vertical wicking height and yarn structure such as twisting and cross-sectional shape [30-34]. Generally, wicking phenomenon occurs when a liquid wets fiber

assembled with capillary spaces and goes through the spaces between them. The resulting capillary forces drive the liquid to move through the capillary spaces. Wicking can be visualized as a spontaneous displacement of a solid–air interface with a solid–liquid interface in a capillary system such as in the vertical wicking height test. Assuming a simple case (i.e. wicking in a capillary tube), the area of the liquid–air interface across the capillary is very small relative to the area of the wetted capillary wall. In this case, we can assume that the tube does not change its shape (i.e. swelling) during the wicking. Therefore, we could say that the only considerable change is the increase of the solid–liquid interface and decrease of the solid–air interface.

Based on an understanding of wicking phenomenon in textiles, the goal of this paper is to establish direction on how to control the liquid transport mechanism in order to quickly remove moisture away from textile fabrics through liquid flow pathways. In the following review, we will discuss the factors that might affect liquid movement in textiles. Also, further studies are necessary regarding how to design the improved liquid transport system in textiles in order to improve physiological comfort.

3.2. Wicking in Porous Media

3.2.1. In-plane wicking

The moisture absorption capacity of fibers (hygroscopy), as well as their surface properties (hydrophilicity or hydrophobicity) are very important parameters to determine the wicking properties of a fabric. In terms of yarn-level, the geometric configuration of the pore structures (inter- and intra-yarn capillaries) play a determinant role on liquid transport. For wear comfort of a textile, both its trans-planar and in-plane wicking properties are important. Trans-planar wicking means the liquid movement through thickness of fabric i.e. perpendicular to plane of fabric.

Typical wicking behavior tests of textile fabrics are operated with a fabric strip, suspended vertically or horizontally with one end dipped into infinite liquid reservoir, and thus are in-plane wicking experiments. To investigate the fabric wicking performance, either how much time it takes for the liquid to reach a certain level or how far the height of the advancing liquid front can go is recorded as a function of time. For instance, to conduct the vertical wicking test, a vertically suspended fabric strip is placed on the fixed clamp to make one end of fabric strip immersed into the infinite liquid reservoir, and the masses of fabric and wicking height versus time are recorded separately. The fabric mass increases with time passed because of the moisture absorption. Water also transits through the thickness of a fabric in its plane and the rate of uptake of water is recorded. Even though the vertical wicking measurement by the gravimetric technique is easy to perform, this test cannot determine the exact quantity of liquid absorbed by the fabrics at different heights (the degree of saturation level). Thus, the testing results have limited implication to clothing comfort.

Simile and Beckham (2012) developed a new wicking test because the results from numerous wicking tests, including strip, spot, plate, siphon, moisture management, or trans– planar

liquid transport tests, do not allow for predictive design of fabrics with defined wicking behavior (Figure 3-9). The new integrated upward–horizontal–downward test provides intrinsic quantitative descriptors of fabrics that can be used to predict wicking behavior. These descriptors are capillary pressure (P_c) and permeability (k) as functions of saturation (S). Wicking tests were conducted on single strips of hydrophilic-treated polyester mesh knit fabrics manufactured for performance athletic apparel. A single fabric strip was positioned to allow sequential upward, horizontal, and downward wicking of fluid from an infinite reservoir. The upward segment governs the liquid saturation, the horizontal section is analyzed to predict capillary pressure from Laplace equation using the Washburn equation, and the downward segment is investigated to determine permeability from Darcy's equation. Through this UHD test method, saturation–capillary pressure–permeability ($S - P_c - k$) relations were determined for this hydrophilic polyester fabric.

From this study, the average effective capillary radii of the substrate was calculated from the horizontal slopes using Lucas-Washburn equation (Eq. 3-18). And these radii were used to calculate capillary pressures using the Laplace equation (Eq. 3-9). However, the effective capillary radius value is not well defined because the capillary radius size in a fabric has a broad range in a fabric. Also, they assumed the same saturation level for each sample because they converted the weight changes by absorbing liquid to wicking length under the assumption that the wicked length is just the mass of water times a constant. However, in reality, even a fabric strip has various saturation levels which can be verified from the diverse range of color intensity at different heights. For example, Figure 4-5a shows when one end of a fabric strip was immersed into infinite dye solution, the color intensities between inside of a blue and a green circle are different even in the fabric strip.

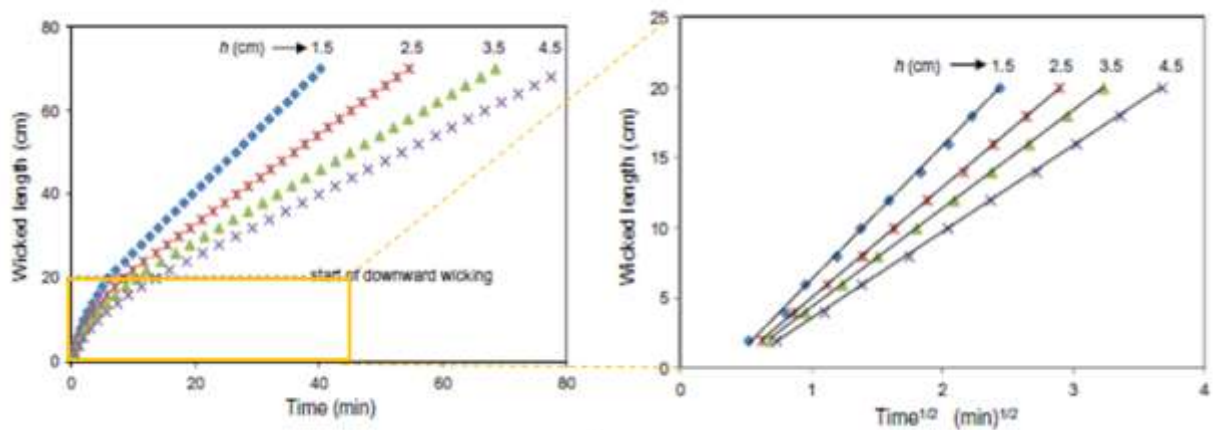


Figure 3-9. (a) Horizontal–downward wicking data, wicking length vs. time, and (b) horizontal wicking data, wicking length vs. the square root of time, for a single knit fabric at upward wicking heights (h) of 1.5, 2.5, 3.5, and 4.5 cm, corresponding to saturations of 0.87, 0.78, 0.74, and 0.69, respectively.

*Data were measured as mass vs. time but are plotted as wicked length vs. time.

Several techniques, including measuring and image processing, are available to investigate wicking behavior of textiles. The most common method is measuring wetting area manually or using image processing software as shown in Figure 3-10. Even though the advanced technique enables us to extract information easily and automatically by counting pixels [35] and with the edge-enhanced image [36], we need to think about whether typical wicking mode such as vertical wicking and dropping liquid is relevant to sweating situation with continuous microfluidic flow.

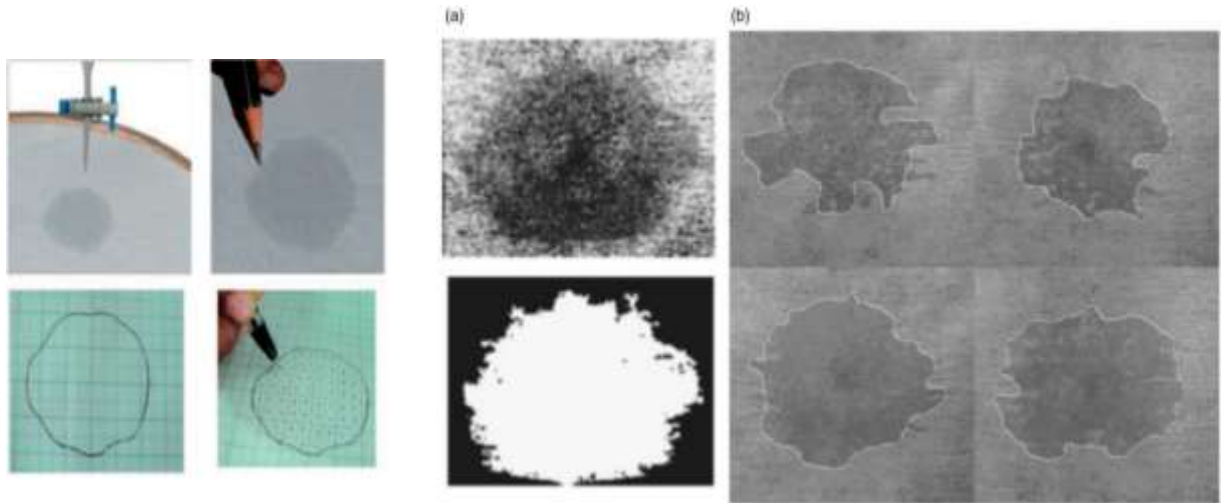


Figure 3-10. Manual method for measuring wicking area (left). [35, 37] (a) Results of the morphological segmentation technique and (b) the region merging technique.[36, 37]

3.2.2. Trans-planar wicking (Through-thickness wicking)

Unlike wicking in the lengthwise direction, transverse wicking is the transmission of water through the thickness of a fabric, which is perpendicular to the plane of the fabric. Compared to longitudinal wicking, transverse wicking is more important because the mechanism of removal of liquid perspiration from the skin involves its movement through the fabric thickness. However, transverse wicking is more difficult to measure than longitudinal wicking. Because the distances involved in transverse wicking are very small, a liquid may transverse the thickness of fabric in less than second [38]. For these reasons, we will discuss which factors might influence the transverse wicking in porous media.

Miller and Tyomkin [39] suggested a sensitive gravimetric method, which is able to measure the rate and total amount of liquid uptake in the perpendicular direction to the plane of fabric. This study shows that liquid entry into a fabric pore happens in essentially all cases when the pore walls are curved. Conventionally liquid entry movement will occur only when the advancing contact angle is less than 90° . However, this study insisted that, especially for fibrous materials, almost all pores have a splayed opening with a concave meniscus formation.

When a liquid front contacts with the entrance of a pore (Figure 3-11a), if the advancing angle is greater than 90° (Figure 3-11c), it is not possible to make the liquid rise up. The convex meniscus shape would produce a pressure gradient opposing the uptake direction. The only way the liquid steps into a pore is to produce a concave meniscus as shown in Figure 3-11d. For this, the contact line of a pore needs to move into the pore to some extent. The liquid front advances continue, keeping a balance between the concave pressure gradient (which gets smaller as it moves into the pore) and the opposing gravity effect of the elevated liquid.

It is important to understand that the formation of a concave meniscus exerts a driving force for the liquid to move into the porous medium and the contact angle is less than 90° . This study suggested the instrumentation to investigate the pore entry phenomenon considers the two key features: 1) investigation of a negative pressure gradient to act against spontaneous uptake, and 2) a rapid response and continuous measurement of mass uptake for wicking.

This research suggested a sensitive gravimetric method in order to investigate the liquid uptake in the perpendicular direction to a fabric (transverse wicking) through theoretical approach. Because most of the studies in the textile field have focused on vertical wicking, this study is noteworthy. Furthermore, if we want to know the liquid transport mechanism in textiles, firstly we should consider how a single liquid droplet moves into the space in fabrics rather than how far the liquid is absorbed through fabrics based on vertical wicking height.

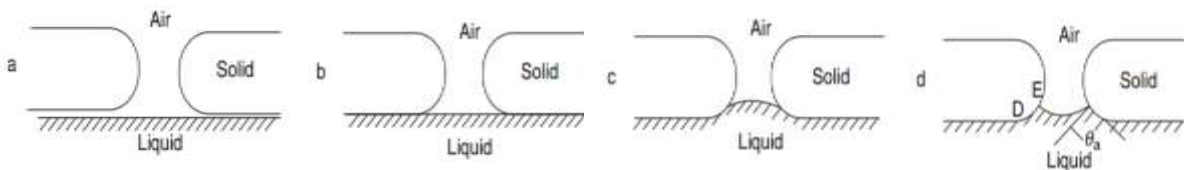


Figure 3-11. Entry of a liquid into a fabric pore: (a) liquid surface just before contact with the pore; (b) when liquid surface is contacting the pore, the angle between liquid and solid surface becomes $\theta_a = 180^\circ$; (c) not possible with convex meniscus; (d) allowable mode of liquid entry [39].

Trans-planar wicking is the transport of liquid through the thickness of a fabric. The apparatus consists of a horizontal plate fed with liquid from liquid flow tube upward to the surface of plate. The most popular trans-planar wicking test is moisture management test (MMT, AATCC 195[7]). MMT investigates changes in electrical resistance with seven concentric sets of pins for each of upper and lower side of fabric in order to evaluate moisture absorption rate. According to

the amount of liquid fed, the upper surface of the plate would be kept damp, thereby simulating a perspiring skin surface. Because perspiration wicks from the skin through a fabric to external environment, through-thickness wicking is critical to clothing comfort. However, if we want to develop a better wicking performance fabric, which can move sweat liquid faster and further, it is more related to in-plane wicking effect than trans-planar wicking because transport distance through the fabric thickness is much shorter than that on fabric surface (in-plane).

3.2.3. Yarn-level Wicking

Depending on the relative amount of liquid used and the setting of the liquid-fabric contact, the typical wicking performance testing can be divided into two groups: wicking from an infinite liquid reservoir and wicking from a limited amount of liquid (usually a single droplet wicking into a fabric).

When we release a drop of water on a textile fabric, wetting starts on the surface of fabrics [40]. However, depending on droplet volume and substrate wettability, we could investigate wicking and/or flooding phenomenon. When droplet volume is more than substrate can absorb during the observation time, the remaining liquid floods on the surface.

After a liquid drop spreads under capillary forces, the water drop fills large openings by penetration through the whole fabric. If a fabric is thoroughly wet, wicking phenomenon begins into the yarn structure. Moreover, generally the liquid transport mechanism in textile fabrics depends on the wetting behavior of the whole yarn rather than the influence of individual fiber materials [41]. For these reasons, the liquid movement in yarn structure has been studied in the textile research field.

To simulate sweating, typical wicking tests of textiles use an infinite reservoir via immersing the fabric end or a limited volume by dropping liquid onto the fabrics. However, during strenuous exercise humans start to sweat and generate sweat flow continuously. In capillary theory, the smaller pore sizes generate higher capillary pressures and thus increase the liquid spreading distance. The capillary action is determined by the interaction of the liquid and the fabric materials through the liquid properties such as viscosity and surface tension, and by the geometric structure of the pores. The size and shape of the fibers, as well as their alignment have an effect on the geometry of the void spaces or pores through which the liquid is transported. Furthermore, the inter-fiber pore should have the proper dimensions to provide sufficient capillary pressure, interconnection pathways to transport the liquid, and overall porosity to retain the liquid. Water transport as well as absorbency in a fibrous material depends on the fiber-water interaction and the geometric configuration of the fibrous materials.

Rajagopalan, Aneja [34] developed a mathematical model of surface-tension-driven flow in capillaries of arbitrary cross-section to predict liquid rise in fiber bundles of specified void fraction, fiber shape, and size. Through previous studies, mathematical models have been derived by considering liquid rise in vertical cylindrical capillaries using a macroscopic force balance approach. However, in this study, they have compared the analytical model with the computational fluid dynamic model, Poly-flow, and with consideration of the shape factor to prove the computational model's validity against the previous studies. Even though this research insisted that they have extended the analysis to more complex geometrics, the difference between the previous and this study is only the consideration of the shape factor as a function of void fraction. Additionally, because they considered the shape factor for both an analytical and a computational model, it seems like that is natural consequence to have excellent agreement between these two

models. Furthermore, because this shape factor usually depends on the shape of the flow geometry and not on its size, they claimed the shape factor can be calculated by capillary-related equations for laminar and pressure-driven axial flow by putting the value of this factor into the equations. According to the models, the maximum liquid height increases by decreasing the void area between the filaments in vertical wicking while the initial rate of penetration decreases.

Although this study derived mathematical capillary models of arbitrary cross-section, these models were based on a unit cell considering the homogeneous cross-section and the flow direction for unidirectional fibers. For understanding the capillary action in textile fabrics thoroughly, we also need to consider fiber bundles as well as yarn bundles. However, this study only considered a single yarn structure consisting of fiber bundles in an axisymmetric plane.

Nyoni and Brook [30] extended the wicking behavior of fabrics to the influence of the yarns including structural features such as twist, diameter and tension through experiments with nylon 6.6 continuous filament yarns in unsaturated, saturated and dry zones. Generally, the yarn specific volume decreases with increase of twist, which would result in the disruption of the continuity, length, and orientation of the capillaries. However, this study showed that at low twist levels, the diameter increased with increase in twist while in medium and highly twisted yarns, increasing the amount of twist led to a decrease in diameter (Figure 3-12a). Moreover, Figure 3-12b shows that when the yarn twist level was increased, the wicking performance decreased due to the reduction of capillary space available. After that twist level, the wicking performance increased again due to spiral wicking along the capillaries following a helical path of less tension near and on the surface of the yarn. Additionally, due to insignificant liquid diffusion into the nylon filaments, swelling was not observed. So, we can assume the capillary action is closely connected with the degree of twist in a yarn.

When they explained the relationship between the retention period of wet yarn and evaporation time, they claimed yarn weight loss was determined by the liquid dispersion through the yarn structure. Although there was an insignificant difference in liquid uptake for all wicking time intervals (i.e., 15, 30, 45 and 60 min), an inevitable question comes to this study result for the rapid drying for yarn after wicking for 60 min compared to that for 45 min. Longer retention period generally has more liquid loss but this experimental study cannot provide a valid reason for the exceptional cases.

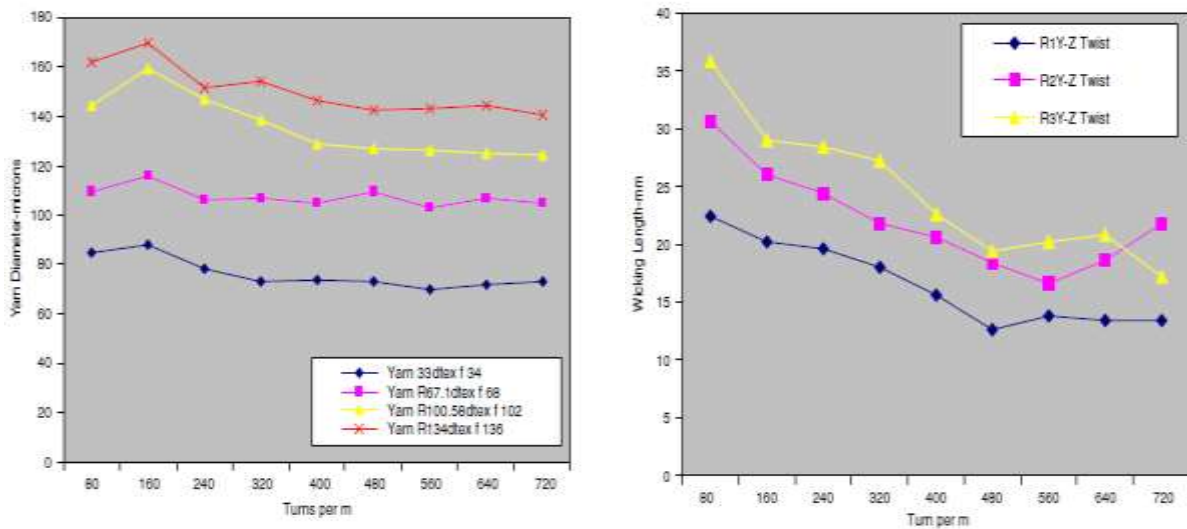


Figure 3-12. (a) Effect of twist on yarn diameter, and (b) the effect of twist level on yarn wicking performance of continuous filament yarns[30].

Wang, Zha [31] studied the effects of twist and monofilament cross-section shape on the wicking height through experiments with polyester filament yarns. With the increase of twist, the wicking height goes up until the maximum height is reached, and then it descends with further increase of the twist (Figure 3-13a). The results of this research are in disagreement with the earlier study [30]. In the wicking comparison between two different cross-sections such as five-leaf and circular cross-section, the wicking height of the yarns with circular cross-section is obviously

higher than that with five-leaf cross-section under the same twist levels (Figure 3-13b). Furthermore, the wicking of the low-stretch yarn is much larger than that of the parallel-drawn yarn at the same twist levels (Figure 3-13c). For these experimental results, we can make a conclusion that twist level, cross-sectional shape, and processing style would affect the wicking properties of yarns. This study asserted that low-stretch yarns have more curls and pores between them, thus this yarn is difficult to be packed closely with a favorable structure for the capillary effect. However, from this experimental result, it is hard to understand what the fundamental reason for the effect of cross-sectional shape on the liquid movement is.

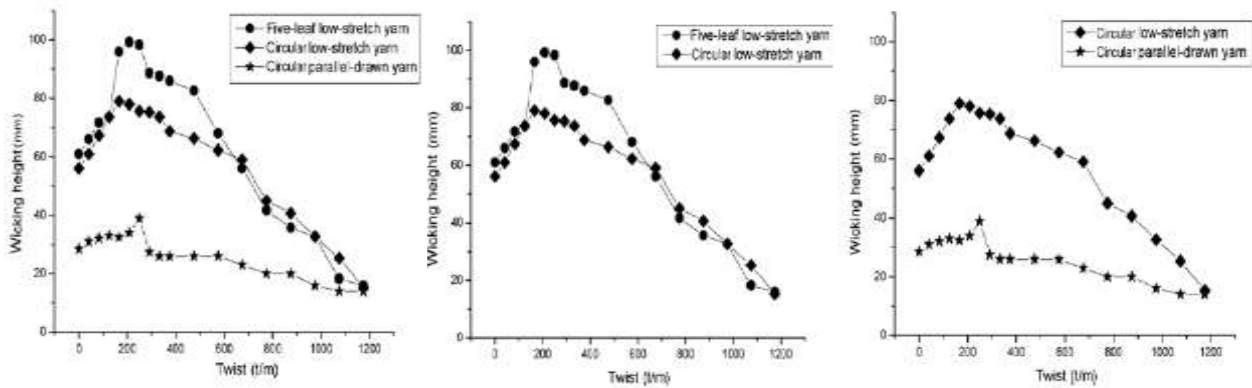


Figure 3-13. Effect of (a) twist, (b) cross-section, and (c) texturing on wicking height of yarns[31].

Sengupta and Murthy [32], [33] have found that wicking phenomenon was highly sensitive to the structure/twist of ring and open-end spun yarns[32], and the twist of circular- and trilobal-filaments[33] in two articles. In the former study[32] of this group, viscous rayon staple fiber (0.17 mg/m, 41mm) was spun to 32.8 tex ring spun and open-end yarns with the different tex twist factors (i.e. 23.95, 28.75, 38.32, 47.90 and 57.48 respectively). They investigated the vertical wicking height for ring and open-end spun yarns according to the twist level with a test length of 30 cm of the yarn. For the ring spun yarns, the wicking time increased steeply as the twist level

rose, whereas for the open-end spun yarn the increase was gradual (Figure 3-14a). The results of overnight vertical wicking height also showed a similar trend (i.e. for any given twist, open-end yarn wicked more than ring-spun yarns) (Figure 3-14b).

From these results, we can determine that highly twisted yarns have a lower wicking tendency than soft-twisted yarn, and also the wicking time increases as the twist increases. However, what they found does not agree with the previous study's result[31] that the wicking height goes up until an optimum twist level, and then it descends with the increase of the twist.

In the latter study[33] of this group, polyester yarns of 68 circular- or trilobal-filaments were textured with the different spin finishes. Air-jet texturized yarns were produced with the texturing parameters of 33.3% overfeed, 9kg/cm² air pressure 30m/min speed under both dry and wet texturing condition. Figure 3-14c shows the trilobal-filament yarns have better wicking properties than circular-filament yarns at the same percentage of floats and arcs. They explained that presence of long drawn out loops like floats and arcs offers less tortuous path for the liquid movement, so higher percentage of floats and arcs results in higher wicking height. It is closely related to the relationship between wicking and core diameter of textured yarns that yarns of trilobal-filaments have faster wicking rates than circular-filament yarns (Figure 3-14c). The increase in core diameter with an increase of long drawn out loops (floats and arcs) provides more spaces in the cores and less tortuous path to the liquid to travel. In this study, the trilobal-filament yarn had a larger core diameter (0.388 mm) compared to that of the circular filament yarn (0.326 mm). This study insists that the inherent bulkiness of trilobal-filament may be the reason for the better wicking rate in trilobal- filament yarns.

Even though this research studied the relationship between wicking and texturing, this study focused more on textured yarn itself by explanation of core diameter for bulkiness and

surface loops. Based on the other study result [31], it appears that their highest twist level is not over an optimum twist level of their yarns. This may be why they did not observe the decrease of wicking height, which is derived from insufficient capillary force. However, based on bulkiness and surface configuration, we can assume the fraction of capillary space between yarns over liquid-occupied space might be the fundamental reasons to induce wicking behavior.

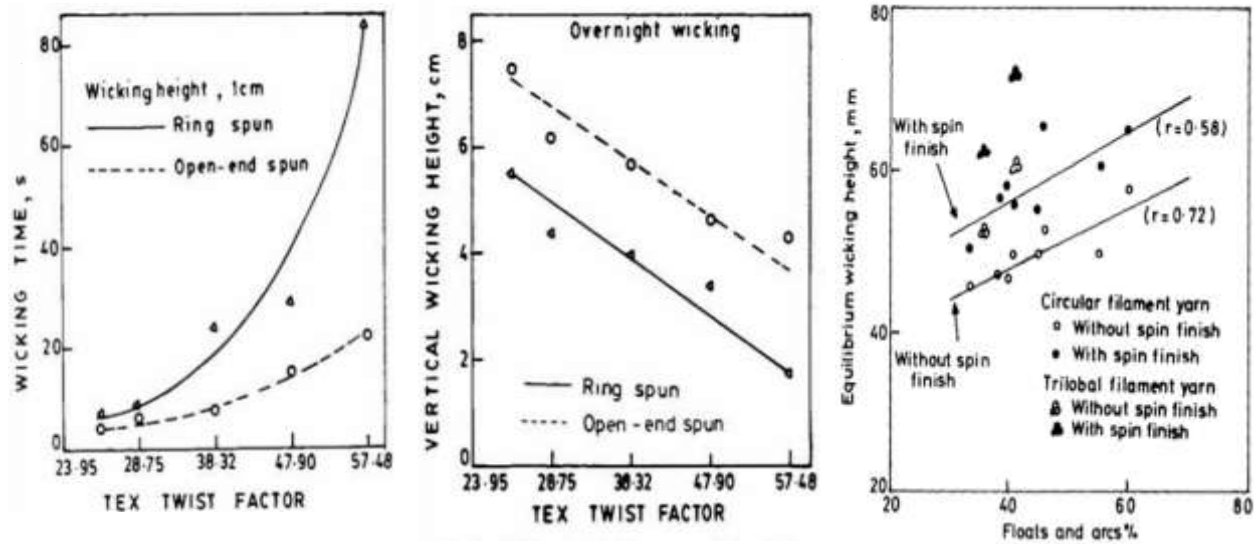


Figure 3-14. Effect of twist factor on (a) wicking time, (b) wicking height [32], and (c) relationship between equilibrium wicking height and percentage of floats and arcs for wet- and dry-textured yarns with and without spin finishing [33].

In order to investigate capillary penetration of liquid, numerous studies used the macroscopic observation of vertical wicking height with the infinite reservoir of test liquid or water. When fabrics absorb sweat from a body, however, the liquid movement starts at a drop rather than relatively infinite amount of liquid. Therefore, in order to control the liquid movement in textiles for a better physiological comfort, previous studies should have considered the droplet amount of water movement first instead of vertical wicking height.

Furthermore, from these previous studies regarding the relationship between yarn structure and liquid movement, we know there is simultaneous occurrence of wetting, wicking, liquid dispersion or retention and evaporation. In order to control the complicated liquid transport mechanism considering time and pathway of liquid flow in textile fabrics, we also need to understand the capillary action in yarns. From these studies, liquid transport mechanism is determined by the liquid's properties, fiber parameters, yarn structure including twist, fiber cross-section, tension, and texturing, and textile structure including geometric configurations of the void space. However, even though we figured out the several factors which affect liquid movement, we still do not know exactly why these factors have an effect on liquid transport mechanism in textiles.

For a better understanding of liquid movement in textiles, we need to know why these factors influence liquid transport mechanisms and which parameters are the most critical ones. Focusing on the factors related to the capillary space, there are three categories: 1) fiber parameters which represent the mechanisms between fibers, 2) the yarn structures related factors which focus on the liquid movement between yarns, and 3) the textile structure related factors which are interested in the mechanism at the point of contact between skin and textile. Based on these three categories, we need to reconsider new approach for liquid transport mechanisms by extending the research regions to other fields.

Most studies in liquid movement have only focused on the fragmentary experimental result without the consideration of the whole wicking process to reach to a maximum wicking distance. However, in this study, they provided a new model considering the integrated imbibition phenomenon from adsorption up to complete saturation. In order to control liquid movement in textiles, the liquid–vapor interfacial configurations should be a priority during transition from adsorption to capillarity.

Much research considering the influence factors of liquid movement in porous media, have considered liquid–vapor configuration, interfacial area, and saturation state. For this reason, from these studies we can get a better understanding of liquid movement in textiles. However, textiles have more complicated structure than porous media because their structure is based on fibers, yarns, and the capillary space between fibers and yarns. We should keep the textile structure in mind: yarn is a long continuous length of interlocked fibers, and yarn is the basic component of weaving or knitting textiles. Even though Lee, Nam [42] considered the void space and throats as the interconnection between pores in porous media, textiles have more complex void space between fibers and yarns respectively and in combination.

3.2.4. Between Two Plates

With a continuous supply of liquid, we could investigate whether a capillary bridge forms between skin and fabric when the wet fabric sticks to the skin. Especially for textile substrates, a capillary bridge affects the wicking mechanism as well as brings discomfort[43]. However, only a few studies have examined capillary bridges between a fabric and another material and none of them have investigated how the capillary bridge would affect wicking through a fabric.

Wang, et al.[44] studied symmetric and asymmetric capillary bridges between a parallel surface with glass and fabrics. Considering the liquid volume, separation distance between surfaces, and the advancing or receding contact angles, they investigated the shape of capillary bridge between parallel surfaces where the effect of gravity could be ignored. Figure 3-15a shows the profile of the bridge can be determined using only one quadrant because the concave capillary bridge between identical parallel surfaces is symmetric about the X- and Z-axes. However, different parallel surfaces make asymmetric bridge, which can be separated into two regions, as shown in Figure 3-15b, the upper half of a symmetric bridge and the lower half of a different symmetric bridge. They found excellent agreement between theory derived from the profile information and experimental results with the microliter-level liquid i.e. ~ 1 , ~ 2 and ~ 5 μl . However, in the case of wicking performance fabrics, which are hydrophilic substrates, the capillary bridge would be only formed at a certain spot where a fabric becomes fully wet. Capillary bridge can also supply liquid to a fabric instead of sweat gland, so it could change wicking phenomenon as compared to when there is no capillary bridge wicking.

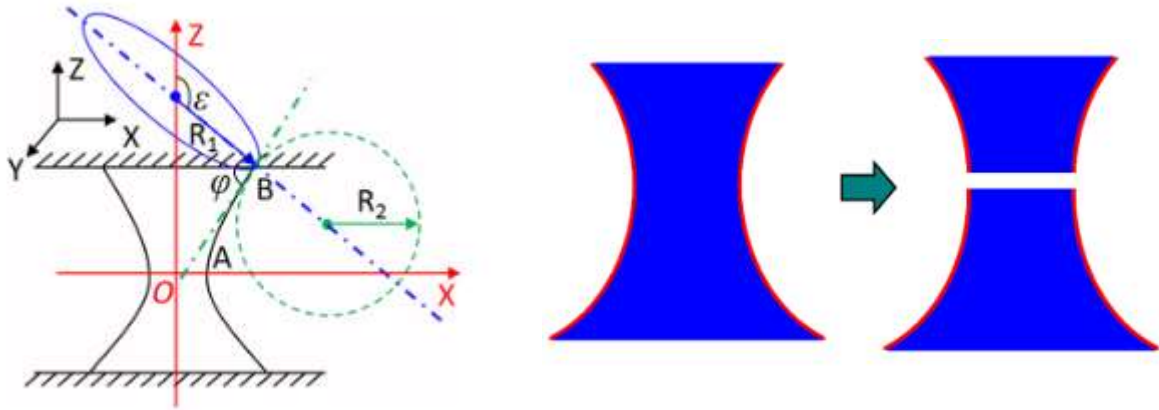


Figure 3-15. Schematic diagram for (a) a liquid bridge between identical parallel surface and definition of symbols and (b) an asymmetric liquid bridge between different parallel surfaces. The profile can be separated into a combination of two different symmetric half bridges[44].

Luo, Heng [45] studied the behavior of a liquid drop between two nonparallel plates, which may be fixed or movable relative to each other. Unlike other previous studies, this study proved through theoretical and experimental investigation that when the two plates are fixed, a liquid drop may not necessarily fill the corner of the two plates. Moreover, this research demonstrated that a liquid drop may fill the corner if more liquid is added to the drop or when the top plate is lifted. Additionally, this research suggested a physical model to interpret the shifting effect of a liquid drop when the drop is squeezed and relaxed between two nonparallel plates. This proposed model indicates that when none of the leading and trailing edges are pinned, the difference of liquid pressures on two edges creates a horizontal flow. This flow makes a liquid drop move from the trailing edge (edge 2 in Figure 3-16) to the leading edge (edge 1 in Figure 3-16). Consequently, after a processing cycle (squeezing and relaxing processes), a liquid drop translates toward the plate corner.

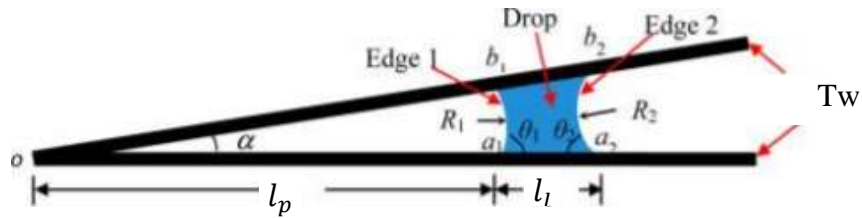


Figure 3-16. Cross-sectional schematic of a liquid drop placed between two nonparallel plates[45].

Note that l_p was defined as the distance between o and a_1 , and l_l as the length of a_1 and a_2 .

In terms of experiment in this study, water drops were placed between two non-parallel SiO_2 -coated Si plates. Water volume is not mentioned but they said the drop size is much smaller than the distance between edge 1 and o . The flow directions were observed for different conditions of a liquid drop position and tilt angle between the non-parallel plates. The values of θ_r (receding angle) and θ_a (advancing angle) were measured to be 50° and 67° separately. When l_l was more than 5 times larger than l_p , a water drop was found to be stationary as shown in Figure 3-17a. This study proved that l_l was increased while l_p was reduced in order to achieve a new balance between p_{w1} (liquid pressure at edge 1) and p_{w2} (liquid pressure at edge 2). From Figure 3-17b, when l_l was increased from 6.0 to 8.5 mm and l_p was reduced from 13.0 to 10.0 mm, the drop started to move toward o until it finally filled the corner. In Figure 3-17(c-1) and (c-2), a stationary drop moved toward o at the beginning but after adding more water it suddenly stopped. If α was increased from 7.2 to 17.2° , the drop began to move again and eventually filled the corner (Figure 3-17(c-3) and (c-4)).

From all of these tests, they figured out that the water drop was observed to stay or to move for filling the corner rather than continuing to move away from the corner. This study uniquely considered the situation of adding more liquid after starting the liquid movement. If we consider

sweat dripping continuously, it has a different wicking phenomenon from that with a single liquid drop.

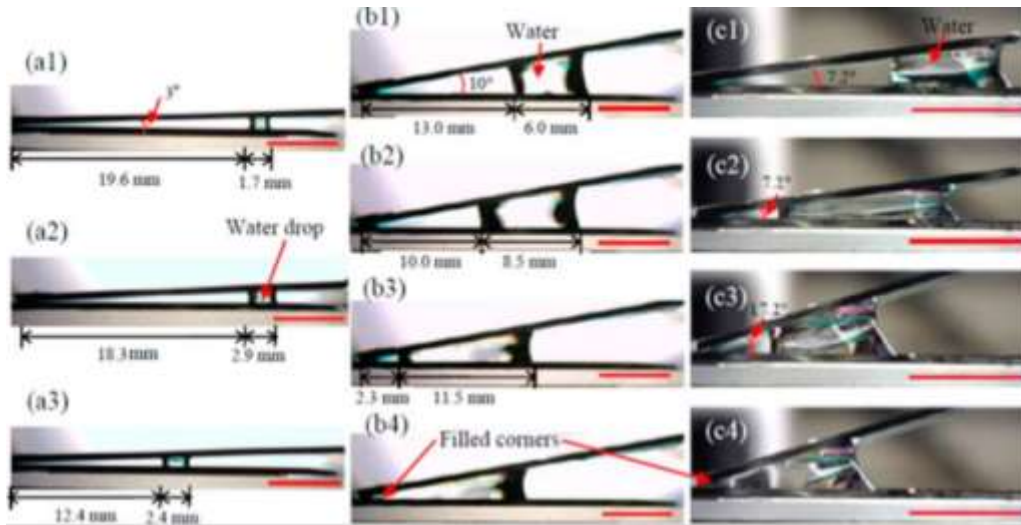


Figure 3-17. (a) When $l_p/l_l > 5.1$, a water drop was at rest. (b) A water drop was initially at rest. And then when water was added to increase l_l , the drop started to move toward the apex edge, and finally filled the corner. (c) A water drop was initially at rest, and after water was added and the top plate was lifted up, and finally filled the corner. The scale bars represent 6 mm.

Xu, Lan [46] studied the behavior of droplets trapped in geometric structure in order to investigate the directional droplet movement through a V-shaped groove, which is folded from a copper sheet. The V-shaped grooves are controlled by surface wettability of the inner wall and the cross sectional angle of the groove shape. The groove inner walls were treated with a self-assembled monolayer (SAM) of n-octadecyl mercaptan, chemical etching.

Compared to this study, the previous research[45] only considered that the droplet transport proceeds toward the corner for the immersed state. However, this study demonstrated liquid movement from the immersed state to the suspended state on the surface having different

wettability derived from roughened and smooth surfaces. Therefore, we can assume that these factors including the state of a liquid and the surface wettability might be critical to control the liquid movement in textiles.

Figure 3-18(a-1) shows that when the cross sectional angle of the groove decreased, the suspended droplet departed from the groove bottom as the droplet volume increased. From the liquid movement, depending on the change of a droplet shape and the cross-sectional angle, it could be helpful to control the liquid transport mechanism to move the liquid away from skin. Specifically, for the etched SAM having hydrophobic characteristics, the transition from immersion to suspension (IM-to-SU) occurred around $\beta = 106^\circ$ (Figure 3-18(a-1)). However, the SU-to-IM transition occurred around $\beta = 109^\circ$ (Figure 3-18(a-2)). Furthermore, the results in Figure 3-18(b-2) with smooth surface show that the droplet departed from the groove bottom with decreasing β , which is the same trend as for the etched surface.

This phenomenon is in contrast with the studies conducted by Prakash, Quéré [47] for the shorebirds' case in which they use their long beaks to drink water. In this shorebird case, the beak acts as a V-shaped groove, and the droplet is transported from the tip of the beak into the mouth as the shorebird closes its beak. However, Xu, Lan [46] demonstrated that the droplet moving direction changes when the surface wettability of the groove inner wall is modified from hydrophilic (Shorebird beaks) to superhydrophobic (Etched SAM groove). Furthermore, this study explained the droplet resting mode is not only controlled by β and θ , but also by the contact angle hysteresis derived from surface wettability i.e. this makes the difference of immersion and suspension in Figure 3-18a and b.

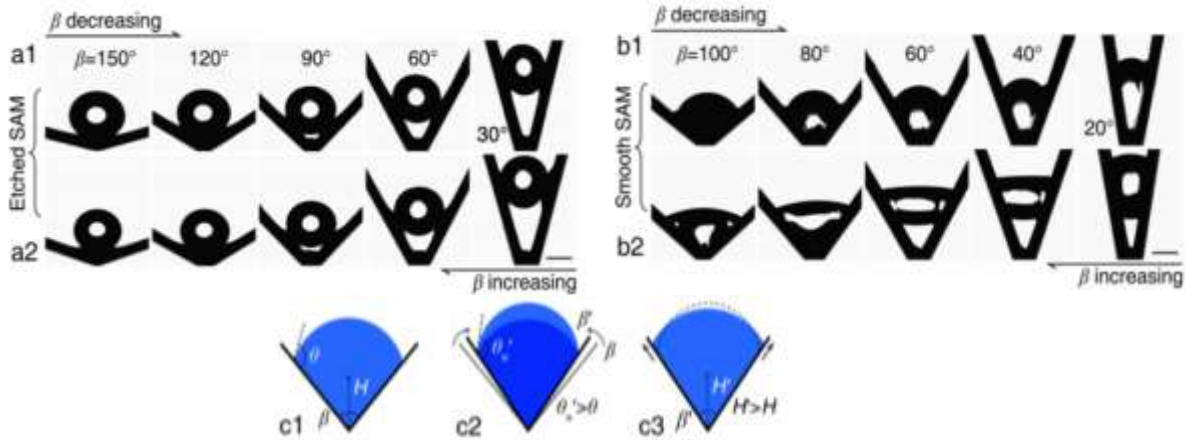


Figure 3-18. IM-to-SU and SU-to-IM resting mode transitions for (a) the Etched SAM and (b) Smooth SAM grooves as β changed. (c) Schematic diagram of a droplet in the stable IM mode depending on β (the cross sectional angle) and θ (the apparent contact angle of the groove inner wall) θ .

3.2.5. Saturation-level

Since Washburn's equation presents linear dependence of square of wicking height in the tube versus time (h vs. \sqrt{t})[48], it has been applied to numerous studies regarding wicking performance of various porous substrates for a long time. Despite the analytical strength of Washburn equation, it has several limitations. Firstly, Washburn equation assumes the porous media is a bundle of cylindrical capillary tubes that have the same radius. According to Washburn equation, the rate of liquid transport is a constant for the penetration of a given liquid into a bundle of fibers, which has a characteristic value of radius, called the average effective capillary radius [41]. Besides the radius of channel, liquid transport rate also is affected by yarn construction features including size, number of fibers, fiber size, alignment, twist, and crimp as they control the level of the inter-fiber capillaries producing higher wicking rates[41]. Because the complexity of yarn structure makes it hard to predict the fluid movement in textile fabrics, it is not acceptable to

apply Washburn equation to textiles' substrate to explain wicking performance of them. Furthermore, movement of liquid through pores could cause shifting and swelling of fibers as well as changes in the pore structure so these changes may make it more difficult to understand wicking mechanism.

Additionally, the Lucas-Washburn model supposes complete saturation of a substrate behind the wetted front. However, in many of the porous materials used, there is a broad pore size distribution, and the porous material behind the visible wetted front is not fully saturated as shown in Figure 3-19. Because liquid can move through capillary channels, the void spaces between fibers or yarns determine wicking performance [49]. Especially since textile substrates have diverse range of void spaces between fibers within a yarn (or in-between yarns), it is hard to investigate the saturation level with wicking performance. Furthermore, Washburn model does not consider slip effect at solid-liquid interface as well as gravity force.

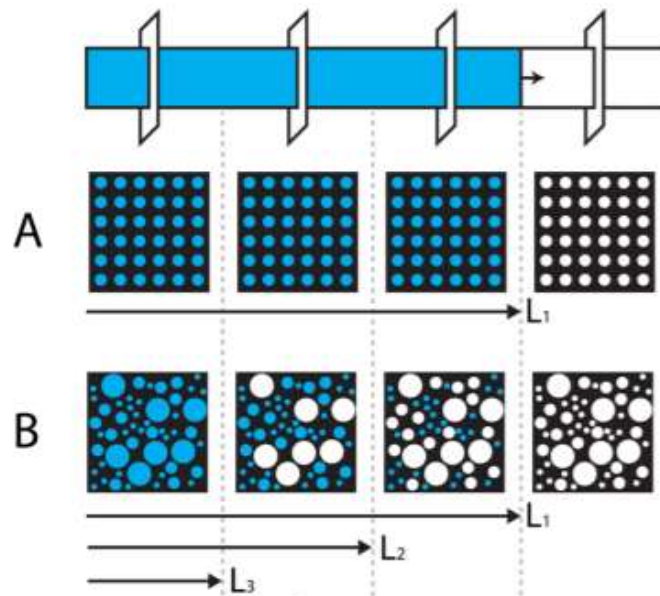


Figure 3-19. Schematic of fluid transport through a rectangular strip of porous material. Planes indicate positions of cross-sectional areas during transport of a perfectly wetting fluid in a porous material. (A) Cross-sectional areas for a strip of material with a single effective pore size show

complete saturation behind the visible wetted front, L_1 . (B) The cross-sectional areas of a material with three different pore sizes show a position-dependent saturation behind the visible wetted front, L_1 . The wetted front positions for the two larger pore sizes, L_2 and L_3 , are also shown [50].

From a macroscopic viewpoint, the capillary pressure in porous media can be expressed as a function of the wetting or non-wetting phase saturation. The curvature of the liquid–gas interface generally increases with the volume content of the non-wetting phase due to the limited pore space available. The Leverett J -function $J(S)$ is a typical equation to explain the correlation between the macroscopic capillary pressure and the phase saturation in porous media. The Leverett J -function can be expressed in terms of the water saturation S_w as follows:

$$J(S_w) = \frac{P_c \left(\frac{K}{\varepsilon}\right)^{1/2}}{\sigma \cos \theta_w} \quad (3-20)$$

where K is the absolute permeability and ε is the porosity. Because $J(S_w)$ is a monotonic increasing function of the water saturation, the pressure of liquid water increases with S_w .

Lee, Nam [42] studied the water transport mechanisms through a pore-network model in hydrophobic gas diffusion layers (GDLs) of polymer electrolyte membrane fuel cells. This study considered the microscale behavior of liquid movement in pores and through throats (interconnections between pores). Based on modeling, this study proved the water saturation distribution in GDLs has a concave shape along the flow direction through the invasion percolation process. For hydrophobic porous media, liquid water does not wet the surface because more energy is required for wetting. For this reason, non-wet space in large pores remains to reduce the contact area with hydrophobic surfaces (Figure 3-20b). In hydrophilic porous media, however, the liquid water behavior is exactly opposite to that in hydrophobic media. Because the liquid was absorbed

well into the surface, the formation of liquid films preferentially resides in smaller pores as shown in Figure 3-20a.

As mentioned in eq. 3-20, $J(S_w)$ is a monotonic increasing function of the water saturation, and the pressure of liquid water increases with the water saturation (S_w). As a result, the macroscopic transport of liquid occurs from a higher saturation region towards a lower saturation region as shown in Figure 3-20c. The capillary pressure in porous media is governed by the interfacial curvature between the two phases derived from saturation level. For this reason, liquid flow is affected by the capillary pressure in the pores, the entry pressure, viscous pressure, and the voids, as well as the saturation distribution.

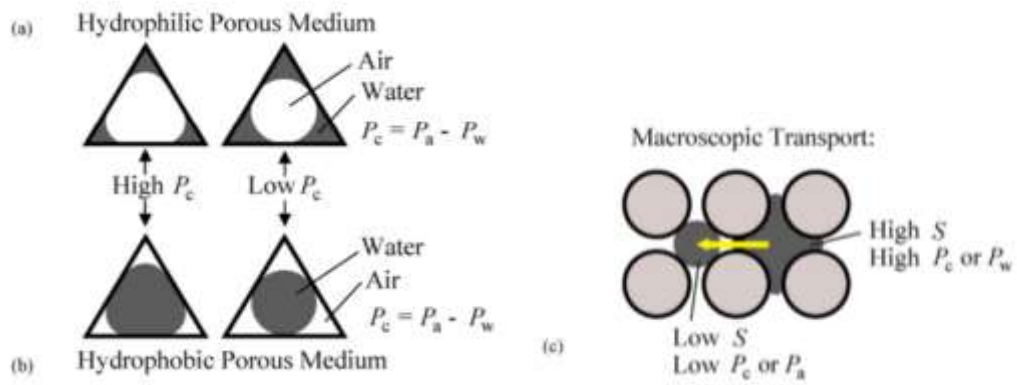


Figure 3-20. The microscopic configuration of liquid water in (a) hydrophilic and (b) hydrophobic porous media, and (c) the macroscopic water transport due to a saturation gradient [42].

In this study, the authors focused on how macroscopic transport of liquid occurs from a higher saturation region towards a lower saturation area based on capillary pressure. It is important for the liquid movement in textiles to understand transverse wicking rather than longitudinal movement in length direction of fibers or yarns. In order to control liquid movement to quickly remove moisture away from fabrics for evaporation, we need to focus on the liquid uptake in the

perpendicular direction to a fabric through transverse wicking. From this study, we can assume the configuration of a single liquid droplet during transverse wicking and why the liquid movement occurs in transverse direction.

Tuller, Or [51] studied adsorption and capillary condensation in porous media focusing on pore spaces through a theoretical approach and modeling. The conventional models of liquid distribution, flow, and transport mechanism have limitation. Specifically, from the conventional models, the liquid movement has been explained in partially saturated porous media through a bundle of cylindrical capillaries. Additionally, the traditional capillary model does not consider the dominant contribution of adsorptive surface forces and liquid films in the low saturation state. This new model considered the liquid–vapor interfacial configurations from adsorption to capillary dominated imbibition unlike the conventional models for partially saturated states. Based on the new model, we can have a better understanding of liquid configuration and movement in porous media. This study also considered the individual contributions of adsorptive and capillary forces until a complete saturation as shown in Figure 3-21d. The pore space geometry with surface area is also considered in this new realistic model. New pore space geometry composed of an angular pore cross section (or capillary) are connected to slit-shaped spaces with internal surface area (for adsorption). Figure 3-21 shows liquid–vapor interfacial configuration during transition from adsorption to capillary dominated imbibition. At low absorption state, thin liquid films coat pore and slit walls. Some liquid is held behind liquid–vapor interfaces at the corners and it contributes to capillary forces (Figure 3-21a). With increasing the amount of liquid, liquid films thicken to a point where the slits spontaneously fill up with liquid (capillary condensation (Figure 3-21b)). A further increase in liquid amount results in a further increase in film thickness within the pore. And a reduction in the radius of curvature of liquid–vapor interfaces continues until they contact and

form an inscribed circle (Figure 3-21c). Consequently, the pore spontaneously fills up (snap off) to complete saturation (Figure 3-21d).

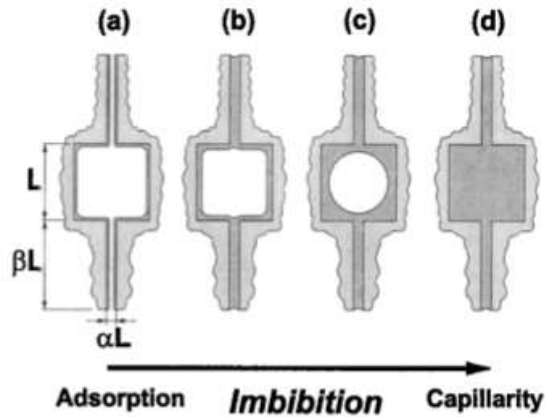


Figure 3-21. Schematic diagram of liquid-vapor interfacial configurations during transition from adsorption to capillary dominated imbibition in the unit cell: (a) Liquid films adsorbed on pore and slit walls and liquid held in corners due to capillary forces at low matric potentials, (b) spontaneous slit fill up (capillary condensation), (c) pore snap off, and (d) full unit cell[51].

*Note that the pore width (L) and the proportions of exposed surfaces (determined by the slit width αL and the slit length βL) are considered.

3.2.6. Effect of Wicking Properties on Physiological Comfort

The main task of textiles and clothing is to protect the human body from weather conditions with sufficient comfort consisting of physiological, psychological and physical aspects, regardless of the type of activity [52, 53]. Performance fabrics, especially moisture wicking ones, are engineered to keep the skin dry during vigorous athletic activities. As keeping the skin dry especially during cold weather sports, the wearer does not lose heat unnecessarily by having wet skin. Clothing comfort has two main aspects which combine to create a subjective perception of satisfactory performance: 1) sensorial comfort and 2) thermophysiological (thermal) comfort [52].

Sensorial comfort relates to the interaction of the clothing with the sense of the wearer, particularly with the tactile response of skin. The main mechanical and surface properties of fabrics that influence the sensorial properties of fabrics are tensile, bending, shearing and thickness. Because this subjective assessment treats fabric hand as a psychological reaction obtained from the sense of touch, the assessment of the fabric handle is carried out subjectively by individual judges[54]. The most widely recognized and used around world is probably the Kawabata's Hand Evaluation System of Fabrics (KES-F) system to measure the fabric handle properties objectively[55].

Thermophysiological comfort relates to the way clothing buffers and dissipates metabolic heat and moisture[52]. When insensible perspiration is continuously generated by the body during normal wearing state, steady heat and moisture vapor fluxes are created as maintaining thermoregulation and a feeling of thermal comfort. In this state, the clothing becomes a part of the steady state of thermoregulatory system by dissipating heat and moisture. However, in transient wear conditions, derived from heavy sweating and intermittent pulses caused by strenuous activity, sensible perspiration and liquid sweat occur. In this case, human body must maintain normal body temperature by maximizing heat loss. Clothing features a wicking fabric that pulls sweat away from the sweat generating spots, where it can quickly evaporate into the environment, and thus it produces a cooling effect. For this reason, how fast and how far sweat liquid goes through capillary channels within fabric is critical for developing a better wicking performance textile. The behavior of functional clothing in normal and transient wear condition can be predicted by fabric properties' measurement, including moisture transport, water vapor permeability, and thermal insulation. Generally, the sweating guarded hot plate method (ASTM F 1868), simulating the heat and moisture transfer from the body surface through clothing material toward the environment, allows

us to measure evaporative and thermal resistance, relating to comfort characteristics of the garment[56].

For sweating guarded hotplate method (Figure 3-22), a 30.5 cm × 30.5 cm fabric sample is mounted on a square porous plate, which is heated to maintain a constant temperature of 35 °C (approximately human skin temperature) and controlled at 65% relative humidity. Air speed generated by the air flow hood is 1 ± 0.05 m/s and DI water is fed to the surface of the porous plate to measure the evaporative resistance of the sample. The plate temperature is measured by the sensor sandwiches directly underneath the plate surface. After the system reaches steady state, total thermal resistance of the fabric is calculated by the following [57, 58]:

$$R_{et} = \frac{A (p_s - p_a)}{H} \quad (3-21)$$

where :

R_{et} = total evaporative resistance provided by the fabric and boundary air layer, m²kPa/W

A = test area, m²

p_s = water vapor pressure at the plate surface, kPa

p_a = water vapor pressure of the air, kPa

H = electrical heating power, W

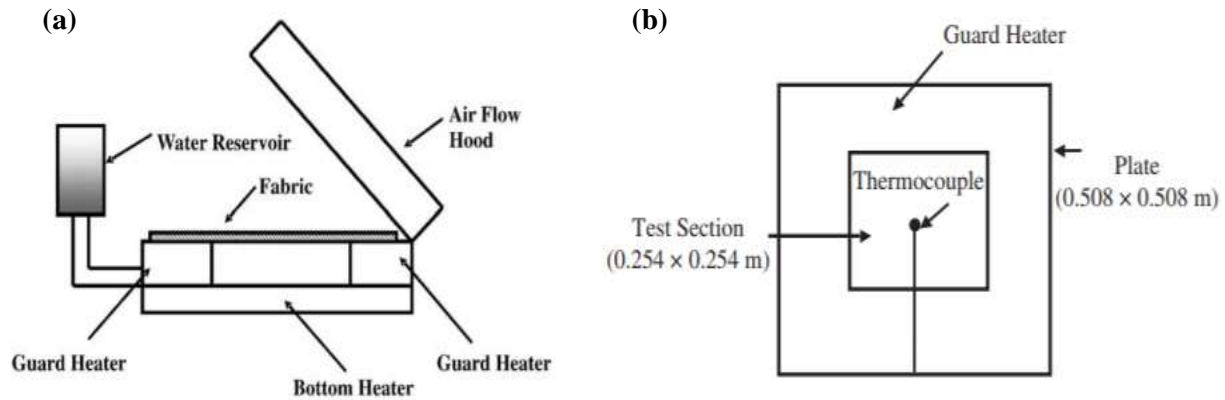


Figure 3-22. (a) Schematic diagram of sweating guarded hot plate and (b) top view of measurement unit of sweating guarded hot plate [56].

The water vapor pressure at the fabric surface at the steady state is assumed to be equal to the saturation vapor pressure at 35°C. If the fabric is saturated with water, the amount of power required to maintain it at constant temperature is related to the rate at which water evaporates from the surface of the plate and diffuses through the fabric. Likewise, the intrinsic evaporative resistance of the fabric (R_{ef}) is obtainable by subtracting the evaporative resistance provided by the boundary air layer (R_{eb}), which can be measured by conducting a test on the bare plate without a fabric over the liquid barrier[56].

$$R_{ef} = R_{et} - R_{eb} \quad (3-22)$$

Sweating is a bodily function that helps to maintain body temperature by tightly controlled self-regulatory mechanisms. At the initial stage of athletic activity, the human body produces heat and a certain amount of water vapor. If the heat production is higher than the heat loss, the body usually starts to produce liquid sweat secreted by the sweat glands on the skin. However, when higher-sweat rate makes sweat liquid dripping down the sweating torso due to the over saturation

of a fabric, there is no more available contribution towards the wet heat loss from this perspiration [59].

Even though the sweating guarded hot plate method allows us to compare evaporative resistance between fabrics, we should remember that the evaporative resistance value of the sample is derived from a fully saturated fabric. However, in order to improve wicking properties, the functional fabrics could remove liquid away from sweating source as well as evaporate faster before getting into the saturation-level. For this reason, we tried to develop a new measurement system which can investigate wicking behavior of fabrics focusing on the initial wicking stage before the fabric become saturated.

In terms of physiological comfort, the relative humidity, the sweat rate and the material composition of fabrics will affect how much heat can be transferred due to evaporative cooling effect. Primary motivation to develop functional textiles with moisture wicking properties is to improve the physiological comfort by optimizing moisture management especially for intense athletic activity.

3.2.7. Limitations of Current Textile Wicking Test Methods

Several equations have been used in many textile studies to analyze wicking performance in quantitative ways (Table 3-1). Usually, these precedent studies have proceeded with typical liquid moisture management property tests of textiles, and then, tried to investigate data through the various equations, shown in Table 3-1. However, those wicking-related equations were not designed for the wicking performance of fabrics under the human sweating circumstance but generally for a straight capillary channel with a constant circular cross-section in contact with an infinite reservoir. However, fabrics have complex capillary channels due to their own structure such as knit and woven. Specifically, the twist level and the cross-sectional area of a yarn within a fabric keep changing over the locations within the fabric. For example, Lucas-Washburn equation has been frequently used for the vertical wicking test with a fabric strip because this test is conducted with infinite reservoir. Even though the average effective capillary radius of a substrate can be calculated through Lucas-Washburn equation and wicking experimental data, this radius does not have any particular significance for the textile substrate. Even though the capillary channel from the calculated radius is assumed as a circular shape in the equations, the actual liquid in the capillary channels of a textile substrate exists in an effective medium space between fibers of arbitrary shape and with arbitrary arrangements, shown in Fig. 5-6. Additionally, the typical wicking test methods may not represent human sweating because those methods are conducted with either infinite reservoirs or limited, but large amounts of liquid (Table 3-2). However, because human sweat is generated from each sweat gland with a continuous flow, continuous liquid flow should be used for the wicking performance test of apparel.

From microscopic video analysis of the vertical wicking as shown later, we found that liquid moves along individual yarns within a fabric, even though the wicking length of a fabric

strip seems to be a single line from a distance, as assumed in the standardized tests. However, because typical test methods focus on either the whole-fabric-level or the single-yarn-level, these textile wicking methods could not explain the yarn-level wicking within a fabric. For this reason, we found that we need a better wicking test method, which can simulate realistic human sweating circumstance (i.e. by using continuous liquid flow) as well as investigate the yarn-level wicking within a fabric. We believe that this new method should be able to explain how liquid is transported in fabrics based on within-a-yarn and yarn-to-yarn transfer wicking, which has not previously been reported. If we could measure the wicking performance along all individual yarns within a fabric, we might find the wicking principle in textiles and it might help to predict the wicking performance of fabrics.

Table 3-1. Wicking performance-related equations and their assumptions.

Wicking-related equations		Assumptions/ limitations
Laplace equation (eq. 3-9)	$\Delta P = \gamma \cos \theta \left(\frac{1}{R_1} + \frac{1}{R_2} \right)$	<ul style="list-style-type: none"> • If $R_1 = R_2$, a capillary channel has a perfectly circular cross-sectional shape • In case of a capillary channel contacting with infinite reservoir
Poiseuille equation (eq. 3-13)	$\Delta P = \frac{8\eta h Q}{\pi r^4}$	<ul style="list-style-type: none"> • Assumed liquid flow through a long straight cylindrical pipe of constant cross section [60]
Lucas-Washburn equation (eq. 3-18)	$L^2 = \frac{r \gamma \cos \theta_E}{2\eta} t$	<ul style="list-style-type: none"> • Assumed a cylindrical capillary channel in contact with an infinite reservoir [61] • Neglect both gravity and inertia [62] • For textile substrates, ‘r’ is the average effective radius determined from the wicking length and assumed to be constant for a given type of textile, but it does not have any actual meaning
Darcy equation	$k = \left(\frac{\left(\frac{dL_d}{dt} \right) H_L \eta S \varepsilon}{P_c - P_{hydro}} \right)^{1/2}$	<ul style="list-style-type: none"> • Assumed a cylindrical capillary channel in contact with an infinite reservoir [61] <p> k: permeability $\frac{dL_d}{dt}$: constant downward wicking rate ε: fabric porosity $= \left(1 - \frac{\rho_{fabric}}{\rho_{fiber}} \right) \times 100\%$ H_L: Total wicking distance P_{hydro}: hydrostatic pressure P_c: capillary pressure </p>
Saturation level	$S = \left(\frac{m_{fluid}}{V_{total} \times \rho \times \varepsilon} \right)$	<ul style="list-style-type: none"> • Defined as the fraction of the void spaces that is filled with a liquid in a porous media • For textile substrates, the saturation level is not constant because as wicking length increases capillary pressure increases due to the saturation level of the fabric decreasing <p> S: saturation m_{fluid}: fluid mass ρ: fluid density </p>

Table 3-2. Limitations of typical fabric wicking test methods.

Substrate scale	Wicking mode	Wicking test method	Liquid source type	Limitations/ assumptions
Fabric	In-plane	Vertical wicking	Infinite reservoir	<ul style="list-style-type: none"> • Focus is on finding textile substrates' absorbency from infinite reservoir • Vertical wicking method was introduced to evaluate the instantaneous absorbency of commercial surgical gauzes • Due to using infinite reservoir, there is no relationship with human sweating circumstance • Cannot explain the yarn-level wicking within a fabric • Lucas-Washburn equation is not appropriate for fabrics because the capillary channels of a fabric are not straight cylindrical pipes of a constant cross-section
		Horizontal or transverse wicking		<ul style="list-style-type: none"> • Wicking phenomenon only from big pores • Due to using infinite reservoir, no relationship with human sweating circumstance • Cannot explain the yarn-level wicking within a fabric
		Integrated upward-horizontal-downward (UHD) wicking [63]		<ul style="list-style-type: none"> • Tries to provide fabric characteristics such as capillary pressure, permeability, and saturation from sequential directional wicking with infinite reservoir • Wicking data are collected not visually as wicking distance but gravimetrically with fabric weight changes • Due to using infinite reservoir, no relationship with human sweating circumstance • The average effective capillary radius can be obtained but it does not have actual meaning because of complexity of textile wicking channels • Even in a certain fabric strip, the saturation level would vary depending on the wicking length

Table 3-2. (continued)

Fabric	In-plane	Droplet wicking	Single Droplet	<ul style="list-style-type: none"> • Use the limited but still much larger amount of liquid (i.e. a single droplet) instead of infinite reservoir • Still much larger amount compared to the realistic human sweat situation • Measure wicking area with the edge-enhanced image without consideration of individual yarn wicking within a fabric and textile structure
	In-plane/trans-planar*	Moisture Management Test (MMT [7])	Multiple droplets	<ul style="list-style-type: none"> • Use multiple droplets instead of continuous liquid flow • Evaluate wicking performance of textiles from total 220 µl liquid dispensed for a period of 20 sec
	-	Gravimetric Absorbency Testing System (GATS)	Infinite reservoir	<ul style="list-style-type: none"> • Use a sintered glass with fine pores instead of a single hole to supply fluid to the system • Measured only the weight of water drawn toward a textile substrate from an infinite reservoir through a tube connected to a porous test plate • No variation in the textile structures • Does not focus on how far liquid can move through a substrate and in-plane wicking • After taking 0.01g liquid absorption in less than 10 sec, evaporation test with air flow is conducted for 1000 sec
A single yarn	Yarn-level	Single yarn wicking	Infinite reservoir	<ul style="list-style-type: none"> • Cannot apply the yarn-level wicking test result to the fabric-level wicking performance because there is a big gap between a single yarn (thread) itself versus the yarn within a fabric
			Droplet	
Fabric	-	Sweating guarded hot plate	Limited but large amount of liquid	<ul style="list-style-type: none"> • Focuses on heat loss from liquid evaporation derived from the wetting area of a fabric substrate • Cannot explain wicking performance of textiles specifically










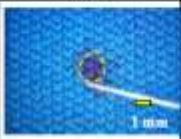

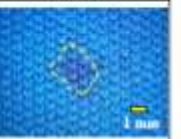
*Accumulative one-way transport capability: the difference between the area of the liquid moisture content curves of the top and bottom surfaces of a specimen with respect to time: [Area ($U_{Bottom} - U_{top}$)]/total testing time.

CHAPTER 4. New Wicking Measurement System to Mimic Human Sweating Phenomena with Continuous Microfluidic Flow

4.1. Needs for a New Wicking Measurement System

When typical wicking test methods were conducted with infinite reservoirs or limited, but large amounts of liquid, such as a droplet, the wicking test results for fabric construction parameters among various textile substrates varied widely and could even have opposite dependencies for the different test methods. For example, in the upward-horizontal-downward (UHD) wicking test with infinite reservoir, a polyester knit fabric provided by EASTMAN, Inc. took ~ 30 min to reach the end of the horizontal direction while a commercial polyester fabric required only ~7 min to arrive the same distance (Table 4-1) (Specific yarn/fabric information can be found in Fig. 5-1). However, when a 1 μ l droplet was placed on the fabric surface, the EASTMAN knit made a considerably bigger wetting area than the commercial polyester fabric. If the wicking performance results vary with the type of test methods and we did not know which method is more appropriate, that means we still do not understand the textile wicking mechanism thoroughly. Additionally, when humans sweat, it is nothing like infinite reservoir or a droplet, rather human sweat is a slow continuous flow generated from sweat glands. Therefore, a better wicking test method should be established to mimic realistic human sweating circumstances by supplying a continuous liquid flow at an appropriate rate to the fabric substrate.

Table 4-1. Wicking performance comparison between the usage of infinite reservoir and droplet.

Wicking test	EASTMAN Polyester Interlock Knit (Flat multifilament yarn, course direction)			Commercial Polyester Interlock Knit (Textured yarn, course direction)		
	7 min	15 min	30 min	7 min	15 min	30 min
Upward-horizontal-downward (UHD) wicking*	 5.6 cm	 6.8 cm	 9.1 cm	 9.7 cm	 13.3 cm	 15.1 cm
Droplet wicking (1 μ l)	 1 sec	 30 sec	 3 min	 1 sec	 30 sec	 3 min

* Fabric strips for the UHD test were 2.5 cm width and ~18 cm length, which is enough for both upward and horizontal segments of 5 cm respectively and the downward sections of at least 5 cm.

4.2. Introduction

Over the past 95 years, many studies have been performed to understand capillary action in complex porous materials in various fields expanding on the Lucas–Washburn equation, which is based on straight capillary channels with an infinite reservoir. However, there are only a few attempts to understand capillary action in the textile field, starting with plain woven fabrics [1, 2], which have a relatively simple structure compared to knitted fabrics that are usually worn close to the skin. Those previous studies have tried to separate in–plane wicking (lengthwise direction) from trans–planar liquid movement (through thickness direction –away from skin) on fabrics [64–67].

Liquid movement in fabrics is driven by capillary action, which is governed by substrate material, capillary channel structure, and liquid characteristics [34, 68]. While it is easy to calculate the rising height of capillary liquid through a single round straight capillary channel, understanding

liquid transport mechanisms of textiles is much more complicated as no such single round channels exist. Even within a single yarn within a fabric, the diameter of a single yarn and the direction of the capillary channels in a yarn keep changing due to yarn twist and fabric construction properties [69]. Many other factors, including void space between fibers and/or in-between yarns, twist level, tension and contact points with adjacent yarns, also affect wicking phenomena simultaneously. Therefore, a better understanding of wicking performance requires a comprehensive knowledge of fabrics: raw material property, fiber-, yarn-, and fabric-structure.

Even though understanding of textile wicking performance is very complicated, typical wicking performance test methods for textiles, including the Vertical Wicking of Textiles (AATCC 197 [70]), the Liquid Moisture Management Properties of Textile Fabrics (AATCC 195 [7]) and the Horizontal Wicking of Textiles (AATCC TM 198 [71]), assume an average material and simply neglect important structural factors (i.e. the details of yarn wicking). All current test methods do not represent human sweating on the skin, which exhibits continuous liquid flow from sweat pores (5–45 nl/min/gland [72]) because these methods are conducted with either infinite reservoirs or limited, but large amounts of liquid, which cannot be generated from a single sweat gland on short time scales (i.e. within minutes). Additionally, typical test methods cannot explain the wicking mechanisms based on within-a-yarn and yarn-to-yarn liquid movement since the large amount of liquid simply overwhelms - ‘floods’ - the fabric wicking phenomena in a split-second. When comparing fabrics’ wicking performance from those typical methods, sometimes the results were opposite between infinite reservoir test and limited amount of liquid test. Such inconclusive and even contradictory results have been discussed widely in industry, yet limited literature is available. The pilot data in our lab suggested that much of the detailed wicking

processes were not fully understood. Therefore, many steps still remain to find out how to improve wicking performance of textile substrates.

The concept of the current vertical wicking method was introduced over a century ago by Hall who, working as a physician, was interested in finding the best absorbency product from commercial surgical gauzes [73]. In his study, he measured the weight difference between a dry and wet gauze strip ($6 \times 0.5 \text{ inch}^2$). To make a strip wet, the double end of the gauze strip was immersed into infinite water, to the depth of one-quarter of an inch for 60 sec. In 2011, the exact same concept of the current wicking test was confirmed as the nonwoven standard method to evaluate absorbency of nonwoven substrates for wipes, diapers and feminine hygiene products (INDA NWSP 010.1.R0 (15) Nonwoven Absorption). The vertical wicking test method was originally made for fabric absorption and has been used in nonwoven field to evaluate how much liquid a nonwoven substrate may have absorbed from an infinite reservoir within a specified amount of time. Due to this background, it may be expected that the current vertical wicking test with infinite reservoir is an inappropriate test to investigate textile comfort on the assumption of human sweating circumstance because human sweat is a slow continuous flow (5–45 nl/min/gland [72]) generated by each of the sweat glands, unlike infinite reservoir. After five decades from Hall's study, the longitudinal and transverse wicking test was firstly used for textile comfort to examine the ability of wool fabrics' moisture transport in sweating circumstance [74]. In 2011, the vertical wicking method became the AATCC standard method TM 197 called Vertical Wicking of Textiles [70]. This wicking test of textiles has been most extensively used by industry as the typical wicking performance test method for textile comfort ever since.

Because a full understanding of fabric-level wicking should start with an understanding of wicking at the yarn-level, most previous yarn wicking performance studies in textile field have

been performed with a single yarn [30, 31, 33]. Those studies have explained the relationship between wicking length and yarn-level properties such as twist level and cross-sectional shape [30, 31, 33]. However, single-yarn wicking performance results cannot be applied to that of fabric-level because various factors are subject to change even in a single yarn: the diameter of a single yarn within the fabric [69], the twist level, the yarn tension and the contact points with adjacent yarns. For these reasons, in order to understand yarn-level wicking within a fabric structure, not only liquid movement within-a-yarn but also yarn-to-yarn transfer wicking should be considered. We postulate here that the liquid in a yarn spills over to the adjacent yarns through the contact points, resulting in fabric-level wicking based on yarn-level liquid movement. Although it still seems quite challenging to predict wicking performance of textiles in high detail, due to their complexity, understanding within-a-yarn and yarn-to-yarn wicking would be a key factor to predict liquid movement considering textile structures and materials.

In the study described below, we aimed to develop a better wicking measurement system, ‘*Single-pore Wicking Evolution Apparatus for Textiles (SWEAT)*’, to understand wicking mechanisms in textiles as well as to mimic realistic human sweating generated from a single sweat pore. With this new measurement system supplying continuous microfluidic flow, with a similar liquid flow rate to a single sweat pore of human body, we studied the liquid transport within-a-yarn and through yarn- on a scale that is realistic for human sweating. Also, we anticipated to measure directional wicking rate by individual yarn and wetting area changes over time. The wicking experimental results from the new measurement system should help to further understand the liquid movement mechanisms through textiles. A better understanding of fabric wicking mechanism should enable us to develop the optimized wicking performance fabrics with the ideal fiber- and yarn-level capillary channels.

4.3. Experimental Section

4.3.1. Fabric Substrates

Two types of commercial blended interlock knit fabrics were used as substrates: 1) cotton–polyethylene blended and 2) polyester–polyethylene blended as shown in Figure 4-1. Cotton yarn (dtex: 197 g/10 km), polyethylene yarn (dtex: 222 g/10 km, 80 filaments/yarn), and polyester yarn (dtex: 233 g/10 km, 68 filaments/yarn) were blended for these two interlock knit fabrics which resulted in 215 g/m² for the fabric weight for the cotton–polyethylene blended and 231 g/m² for the polyester–polyethylene blended fabric, respectively. To compare wicking performance in non-blended fabrics, a 100% cotton twill fabric (186 g/m², Style No. 494, Testfabrics Inc.) and a commercial 100% cotton interlock knit fabric (dtex: 148 g/10 km, Cotton Inc.) were used.

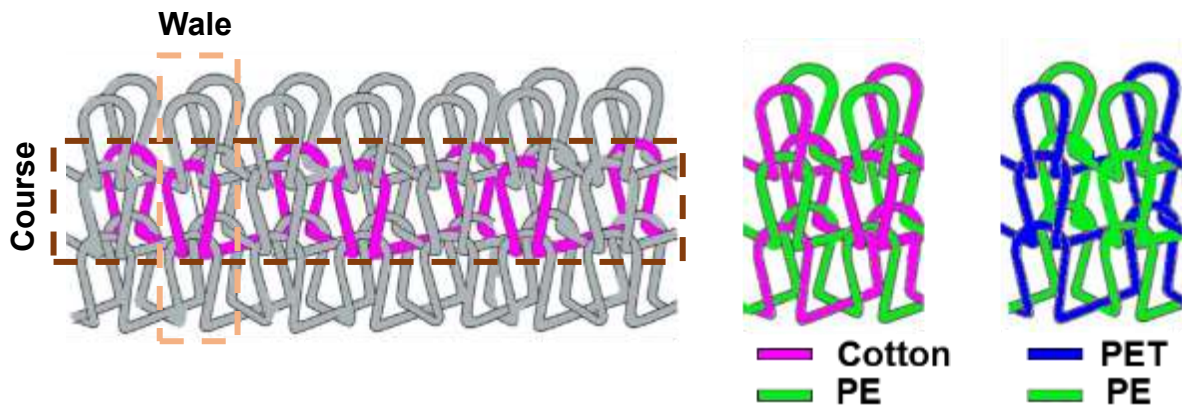


Figure 4-1. (a) Interlock knit structure with a single course yarn layout in magenta color, repeating unit of (b) the cotton and polyethylene blended, and (c) the polyester and polyethylene blended interlock knit.

4.3.2. Dye Solution for Wicking Length Indicator

Dye solutions were prepared for wicking performance indicator by dissolving brilliant blue G (BBG, $C_{47}H_{48}N_3NaO_7S_2$, pure, Sigma-Aldrich), brilliant blue R (BBR, $C_{45}H_{44}N_3NaO_7S_2$, pure, DyStar), and rose Bengal (RB, $C_{20}H_2Cl_4I_4Na_2O_5$, dye content 95%, Alfa Aesar) respectively in deionized water.

In order to indicate wicking distance of fabrics visually, three types of dye were used: two typical types of wicking indicator dyes, including brilliant blue G and R, and a water-soluble dye, called 'rose Bengal'. Since previous studies used 0.6wt% brilliant blue solution as a wicking performance indicator [75], we chose similar concentration levels for making dye solutions ranging from 0.2 wt% to 0.6wt%. Considering rose Bengal dye has 10wt% solubility in water, in this experiment, 0.2, 0.4, and 0.6wt% dye solutions were used after overnight stirring in order to make sure dye dissolved into water completely.

4.3.3. Vertical Wicking Test

According to the vertical wicking test (AATCC 197 [70]), wicking ability of a fabric strip was analyzed under $21 \pm 1^\circ C$ and $65 \pm 2\% RH$ condition. Each fabric was cut into 25 mm-wide and 250 mm-long strips and suspended vertically with the lower 5 mm of the specimen immersed into the infinite reservoir at the test starting time. The test method to investigate a fabric wicking performance allows for two different approaches, either how much time it takes for the liquid to reach a certain level or how far the height of the advancing liquid front travels as a function of time. In this study, the wicking length of liquid was recorded after 30 min of water spreading. Specimens were tested in both course and wale directions.

4.3.4. Droplet Wicking Test

We evaluated the Liquid Moisture Management Properties of Textile Fabrics (MMT, AATCC 195 [7]) method, which uses a pump to supply total 220 μl of multiple liquid droplets for 20 sec. The moisture management tester equipment produces 11 ± 1 droplets for 20 sec instead of continuous flow (i.e. a droplet volume of MMT is the range of 18.3– 22 μl). These multiple droplets are supplied to the fabric specimen with direct contact instead of allowing the droplets to fall onto the fabric. Because even a single droplet from the MMT test (i.e. 18.3-22 μl) still wicks in a short time, it is hard to investigate the wicking progress regarding how liquid moves through the textile substrate. For this reason, we decided to reduce the volume of a droplet down to 4 μl (~fifth part of a droplet volume of the MMT) in our experiment because we assumed the smaller volume might allow us to observe wicking phenomena more precisely than bigger volume. Furthermore, a 4 μl droplet, used for our modified version of the MMT test, has been used in many textile studies to investigate surface wettability for various substrates from hydrophilic to hydrophobic fabrics (i.e. contact angle) [76-78]. We made the droplet in contact with the surface of the fabric sample to simulate the typical test condition, and then analyzed wicking performance over time. This adapted MMT droplet wicking test was conducted at the controlled conditions at $21 \pm 1^\circ\text{C}$ and $85 \pm 5\% \text{RH}$ to prevent evaporation during the experiment process.

4.3.5. New Measurement System: Single-pore Wicking Evolution Apparatus for Textiles (SWEAT) Test

In order to mimic the human sweat phenomenon, a new measurement system was developed to investigate yarn-level wicking behavior within a fabric. Figure 4-2 shows a 10 μl glass syringe (Hamilton Company) and a 33-gauge needle with a customized needle tip (outer

diameter: 210 μm , inner diameter: 108 μm , Hamilton Company), which has a similar inner diameter to a sweat gland pore (inner diameter of eccrine sweat gland at the skin surface: 60–80 μm [79]). A micro syringe pump (Micro4, World Precision Instruments, Inc) was used to supply continuous nanoliter flow (50 nl/min). To simulate the sweat flow generated from a single sweat pore with a needle, a certain point in a single yarn within a fabric was picked with a needle. The microfluidic liquid was injected continuously through this single point. The needle was tilted approximately 1° to prevent it from touching a fabric except at the very tip (Figure 4-2). The experiment of the SWEAT test system was conducted at controlled conditions at $21 \pm 1^\circ\text{C}$ and $85 \pm 5\% \text{RH}$ to reduce evaporation during the experiment. Furthermore, the required space for the SWEAT test equipment setting ($40 \times 20 \times 30 \text{ cm}^3$) is small enough to fit into a glove box or bag to control humidity and temperature.

4.3.6. Wicking Performance Measurements

The wicking performance of the fabric samples was recorded as a video file using a microscope camera. Captured pictures were taken from video files (1, 30 sec, 1, 5, 10, 20, 40, and 120 min after wicking started). For the directional wicking length analysis from the captured pictures, ImageJ 1.51u (National Institute of Health) was used.

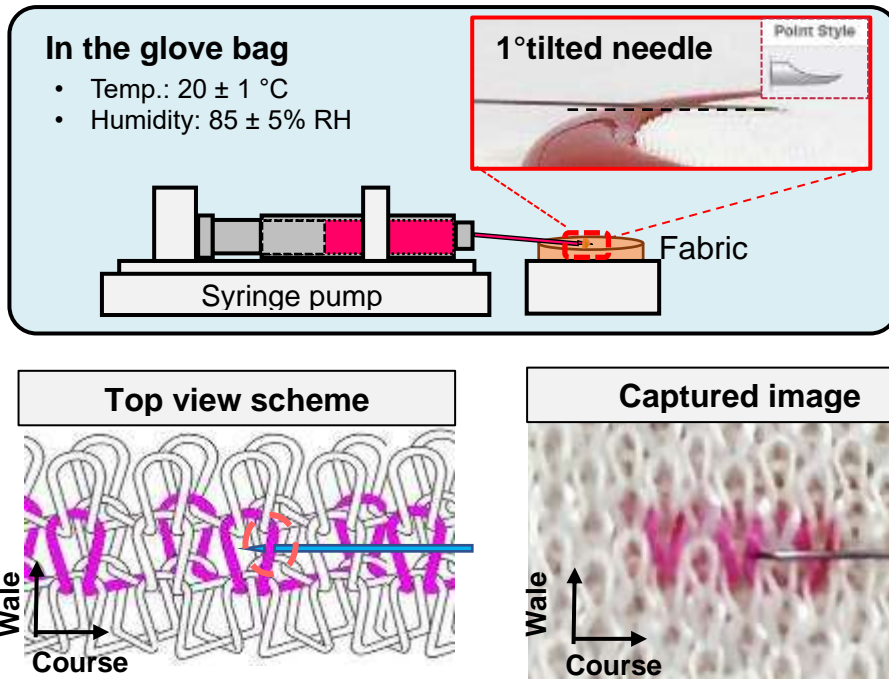


Figure 4-2. SWEAT test experimental setup with top view scheme and actual captured image.

4.4. Results and Discussions

The wicking behavior of a solid substrate is controlled by both the surface energy and the geometric surface of the capillary channel. To investigate wicking performance of a fabric substrate using an indicator dye solution the dye must not affect liquid movement in a fabric specimen. Before starting wicking tests, the dye solutions described in the Experimental Section were tested to determine an appropriate dye for textile wicking tests.

4.4.1. Preparation of Wicking Indicator with Dye Solution

The indicator dye solution for wicking performance must have good visibility, and the dye solution must have no or negligible affinity between liquid and a fabric. If an indicator solution has high affinity to a fabric, it could lead to erroneous wicking lengths. In addition, it could deplete the dye from the solution and separate from the water. Additionally, the dye solution should have a similar surface tension to human sweat because the wicking performance test in textiles is supposed to mimic realistic sweating.

To find an appropriate dye solution, three kinds of dyes, described in the Experimental Section, were compared: brilliant blue–R, –G, and rose Bengal. Even though typical dye solutions used for visual indicators in textiles are brilliant blue–R and –G, those dyes were found to lag behind the actual advancing water front after 3 h in a fabric strip test (Upward–horizontal–downward test (UHD) [63]). Because both typical dye solutions separated from deionized water, they were excluded from further consideration. However, the rose Bengal dye did not exhibit water–dye separation over a 4 h–long UHD wicking test. Since the rose Bengal dye has 10% solubility in water, 0.2, 0.4, and 0.6wt% dye concentrations in solution were prepared as previous studies used 0.6wt% brilliant blue solution as a wicking performance indicator [75]. After

overnight stirring, the rose Bengal dye solution was used to assure that the dye dissolved in water thoroughly. In terms of dye solution affinity with a fabric, Figure 3 shows that the wicking rate of the brilliant blue-R and -G showed slightly slower rates than that of deionized water. However, the wicking rate of the rose Bengal solution was within experimental error range of the deionized water rate. Thus, rose Bengal was used in the remainder of this study.

Electrolyte concentration in sweat depends on a variety of factors: exercise intensity, environmental condition, heat acclimation status, aerobic capacity, genetic predisposition, body size/composition, sex, diet and hydration status [56, 80]. Sweat composition also varies considerably even within and among individuals [81]. For these reasons, we tried to choose a solution which has the most similar level of surface tension to deionized water. Table 1 shows that the 0.6 wt% rose Bengal dye solution has a surface tension of 71.4 ± 0.3 mN/m, which is similar to that of distilled water (72.9 ± 0.2 mN/m). After comparison of different concentrations of the rose Bengal dye solution from 0.2 to 0.6 wt%, we found that the 0.6wt% rose Bengal solution had the same range of surface tension as 0.2 and 0.4 wt% solutions (surface tension of 0.2wt%: 71.6 ± 0.4 , 0.4wt%: 71.6 ± 0.7 mN/m). Moreover, the 0.6wt% solution had better color visibility than lower concentration solutions and a similar level to typical brilliant blue dye solutions shown in Figure 4-4. Based on affinity, surface tension and visibility comparison, the 0.6wt% rose Bengal dye solution was selected as our experimental wicking performance indicator.

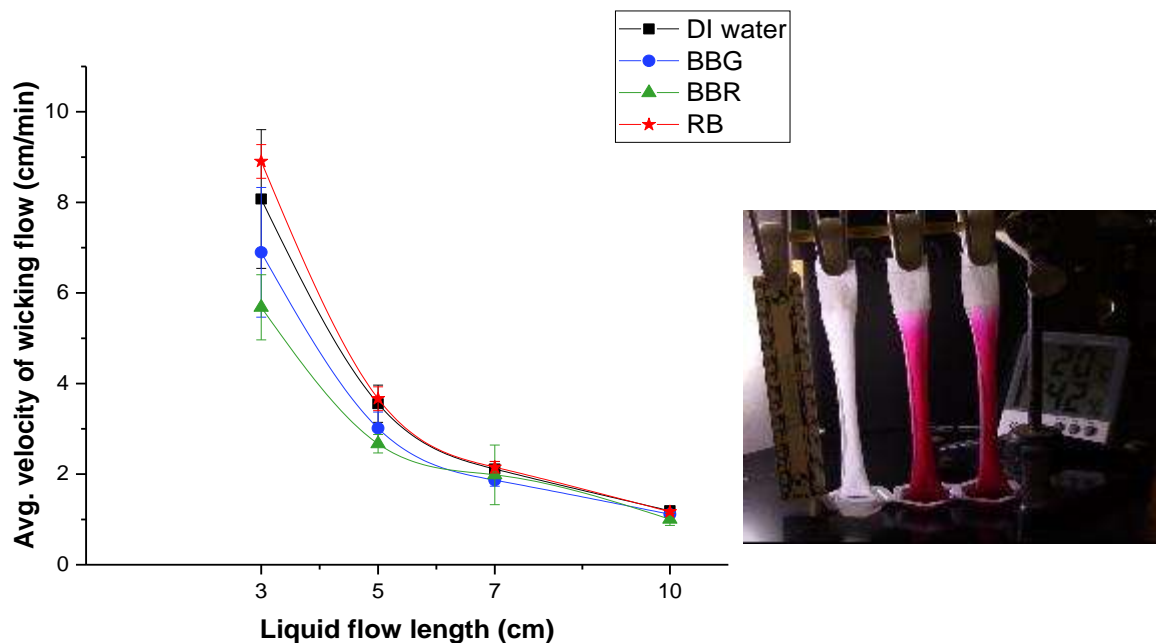


Figure 4-3. Affinity investigation through wicking flow rate comparison among deionized water (DI), 0.6 wt% dye solutions of rose Bengal dye, brilliant blue G (BBG), and brilliant blue R(BBR). The captured picture shows wicking rate comparison, from left, deionized water, and two of the rose Bengal dye solutions.

Table 4-2. Surface tension of dye indicator solutions including deionized water (DI), rose Bengal dye (0.2, 0.4 and 0.6 wt%), brilliant blue G (BBG), and brilliant blue R(BBR).







Surface Tension (mN/m)	DI water	Rose Bengal			BBG 0.6 wt%	BBR 0.6 wt%
		0.2 wt%	0.4 wt%	0.6 wt%		
Average	72.9	71.6	71.6	71.4	69.7	70.7
S.D.	0.2	0.4	0.7	0.3	2.1	0.8
						



Figure 4-4. Dye solution visibility on fabric substrates with 0.6 wt% of (a) rose Bengal, (b) brilliant blue G, and brilliant blue R.

4.4.2. Wicking Performance from Vertical Wicking Test

Vertical wicking test method is operated with a fabric strip, suspended vertically with one end dipped into an ‘infinite’ reservoir, and thus focuses on in-plane wicking performance. This vertical wicking measurement by the gravimetric technique has been widely used in the textile field, because it is easy to compare the wicking length and/or velocity among various fabrics with the results accumulated over many years.

However, as mentioned in the Introduction Section, because the current vertical wicking method was not originally designed to mimic human sweating, it has brought more issues. Figure 5 shows that this method cannot measure the exact front wicking length absorbed by the fabrics, because the wicking length is considerably different at each time, even within a single strip. Furthermore, color intensity was changed even in a single strip depending on different heights since the fabric strip absorbed various levels of saturation. The saturation levels decreased as the vertical distance traveled by liquid increased, as seen by the comparison of the color intensity inside of two circles with lower and higher spots in Figure 5. In the vertical wicking test, the wicking length from vertical wicking method is defined as the extent of wicking. However, the

results from the vertical wicking test have limited implication because it does not explain which factors affect wicking mechanism of a fabric considering fabric structure and yarn–level properties.

Because the experimental test results of the vertical wicking test cannot help to understand wicking phenomenon in textiles, many previous studies have attempted theoretical approaches through the Lucas–Washburn equation [48]. As mentioned in the Introduction Section, the Lucas–Washburn equation has been used to find the effective capillary radius, \bar{r} , based on the relationship between wicking length and time of a fabric strip ($h - t$) in the vertical wicking test from infinite reservoir [63, 82, 83]. However, this procedure is prone to criticism because the Lucas–Washburn equation has been applied to the penetration of liquid into the complex textile substrates by assuming fabrics consist of assemblies of straight cylindrical capillaries. For this reason, even though a single capillary radius, called the effective capillary radius, r , was calculated from the Lucas–Washburn, it cannot be interpreted as applying to an actual three dimensional structure of a fabric with two different levels of capillary sizes: in-between–yarns and in-between–fibers. In textiles, liquid goes within–a–yarn as well as yarn–to–yarn transferring, which causes differences in wicking behavior depending on the strip directions (warp/weft for woven or course/wale for knit) and the fabric structures, not in simple straight capillary channels.

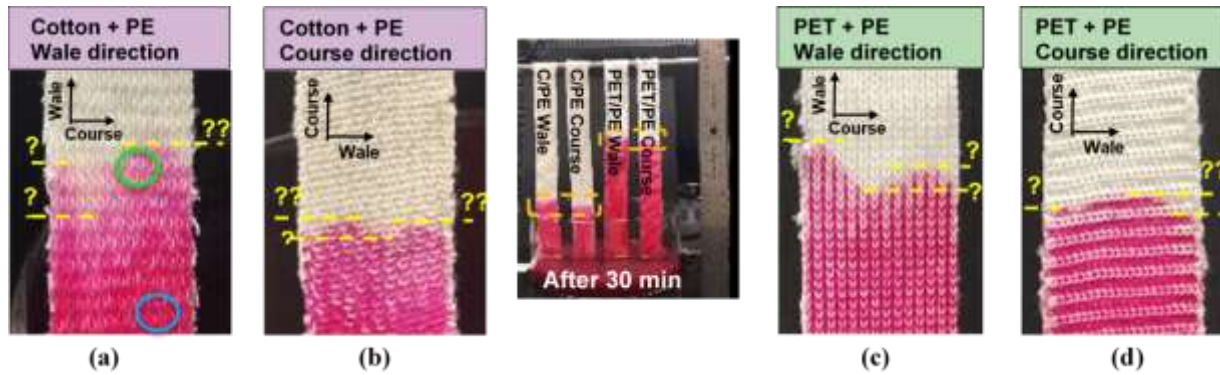


Figure 4-5. The variation of wicking length within a strip as well as the degree of saturation based on color intensity is shown for the vertical wicking test results on the interlock knit fabrics after 30 min: (a) the wale direction, (b) the course direction of cotton and polyethylene blended fabric, (c) the wale and (d) the course direction of the polyester and polyethylene blended fabric.

4.4.3. Wicking Performance from Droplet Wicking Test

Depending on the relative amount of liquid used and the nature of the liquid–fabric contact, the typical wicking performance test methods can be divided into two groups: wicking from an infinite liquid reservoir and wicking from a limited amount of liquid. Using a single droplet on a textile substrate is a common method for limited, but relatively large amounts of liquid when compared to a single sweat gland. When a drop of liquid is released onto a textile fabric, wetting starts on the surface of the porous medium [40]. Wetting is a prerequisite for wicking because a liquid cannot move through capillary channels without wetting [10]. After a liquid drop is placed on a fabric, the liquid drop fills large channels (openings) first, followed by wicking into relatively small channels (i.e. void space within a yarn). However, depending on droplet volume and substrate wettability, the flooding phenomenon can be investigated with or without the wicking stage. If the droplet cannot be absorbed by a substrate instantly, the remaining liquid floods on the

surface which does not proceed along capillary channels (at the initial stage as shown for hydrophilic yarn of the cotton–polyethylene blended fabric in Table 4-3).

The most popular standard method using a limited amount of liquid is AATCC TM 195 called the Liquid Moisture Management Properties of Textile Fabrics [7]. Even though this test method assumes that the wetting area from multiple droplets would make a perfect circular shape with the concentric sensor setting, Table 4-3 shows that the actual wetting area was not a round shape, and it was determined by the fabric structure and the yarn types. Additionally, comparing the supplied liquid amount of this test equipment to the human sweating circumstance (sweat flow rate: 5–45 nl/min/gland [18]), the condition of this typical test method is very far from realistic as it is not from flow and combines a wide range of sweat glands at a much faster flow than actual sweat rate (660000 nl/min/gland, shown in Table 4-4).

Another critical issue about the droplet wicking test is that the wetting area depends on where the droplet was placed on a fabric. Despite being the same fabric, wicking performance may change considerably depending on the initial contacting location (i.e. droplet falls into void space in-between yarns or onto a hydrophobic/hydrophilic yarn). Table 4-3 shows that while a droplet placed on hydrophilic yarn wicked through instantly, that on hydrophobic yarn just sat on the same spot without wicking even in the identical fabric, for the cotton–polyethylene blended fabric. For this reason, each selection of the contacting spot on fabrics may lead to different test results especially for blended fabrics.

In some test methods, instead of placing a liquid droplet directly on a specimen, the liquid is dropped from above a fabric substrate, such as in the adjusted test method of AATCC TM 198 called Horizontal Wicking of Textiles [71]. Depending on the dropping height and the volume, various factors were affected: impact time and position, contact line edge position, wetted length

on the impact surface and drop apex height, which resulted in changes of wicking behavior [84]. Table 5 shows that the size of the wetting area changed depending on various droplet volumes on the 100% cotton fabric (1.5, 2, 3 and 4 μl).

In terms of the droplet wicking analysis, generally, the wetting area and the wicking rate are measured. Most common methods are to measure the wetting area manually (i.e. by drawing the edge line of wetting area) or using image processing software. The more advanced imaging techniques enables us to extract information easily and automatically by counting pixels on the edge-enhanced image [36]. However, because wicking from a droplet happens in a minute and starts from more than one single yarn simultaneously, it is almost impossible to observe the liquid movement within-a-yarn and yarn-to-yarn transferring accurately with the current methods. Although the droplet wicking test is a more relevant method to realistic human sweating than the vertical wicking from an infinite reservoir, still the wicking test with a droplet could not explain how to improve wicking performance of fabrics on the basis of fabric structure and yarn properties. Furthermore, as long as typical wicking methods use infinite reservoir or limited, but large amounts of liquid, any of these test methods cannot be expected to simulate human sweating.

Table 4-3. Wicking performance comparison from dropping liquid (4 μ l) on the cotton–polyethylene, and the polyester–polyethylene blended interlock fabrics by picking hydrophilic or hydrophobic yarns independently.

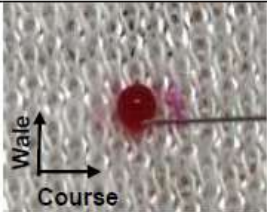
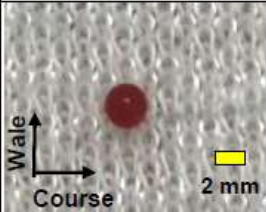
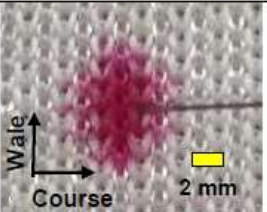
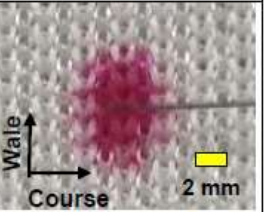
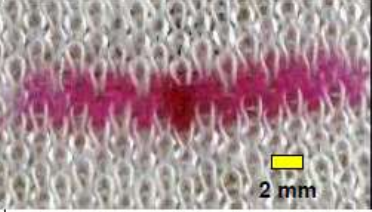
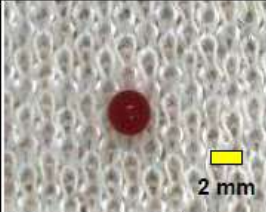
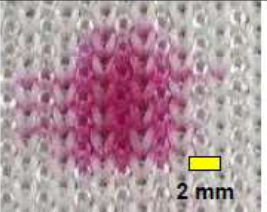
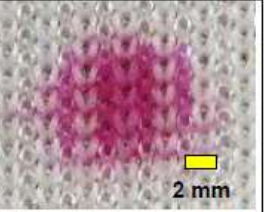
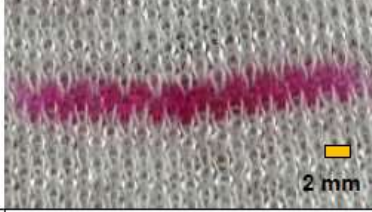
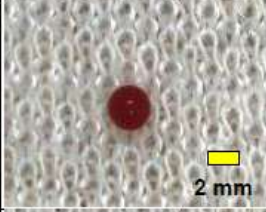
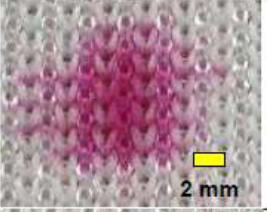
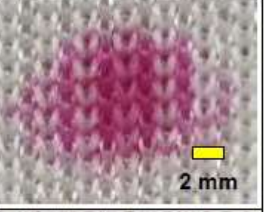
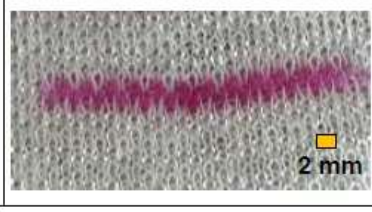
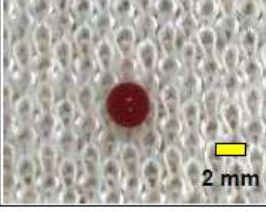
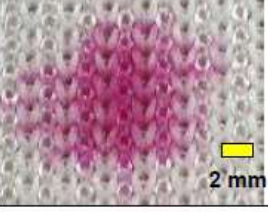
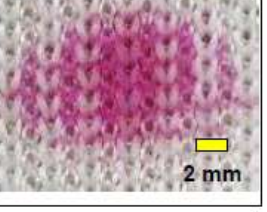
Picked yarn type	Cotton and polyethylene blended		Polyester and polyethylene blended	
	Hydrophilic yarn	Hydrophobic yarn	Hydrophilic yarn	Hydrophobic yarn
1 sec				
30 sec				
60 sec				
300 sec				

Table 4-4. Characteristic comparison between human sweat gland pore and testing methods, including the vertical wicking test (AATCC 197), the moisture management test (MMT, AATCC 195) and the SWEAT (Single-pore Wicking Evolution Apparatus for Textiles) test with a needle.

		Diameter		Flow rate	Wicking rate comparison[†]
<i>Sweat gland pore</i>		60–80 μm [79]		5 –45 nanoliter/min [72]	
<i>Typical test method</i>	<i>Vertical Wicking</i>			Infinite reservoir	2.2 mm/sec (20 mm/ 9.16 sec)
	<i>MMT</i>			660000 nanoliter/min (220 μl / 20 sec)	Top: 7.7 mm/sec Bottom: 7.6 mm/sec
<i>SWEAT test</i>	33 gauge needle	Outer	Inner	50 nanoliter/min	Avg ^{††} 0.16 mm/sec (4.0 mm/24 sec)
		210μm	108 μm		

[†] Results from multifilament polyester interlock knit fabric.

^{††} Average value from all four directions.

4.4.4. Wicking Performance of New Measurement System, SWEAT Test (Single-pore Wicking Evolution Apparatus for Textiles)

Table 4-5 shows that when a continuous microfluidic flow (50 nl/min) was supplied to a single point of a specific course yarn within the knit fabric, the flow progressed by wicking along yarns. Liquid movement within-a-yarn as well as yarn-to-yarn transfer was observed, which had not yet been described in the textile literature. In fact, despite having identical substrates, comparing Table 4-5 to Table 4-3 and Figure 4-5, it is obvious that the wicking performance of the fabric specimens is highly influenced by the specific wicking test method chosen, especially depending on how the liquid is supplied to a fabric specimen. The yarn-level liquid movement within a fabric was investigated by the SWEAT test for the first-time.

The purpose of current wicking test methods is to evaluate liquid transport properties in fabrics. However, it is almost impossible to understand yarn wicking performance through those

methods as they force the wicking to happen from an infinite reservoir or even a droplet that is much larger than a single yarn. Thus, yarn-level liquid movement within a fabric (i.e. how liquid moves along a yarn and transfers to other yarns) cannot be explained. In other words, without understanding of wicking mechanism thoroughly, we cannot develop a better wicking performance substrate or control liquid movement in textiles. Furthermore, typical test methods do not represent realistic human sweating conditions, because in reality liquid sweat generated from each single gland is a continuous microfluidic flow instead of infinite reservoir or limited but large amount of liquid such as droplet which are used for all current test methods.

Table 4-5 shows that depending on the property of the yarn picked by the needle, different shapes of the wicking area were observed, within identical substrates. For example, when the flow was supplied to a hydrophilic yarn of the polyester–polyethylene blended fabric, every other yarn-column became wet because the liquid flow went along hydrophilic yarns only (the polyester–polyethylene structure is shown in Figure 4-7b). However, the liquid flow, starting from a hydrophobic yarn, passed along both hydrophilic and hydrophobic yarns, possibly because the resistance to flow within hydrophilic yarns was bigger than the required pressure for transferring to other yarns.

With the SWEAT test, the wicking rate of each course yarn can be investigated individually because the fabric wicking performance was recorded as a video file. Figure 4-6 shows how the wetting area expanded in all directions in the droplet wicking method (e.g. MMT) and the SWEAT test, respectively. While the larger droplet in the MMT method spreads very rapidly initially, the continuous flow from the SWEAT system exhibits a more gradual growth, with different wetting areas at the same final volume. Compared to the total liquid volume used in MMT (i.e. 220 μl), a 4 μl droplet used in this study is 55 times smaller. However, it is still hard to

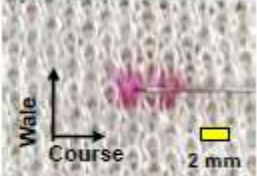
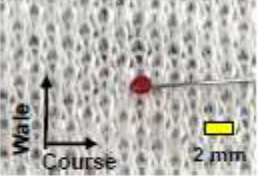
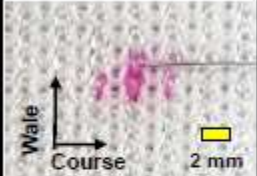

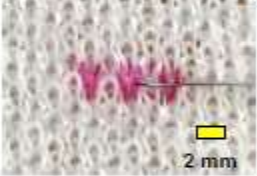
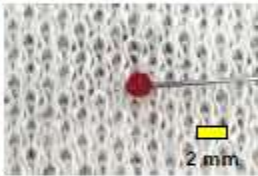
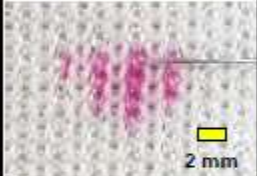
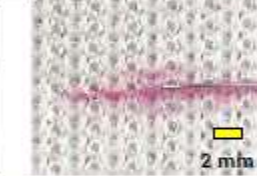
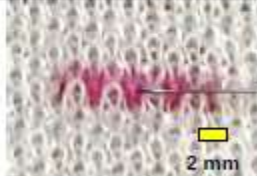

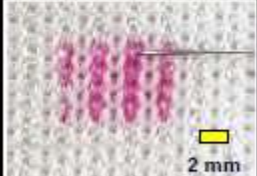

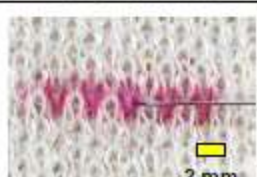
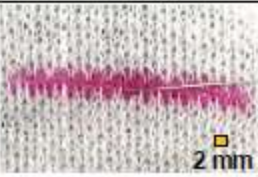
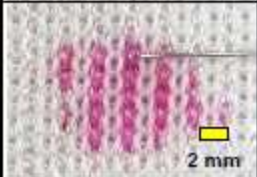
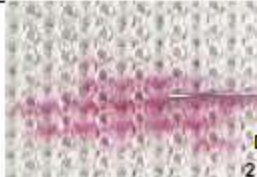
investigate liquid transport within-yarn and yarn-to-yarn transfer wicking because the fabric wicking, even from these small droplets, is still extremely fast and sometimes flooding occurs, resulting in discernible spreading across yarns. Figure 4-6 shows that with the 4 μ l droplet wicking method on the polyester–polyethylene blended interlock fabrics, the liquid reached the maximum wicking length after ~5 min (the wicking length of the course direction: 6.6 mm, for the wale direction: 4.4 mm), whereas the 50 nl flow from the SWEAT test took 80 min to arrive at the same level for all directions (Table 4-3 and 4-5). With this SWEAT test, the speed that the liquid moves along an individual course yarn and when liquid transfers to adjacent yarns can be analyzed as the liquid moves along yarns. For this reason, this SWEAT test seems more appropriate to explain wicking mechanisms of yarns within a fabric for both in–plane wicking as well as trans–planar liquid movement. Eventually, this methodology would facilitate development of an empirical model on how liquid moves through a yarn and transfers to adjacent yarns. Wicking mechanisms in textiles could thus be studied and controlled under conditions that closely resemble physiological conditions and further investigate how these realistic wicking processes may affect human thermal and tactile comfort.

Moreover, the SWEAT method avoided the flooding stage by controlling flow rate and choosing a similar diameter of liquid source to human sweat gland pore size. Supplying liquid to the hydrophilic yarn of the cotton–polyethylene blended fabric, compared to Table 4-3, Table 4-5 showed that all liquid flow was taken into the fabric specimen without flooding. Based on recorded wicking videos, liquid transport phenomenon of fabrics can be analyzed for quantitative measurement, and the level of saturation of substrates can be investigated based on the color intensity. Table 4-6 shows that the wicking performance on the 100% cotton twill and interlock knit fabrics with the SWEAT test and the droplet wicking test, individually. Even though the liquid

amount used for both tests was identical, wicking performance varies depending on the test method. The color of wetting area from the SWEAT test is much darker than the center color from the droplet test, while the size of wetting area from the SWEAT is smaller. Generally, the saturation of a substrate is determined by comparing the corresponding volume of the liquid amount to the expected void volume of the substrate [46]. Table 4-6 shows the saturation level of the droplet test is lower than the SWEAT test and is less than 100% because only the smallest pores can be completely saturated while the larger pores have not filled yet. For the droplet wicking test, the color around edge of the wetting area is lighter than the center at an early stage but it has slowly evened out as time passed.

With this SWEAT test method, the directional wicking rate and the individual yarn wicking performance of the knit fabrics could be determined (Figure 4-6 and 4-7). Figure 7(b) shows that 'C(0)', denotes the yarn that is picked by the needle of SWEAT system and provided with continuous liquid flow. 'C(1)' is the closest adjacent yarn to C(0) and an ordinal number keeps increasing in this way. Figure 4-7 (a) shows that the individual yarn's wicking performance did not follow the Lucas-Washburn law (eq 18) because the slope value was not constant when wicking length was plotted versus the square root of time. According to these experiments, with liquid movement along individual yarns under realistic human sweating circumstance, wicking performance should be understood as how liquid moves within a yarn and transfers to adjacent yarns. A better understanding of wicking performance with this SWEAT test method promises to provide a predictive model of wicking performance fabrics and should result in contributions to the textile industry to improve wicking in products, including sportswear, military apparel and textile printing.

Table 4-5. Wicking performance comparison from the SWEAT (flow rate: 50 nanoliter/min) on the cotton–polyethylene, and the polyester–polyethylene blended interlock fabrics by picking hydrophilic or hydrophobic yarns independently.

Picked yarn type	Cotton and polyethylene blended		Polyester and polyethylene blended	
	Hydrophilic yarn	Hydrophobic yarn	Hydrophilic yarn	Hydrophobic yarn
10 min				
20 min				
40 min				
80 min				

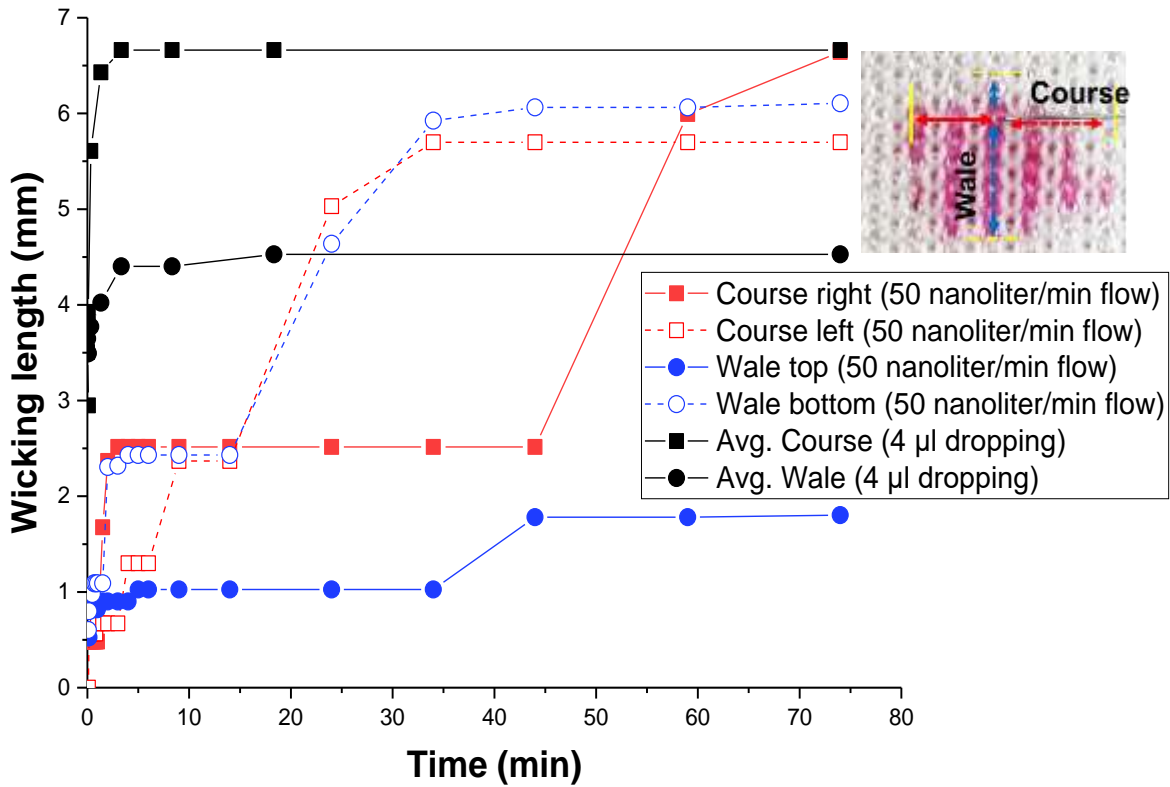


Figure 4-6. Wicking rate comparison of between the SWEAT test (50 nanoliter/min) and the droplet wicking (4 μ l) on the polyester–polyethylene blended interlock fabric. Wicking rate of the SWEAT test is obtained from four directions with the needle’s hole as a center (in the inserted picture on the top right) when a hydrophilic yarn picked from the polyester–polyethylene blended interlock fabric: course direction–right (red solid line) and –left (red dotted line), and wale direction– top (blue solid line), –bottom (blue dotted line). Wicking rate of dropping method is determined by the average rate of course direction and wale direction, respectively.

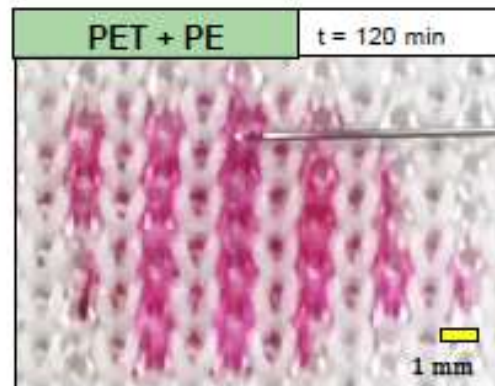
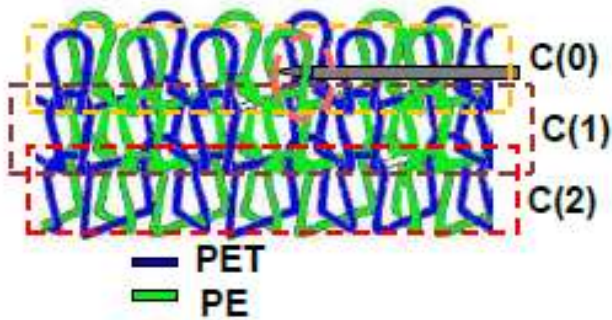
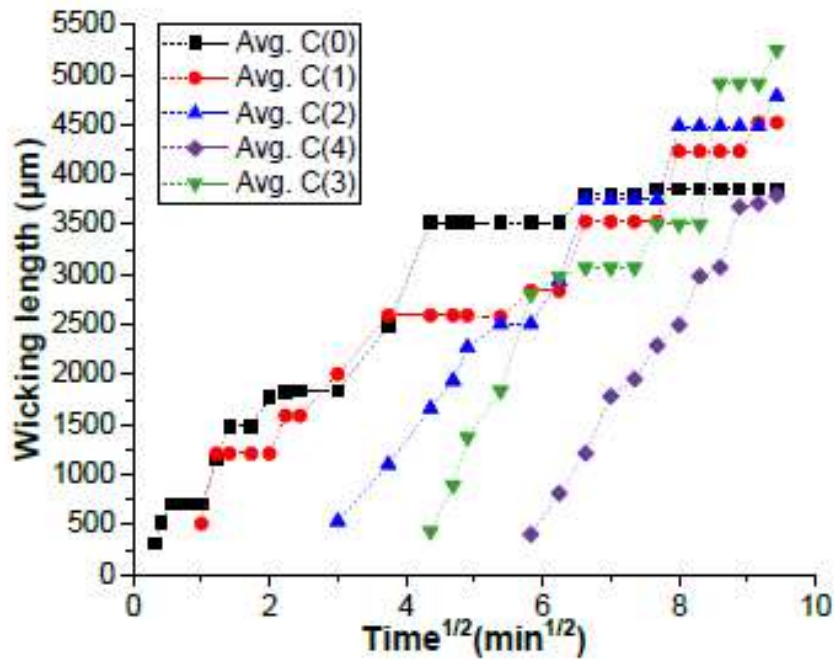
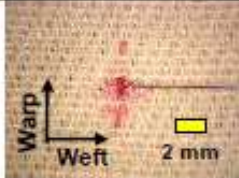
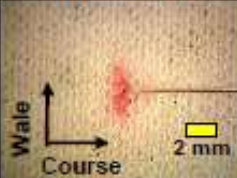

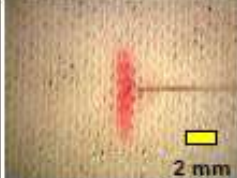

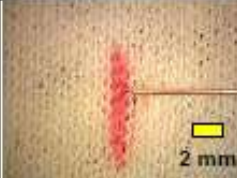
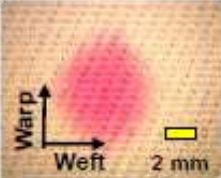


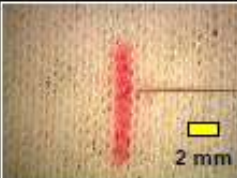
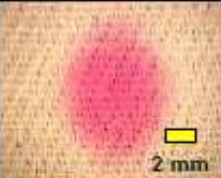

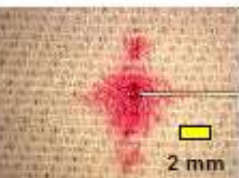
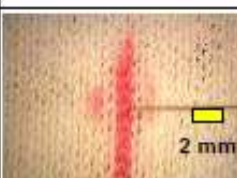
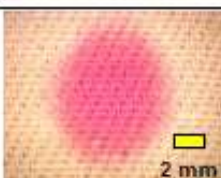







Figure 4-7. (a) Individual yarn wicking performance within the polyester–polyethylene blended interlock fabric with the continuous flow rate through the SWEAT test (50 nanoliter/min) with the square root of time. (b) In the schematic of the interlock knit structure, ‘C(0)’ denotes the yarn picked by the needle of SWEAT system, and ‘C(1)’ is the closest adjacent yarn to C(0). After 120 min, the result of wicking performance is shown in (c).

Table 4-6. Wicking performance comparison between the SWEAT test (flow rate: 50 nanoliter/min) and the droplet wicking test (1.5, 2, 3, and 4 μ l). [†] Picture was taken after 5 min.

SWEAT test			Droplet wicking test [†]		
	100% Cotton twill	100% Cotton interlock knit		100% Cotton twill	100% Cotton interlock knit
10 min					
20 min					
30 min (1.5 μ l)			1.5 μ l		
40 min (2 μ l)			2 μ l		
60 min (3 μ l)			3 μ l		
80 min (4 μ l)			4 μ l		

4.5. Conclusions

An ideal wicking performance test for textile comfort is supposed to mimic the realistic human sweating circumstance by continuous microfluidic flow generated from sweat glands. Wicking performance is composed of two criteria: liquid movement within-a-yarn and yarn-to-yarn transferring within a fabric which result in liquid sweat transport from each sweat gland pore through textile substrates. In order to simulate human sweating generated from a single sweat gland, the SWEAT test was developed with a constant microfluidic flow of 50 nl/min, similar to sweat flow rate from a single sweat gland. A 0.6wt% of rose Bengal dye solution was chosen as a wicking performance indicator, based on surface tension and affinity between a fabric and dye solution. When the liquid flow was supplied to a single point of a course yarn within the interlock knit fabric through the SWEAT test, liquid movement could be observed within-a-yarn and yarn-to-yarn transfer wicking, which had not yet been observed by other typical measurement methods. If we can understand wicking mechanism principle based on within-a-yarn and yarn-to-yarn transferring, that means we could control liquid transport in textiles as well as develop a better wicking performance textile. Additionally, this SWEAT test method avoided the unrealistic flooding liquid stage by controlling flow rate and choosing a similar diameter of liquid source to sweat gland pore size. Without this flooding effect, it allows us to investigate individual yarn wicking performance since in terms of the SWEAT test liquid movement along capillary channels in textiles is fully derived from a continuous liquid flow.

It is also important to note that the wicking performance results from the vertical wicking and the droplet wicking methods (i.e. AATCC 195 [7] and AATCC 197 [70]) in common use today, are inappropriate to determine physiological responses of fabrics to local sweating. To develop an empirical model to explain wicking mechanism in textiles in response to human

sweating, the SWEAT test presented here seems much more appropriate and should be evaluated further.

CHAPTER 5. Time-wicking Length Superposition for Textiles

5.1. Abstract

In order to mimic realistic human sweating, a continuous microfluidic flow is supplied to only a single yarn at a single point within the fabric substrate at similar flow rates to a single sweat gland. This new test method, which we refer to as ‘Single-pore Wicking Evolution Apparatus for Textiles (SWEAT) test, allows us to investigate yarn-level wicking performance within a fabric because liquid moves along yarns and transfers to adjacent yarns in a fabric state instead of making a circular wetting area. Here, we conducted the SWEAT test on knit fabrics characterized by different yarn properties (i.e. textured yarn and flat filament yarn) and knit structures such as single jersey and interlock knit. While fabric wicking performance of the textured yarn occurs randomly and is unpredictable, a fabric with the flat yarns shows the same wicking length (l) for each individual yarn as a function of time (t). These results validate that time-wicking superposition principle could be applied to the liquid movement of each individual yarn within a knit fabric: liquid wicks within a single yarn initially, subsequently it spills over to adjacent yarns through contact points, but the wicking rate in adjacent yarns is identical to the initial course yarn, providing that the relationship between wicking length and time is derived from intrinsic characteristics of yarn properties and textile structures. Moreover, the wicking rate of individual yarn do not follow the Lucas-Washburn equation where the wicking height is proportional to the square root of time because the wicking rate of an individual yarn has stopped when liquid transfers to adjacent yarns. These results indicate that the SWEAT test could be used to predict wicking rate and eventually to control liquid movement in complex porous media.

5.2. Introduction

Understanding of liquid transport in textile substrates is important not only for textile comfort but also many applications in various fields, including the life science industries for pharmaceuticals and biomedicine (such as drug delivery and detection) and wearable devices [85-87]. Over the past 30 years, a number of studies in the textile field have been performed to investigate the single yarn wicking performance from an infinite reservoir. These studies have tried to understand the relationship between wicking performance of a single yarn and various yarn properties such as twist level and cross-sectional shapes, because an understanding of yarn-level wicking should be easier than that of fabric [30, 31, 33]. These studies found that the yarn-level characteristics of a single yarn would affect wicking length. However, we found that we could not apply the yarn-level wicking result to the fabric-level wicking performance because there is a big gap between a single yarn (thread) itself versus the yarn within a fabric. In a fabric, various yarn features, including diameter, twist level, tension and contact points with adjacent yarns, are subject to change constantly depending on each location on the yarn and on the fabric structure (i.e. knit and woven).

For fibrous material such as knit and woven fabrics, main factors of wicking performance are substrate material and capillary channel structure. While most of the studies have been done based on a straight channel with a fixed radius, textile substrates have two different levels of void space size: 1) microscale for the void space in-between fibers within a yarn and 2) mesoscale for the space in-between yarns. In addition, the void size distribution within a yarn is broad and changes constantly along the yarn's length.

In the study described below, we aimed to investigate wicking performance of fabric substrates based on the yarn-level liquid transport within a fabric through a new wicking

measurement system, ‘*Single-pore Wicking Evolution Apparatus for Textiles (SWEAT)*’. By supplying continuous microfluidic flow to a single point of a certain yarn within a fabric substrate, we could examine the liquid transport within-a-yarn and yarn-to-yarn transfer wicking in realistic human sweating circumstances. If we can find a certain principle which can explain the wicking behavior of fabrics with complicated capillary channels, we might anticipate wicking performance and establish a predictive model, which should result in a large contribution to many industrial fields especially textiles, nonwovens, and printing on those substrates.

5.3. Experimental Section

5.3.1. Fabric Substrates

EASTMAN flat filament polyester yarn (84 denier or 9.3×10^{-3} g/m, 220 filaments/yarn) were knitted to make a single jersey knit and an interlock knit (fabric weight: 139.7 g/m², 42 yarns/inch in course and 43 yarns/inch in wale direction) at EASTMAN Chemical Company (Kingsport, TN) (Figure 5-1 (a – c)). Commercially available textured polyester yarns (70 denier or 7.8×10^{-3} g/m, 72 filaments/yarn) were obtained and knitted for a single jersey knit and an interlock knit (fabric weight: 122.5 g/m², 46 yarns/inch in course and 42 yarns/inch in wale direction) at the Knitting Lab of EASTMAN Chemical Company (Kingsport, TN) (Figure 5-1 (d – f)). All fabric was treated with a commercial wicking agent of Feran ICE (Rudolf Group, Germany) to improve moisture management properties. The creation of homogeneous fabrics with well-controlled yarn tension is critical for the reproducibility of the experiments reported in this paper.

According to our previous study, 0.6 wt% rose Bengal dye (RB, C₂₀H₂Cl₄I₄Na₂O₅, dye content 95%, Alfa Aesar) was dissolved in deionized water with stirring overnight and used in

these experiments for wicking performance indicator (solution surface tension $\gamma = 71.4 \pm 0.3$ mN/m).

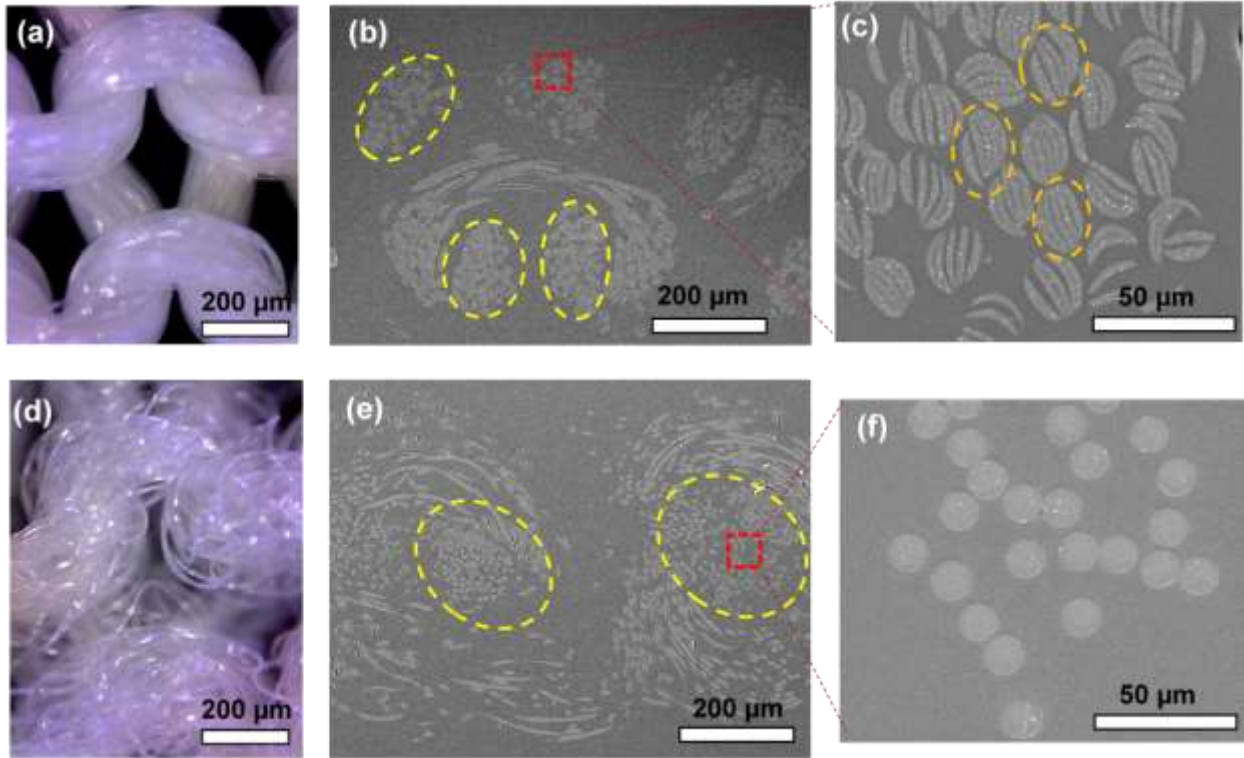


Figure 5-1. EASTMAN flat filament polyester yarns were knitted for a single jersey knit for (a) top view from microscope, and (b) SEM image of the cross-section of course direction in the interlock knit fabric. Yellow circle in (b) and (e) displays individual yarn within a fabric. EASTMAN flat filament yarn has (c) a unique cross-sectional shape of EASTMAN flat filament yarn with 220 filaments per this yarn consist of 44 subunits (orange circle) with 5 filaments. Commercial textured polyester yarn was knitted for a single jersey knit for (d) top view and (e) SEM image of the cross-section of course direction in the interlock fabric. A commercial polyester fabric has (f) the circular shaped filaments.

5.3.2. Upward–horizontal–downward Wicking Test

In order to investigate wicking performance of fabric–level, the upward–horizontal–downward (UHD) wicking test was conducted with infinite reservoir based on the method of previous researches.[63, 88, 89] Fabric strips of 2.5 cm width and ~18 cm length, were sufficient for both upward (h) and horizontal segments (H_L) of 5 cm respectively and the downward sections (D_L) of at least 5 cm. The fabric strips were carefully cut with long axes parallel to courses and wales separately. An apparatus was constructed using metal laboratory rods to conduct the UHD wicking test on these fabric strips according to the schematic shown in Figure 4-2. The framework to support the fabric strip was constructed for the accurate length of each direction. The fabric strip was positioned on the framework and both ends of the fabric strip were clipped onto a rod suspended into the reservoir at the position that kept the fabric end immersed into infinite reservoir without touching the reservoir container. A small load was placed at other end of strip to keep it taut for all three segments. For our experiment, we used a 0.4 g plastic clip placed on each side of the fabric because the plastic had no effect on liquid transport through the fabric strip. It is important that the small load should not affect textile structure especially for knit fabrics to prevent altering the wicking performance of the stretched fabrics due to changes of the void spaces in–between yarns/ fibers and the yarn tension. The laboratory rods at both ends of horizontal segment of 5 cm supported a wet fabric strip during wicking progressed by preventing drooping of the fabric sample. One end of fabric close to infinite reservoir is submerged at the start of a wicking experiment. Three video cameras recorded wicking performance to face the fabric strip from all three directions. The entire setup for the UHD wicking test was placed in a laboratory glove box to protect the fabric strip from air currents, and to control temperature as well as humidity (21 ± 1 °C, 90 ± 5 %RH) to reduce evaporation during wicking performance experiment.

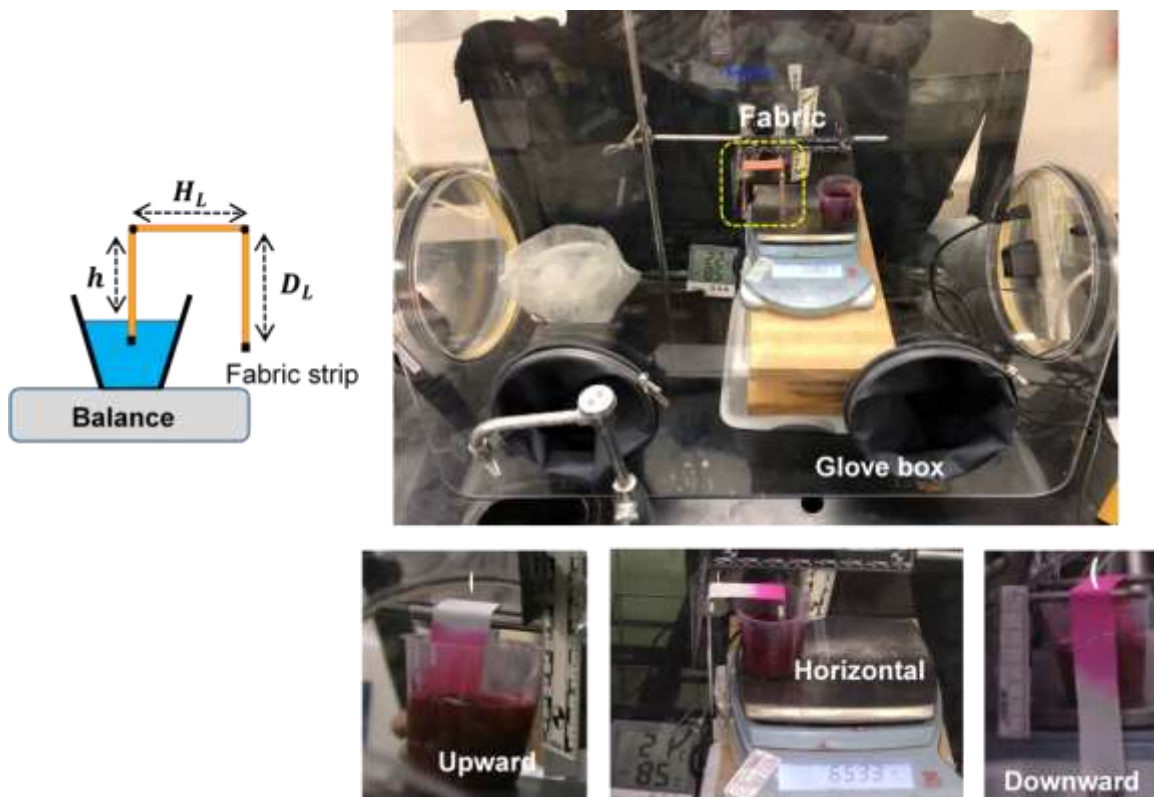


Figure 5-2. (a) Schematic of Upward–horizontal–downward (UHD) wicking test. From (b) the actual UHD wicking test setup in a glove box, wicking performance of a fabric strip is recorded from three video cameras for the views of (ci) upward (h), (cii) horizontal (H_L), and (ciii) downward (D_L) segment, respectively.

5.3.3. Droplet Wicking Test

In the droplet test, a small square fabric sample (10 cm × 10 cm) was placed on an embroidery hoop ring (inner diameter: 6 cm) without tension and secured to the hoop with rubber ring. A 1 μ l droplet of 0.6 wt% rose Bengal dye solution was placed on the fabric surface at the identical spot with the SWEAT test to compare wicking performance between two test methods. By using a 10 μ l glass syringe (Hamilton Company), a droplet directly contacted a substrate surface to prevent dropping effect derived from the dropping height. Rose Bengal dye solution was

used to increase the contrast between wetted and dried fabric for image analysis purposes. From the previous study, we found a 0.6 wt% rose Bengal dye solution does not affect the water wicking performances on fabrics based on surface tension and affinity between a fabric and dye solution.

Droplet wicking tests were recorded as a video from the top view to visualize fluid flow paths using Mighty scope 5M digital microscope (Aven Inc.; Ann Arbor, MI) with eScope software (Tektronix, Inc.; Beaverton, OR). Firstly, a ruler was placed on a fabric along the course direction of a substrate for the calibration during wicking performance analysis, and it was removed before starting wicking test. The captured images from the recorded video files were analyzed with ImageJ 1.51u software (National Institute of Health; Rockville, MD) to determine the wicking length for both course and wale directions as a function of time. The wicking length from the liquid droplet was calculated to obtain the average value for each direction, assuming that the fabric would have homogeneous structure for the upper and lower sides for course direction, and for the left and right side for wale direction. This droplet wicking test was conducted inside of a globe bag to control conditions for 21 ± 1 °C and 90 ± 5 %RH to reduce evaporation during the experiment process.

5.3.4. Single-pore Wicking Evolution Apparatus for Textiles (SWEAT) test

Single-pore Wicking Evolution Apparatus for Textiles (SWEAT) test has been developed to simulate realistic human sweating generated from each sweat gland pore by using a 10 μ l glass syringe (Hamilton Company) and a 33-gauge needle with a customized cut needle tip to hold a yarn. The SWEAT test allows us to investigate yarn-level wicking performance within a fabric by picking a certain point in a single yarn within a fabric with a needle. The dimension of needle (outer diameter: 210 μ m, inner diameter: 108 μ m, Hamilton Company) was chosen to have a

similar inner diameter to sweat gland pore (inner diameter of eccrine sweat gland at the skin surface: 60–80 μm).[79] In order to supply a continuous nanoliter–level flow (50 nl/min) to a certain point of a picked yarn, a micro syringe pump (Micro4, World Precision Instruments, Inc) was used. The needle was placed to be parallel to course direction in order to pick a yarn within a fabric substrate and tilted approximately 1° to prevent it from touching a fabric except at the very tip to inject liquid. The SWEAT test system was placed inside of a glove bag made of a clear film to control temperature and humidity for the specified condition to reduce evaporation during experiment: $21 \pm 1^\circ\text{C}$ and $90 \pm 5\% \text{RH}$.

5.4. Results and Discussion

Polyethylene terephthalate ($(\text{C}_{10}\text{H}_8\text{O}_4)_n$, PET), commonly known as polyester, is one of the most popular textile materials because it has excellent mechanical properties for apparel such as high tenacity, wrinkle free characteristics, and considerable durability for wash and wear [90]. However, because polyester fabrics have poor wicking performance, it is critical for apparel materials to improve their moisture management properties. Thus, after wicking agent treatment, polyester has been widely used for performance athletic apparel.

In this study, wicking performance of polyester knit fabrics with two different yarn types, including flat multifilament yarn and textured yarn, were compared according to three wicking test methods: 1) UHD test with infinite reservoir, 2) droplet wicking test with limited amount of liquid, and 3) SWEAT test through continuous microfluidic flow.

The wicking performance from the UHD wicking test shows that liquid moves faster on the commercial polyester interlock fabric rather than the EASTMAN interlock fabric (Table 4-1 and 5-1). In terms of the UHD test, a commercial polyester fabric takes ~ 15 min to reach the

downward segment (i.e. 13 – 14 cm section from the surface of infinite reservoir), while the EASTMAN fabric requires ~100 min to arrive at the same distance. Because the commercial polyester fabric consists of textured yarns, this commercial fabric has larger and randomly oriented void spaces in-between fibers compared to EASTMAN flat yarn (Top view comparison: Figure 5-1a vs. d, and cross-sectional view comparison: Figure 5-1b vs. e). When one end of a fabric strip was immersed into infinite reservoir, capillary channels with big radius keep taking liquid from infinite reservoir and then, redistributing towards adjacent capillary channels. For this reason, a substrate with bigger channels could wick faster than a substrate with smaller channels when unlimited liquid is supplied to a wide area covering many void channels simultaneously.

Table 5-1. Wicking length comparison over time from the Upward-horizontal-downward wicking test on polyester interlock knit fabrics, including the EASTMAN flat yarn fabric and a commercial textured yarn fabric for 7, 15, 30, and 100 min (unit: cm, [the range] : the range of wicking length of ≥ 4 times repeated tests at the certain time).

Time Substrate	7 min	15 min	30 min	100 min
EASTMAN fabric	5.3 [4.8– 5.6]	6.7 [6.0– 7.3]	8.7 [7.8– 9.2]	13.3 [12.7– 13.6]
Commercial PET fabric	9.7 [9.4– 10.2]	13.5 [13.3–14.1]	15.4 [15.1–15.8]	X

However, the wicking performance results from droplet wicking test is completely opposite to the UHD test: with the limited amount of liquid, liquid of microliter–scale droplet moves further on the EASTMAN fabric with smaller capillary channels than the commercial fabric with bigger

channels (Figure 5-3). The only difference between the UHD test and the droplet wicking test other than the test configuration is the amount of liquid supplied by using either infinite reservoir or the limited amount. However, due to inconsistency between two wicking test methods, we do not know which method is appropriate for textile comfort. In terms of the droplet wicking test, sometimes flooding occurs when either the flow rate or the liquid volume exceeds the threshold value of textile substrates [91]. Furthermore, when the droplet contacts on the surface of a fabric, it covers several course yarns and void spaces in-between yarns. Therefore, wicking begins from the whole contacting area between a fabric and a droplet, which means that liquid movement is initiated from several yarns as well as the space between yarns. For this reason, it is almost impossible to differentiate between the liquid movement along yarns and the wicking from the large void spaces. Another critical issue to investigate wicking performance of textiles is flooding effect. Without flooding, the liquid is spontaneously transported through capillary channels along yarns.

5.4.1. Time-wicking Length Superposition

In terms of the SWEAT test, when a continuous flow (50 nl/min) was supplied to a certain point of a single yarn, within-a-yarn and yarn-to-yarn transfer wicking can be observed over time starting from the single contacting point with the needle (Figure 5-4). Because liquid movement for each individual yarn within a fabric is visually traceable due to the dye solution, how fast liquid moves along a yarn and when liquid spills over towards adjacent yarns can be observed. Figure 5-5b shows that the slope value of wicking length of individual yarn is not constant over square root of time, which means that the liquid movement mechanism of textiles cannot be explain by the Lucas-Washburn equation in which the wicking length is directly proportional to the square root

of time ($l \propto \sqrt{t}$). While the Lucas-Washburn equation (eq. 3-18) assumes that wicking phenomena are controlled by viscosity and the driving forces (i.e. Laplace pressure) from infinite reservoir without restriction of the quantity of liquid, the flow rate of the SWEAT test is restricted by the syringe pumping speed (i.e. feed rate, 50 nl/min in this study). Therefore, the Lucas-Washburn equation is not applicable for the SWEAT test. As the time increases, the wicking length increases, then stops increasing for a while when liquid spills over to the closest adjacent yarns. As time continues, the wicking length increases again until it finally reaches a plateau (Figure 5-5a) where there is a balance between evaporation and liquid supply rate.

However, the slope of initial wicking length graph for each individual yarn seems identical, even though the wicking of individual yarn starts at different times. To identify each individual course yarn within a fabric, 'C(0)' denotes the yarn that is picked by the needle of the SWEAT system and provided with continuous liquid flow. 'C(± 1)' is the closest adjacent yarn to C(0) and an ordinal number keeps increasing in this way. Specifically, C(± 1) represents two course yarns for the nearest upper (+1) and lower (-1) course yarn from C(0), shown in Figure 5-5a. In order to check if the slope value of each individual yarn was identical or not, the wicking graph of each individual yarn from Figure 5-5b was translated toward the wicking start point of the C(0) yarn parallel to the x-axis (time-axis) in order to align the same wicking start points for all graphs, as shown in Figure 5-5c. Figure 5-5c, derived from Figure 5-5b, presents that the initial slope values of individual yarns are considerably identical, especially in the first few minutes. In other words, although each of course yarns have different wicking starting points, the wicking mechanism of all course yarns within the fabric substrate are equal to each other. There appears to be the time-wicking length superposition principle: liquid wicks within a single yarn initially, subsequently it spills over to adjacent yarns through contact points, but the wicking rate in adjacent yarns is

identical to the initiated course yarn. Consequently, the fabric is a collection of yarns which are used as capillary channels for wicking purposes. This time-wicking length superposition principle has the substantial potential to anticipate the liquid movement in textiles. If we know the wicking performance of any individual yarn, liquid movement of other yarns within a fabric substrate might be predictable.

It is important to note that the wicking results of textiles with a constant supplied flow rate from the SWEAT test were not observed because typical wicking test methods such as the vertical, horizontal, and UHD test do not explain within-a-yarn and yarn-to-yarn transfer wicking. Additionally, the experimental data from the SWEAT test cannot be explained by the well-known Lucas–Washburn equation (Figure 5-5b) because the wicking length graph over time shows how liquid spills over to adjacent yarns as well as how fast liquid moves along a yarn without a constant slope value. Based on Lucas-Washburn equation (Eq. 3-18), some textile studies have tried to calculate the average effective capillary radius (r) by using a constant slope value between wicking length and square root of time [63, 92]. However, the average effective capillary channel size means nothing to textile fabrics because even the capillary channel radius of a yarn within a fabric keeps changing due to the own structure. Furthermore, Almoughni et. al. (2015) has tried to narrow the space between theoretical and experimental investigation in capillary flow along yarns but they cannot examine the actual liquid location in the cross-section of yarns in their experiment. Even though the parallel fibers within the certain yarn cross-section area are aligned evenly, they found that liquid in textiles theoretically gets settled in an effective medium space between fibers with arbitrary arrangements, shown in Fig. 5-6 [93].

Dropping Liquid Test (1 μ l)
With the limited amount of liquid

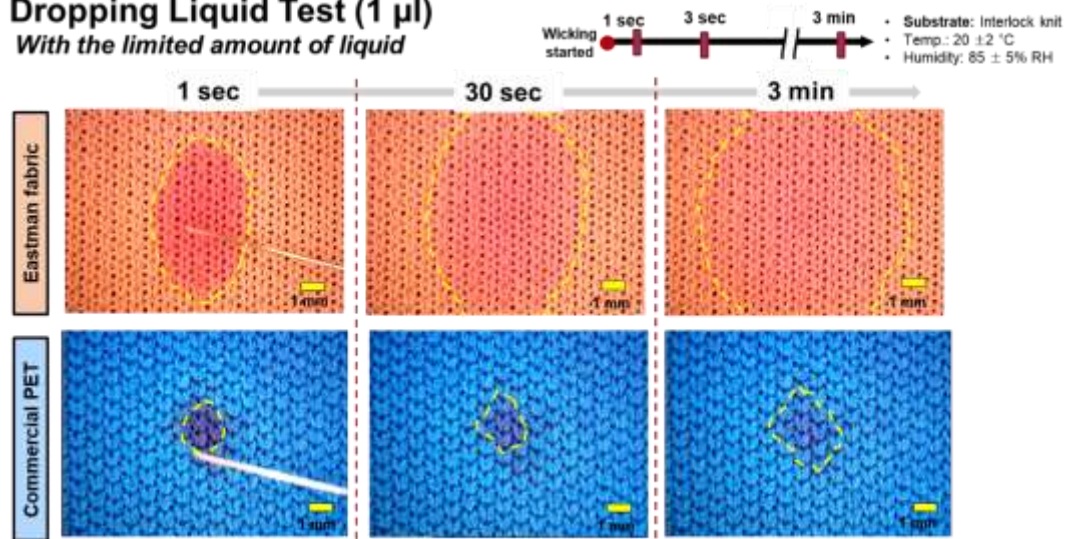


Figure 5-3. Wicking performance comparison from the droplet wicking test (1 μ l) on the EASTMAN interlock knit fabric with flat filament yarns and a commercial PET interlock knit fabric.

Single Point Measurement System
With continuous microfluidic liquid (50 nanoliter/min)

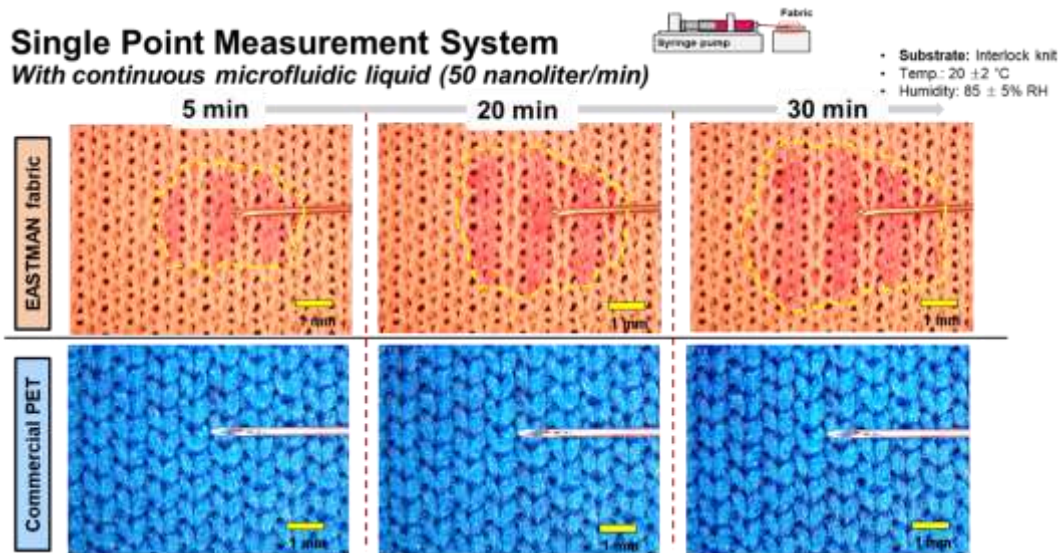


Figure 5-4. Wicking performance comparison from the SWEAT test (continuous flow rate: 50nl/min) on the EASTMAN interlock knit fabric with flat filament yarns and a commercial PET interlock knit fabric.

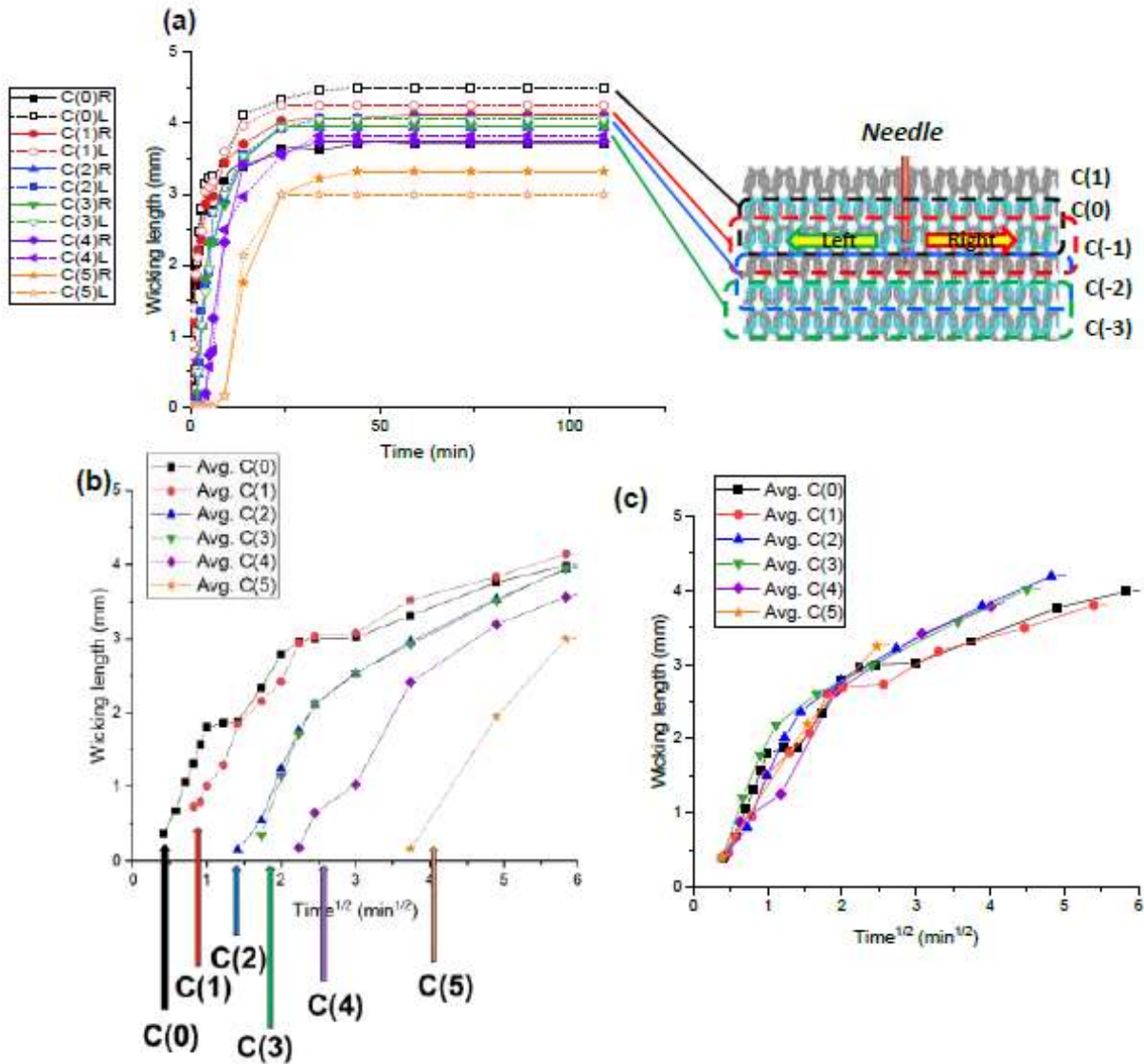


Figure 5-5. Apparent wicking length of EASTMAN single jersey knit from the SWEAT test (continuous flow rate: 50nl/min): (a) apparent wicking length over time, (b) apparent wicking length over square root of time. And (c) shows the wicking length graph of each course yarn over square root of time ($L - \sqrt{t}$) overlap each other when the graph of each yarn's wicking is shifted to place all starting points at the wicking beginning point of the C(0) yarn in order to check the time-wicking length superposition principle.

Even though the properties of a single yarn within a fabric, including diameter, twist level, tension, and contact points with adjacent yarns keep changing depending on location due to textile structures, the wicking performance of each individual yarn follows the time–wicking length superposition principle: the wicking performance of the first yarn (i.e. $C(0)$), which is picked with the needle, is same as all other yarns ($C(i)$, ‘i’ is the number to indicate how close to the initial yarn. From wicking videos, we found that liquid transferred to adjacent yarns only at the direct contact points with adjacent yarns instead of transferring through the relatively big void space in-between yarns. That means that the liquid flow probably wicks through capillary channels in-between fibers or peripheral region around fibers (Figure 5-6). It can explain why every other column of the EASTMAN interlock knit became wet. That’s because a wet yarn of an interlock knit fabric went through the two layers of interlock knit structure and the liquid along the wet yarns was transferred to adjacent yarns with contact points (Fig 5-7c and d). Therefore, we know liquid moves along yarns (open space inside of a yarn) and spills over to adjacent yarns only through their contact points instead of using the big void spaces between yarns. Even though we know that the actual cross-sectional shape of the capillary channel of textiles is not circle, it is hard to examine what the capillary channels look like in a yarn and how big they are (i.e. capillary channel area).

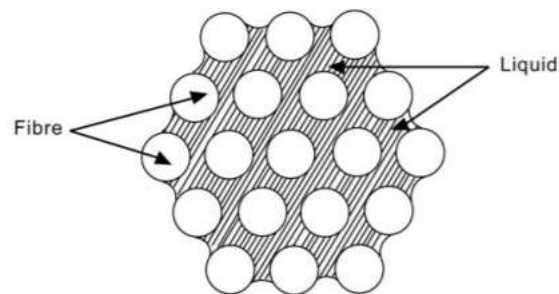


Figure 5-6. Theoretical schematic illustration of liquid moving in yarn [93].

The time-wicking length superposition principle for individual yarn wicking performance can be explained further, if we make four assumptions: 1) all liquid goes into yarns (in-between fibers), 2) the yarn diameter and the porosity in a yarn is constant, 3) each individual yarn in a fabric has same structure within a fabric, and 4) the saturation level of individual yarn is considered equally.

Figure 5-7b shows the apparent wicking length and the actual wicking length of individual yarn. The actual wicking length was defined to analyze the wicking performance based on the actual yarn length. The wicking performance of EASTMAN fabric with multifilament flat yarns shows the time-wicking superposition principle. However, when a continuous liquid was supplied to a commercial polyester knit fabric with the textured yarn, wicking performance becomes unpredictable and random because of uneven, widely varying capillary channel size obtained from texturing (Figure 5-8). However, the knit with flat yarns without texturing (i.e. EASTMAN single jersey knit and interlock knit) shows symmetric wetting area for both course and wale direction.

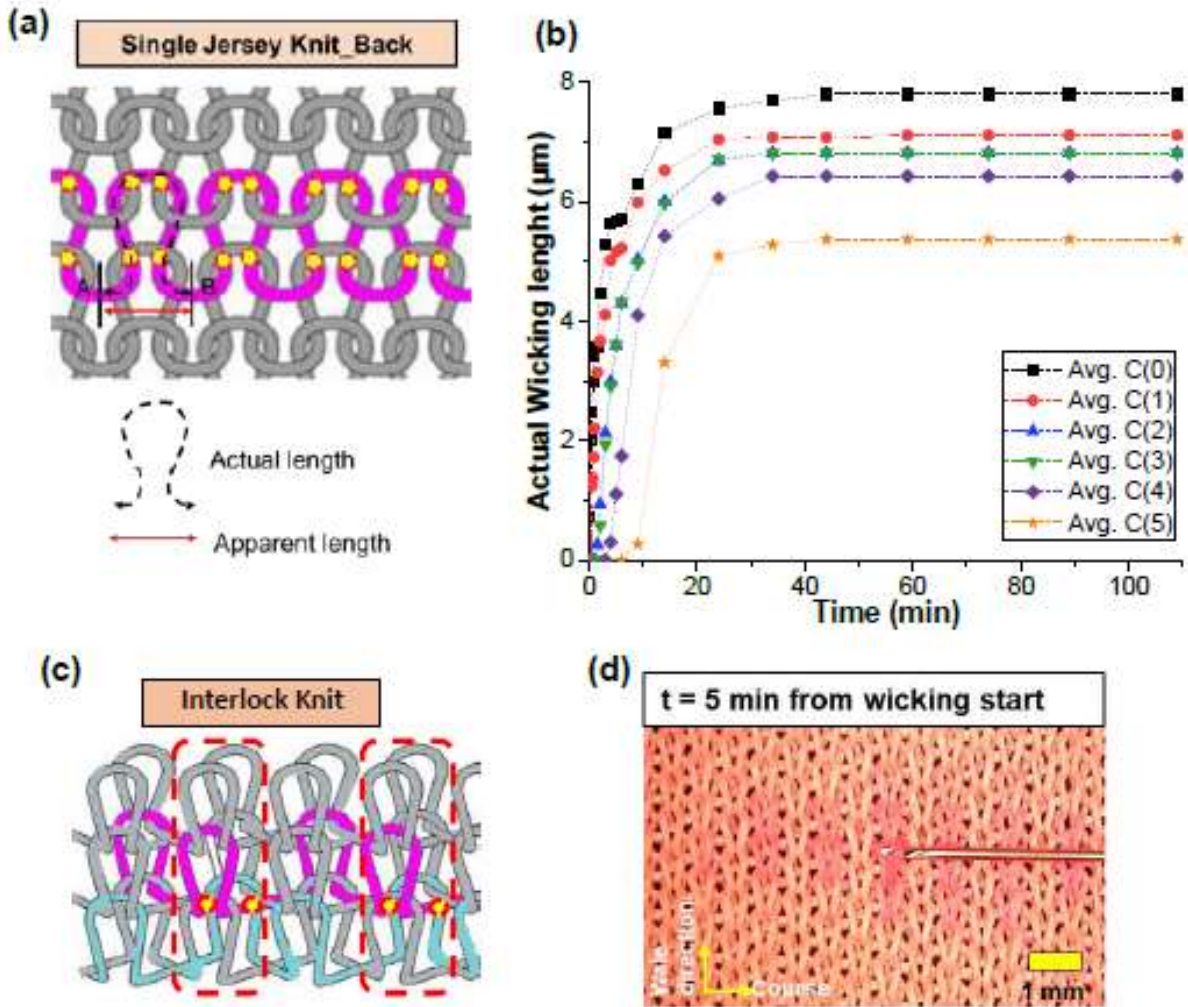
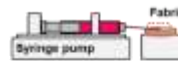


Figure 5-7. (a) Actual wicking length presents the yarn length considering textile structures, but apparent wicking length is the shortest distance from the wicking start point (yellow circles shows the contacting points within a fabric). (b) shows wicking performance based on actual wicking length over time. (c) shows that the contacting point of the interlock knit fabric and (d) the actual yarn-to-yarn transfer wicking happens through the connecting point in-between yarns. For the interlock knit fabric, every other column becomes getting wet due to the contact points.

Wicking Performance Comparison

30 min after wicking started



- Temp.: 20 ± 2 °C
- Humidity: $85 \pm 5\%$ RH
- Flow rate: 50 nanoliter/min

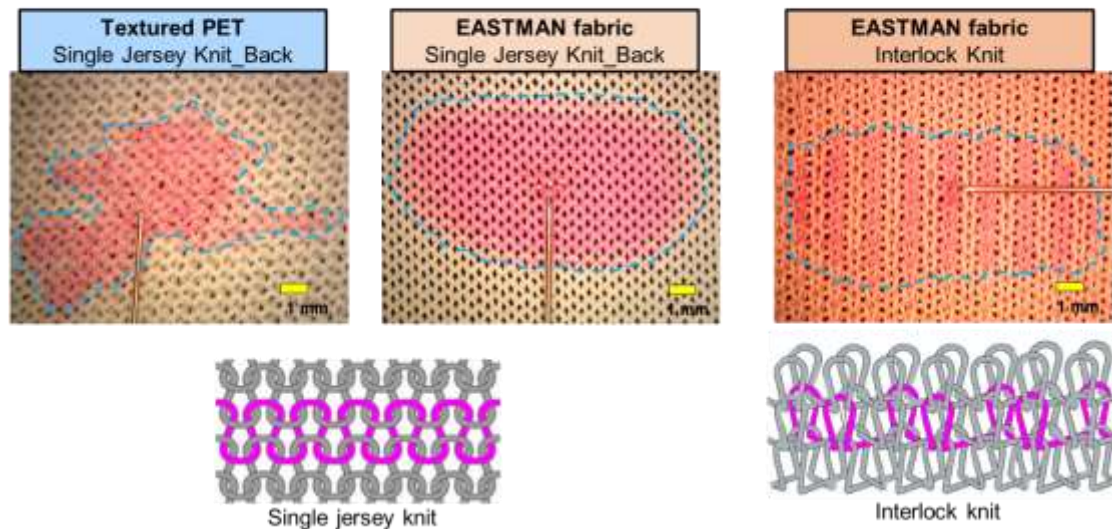


Figure 5-8. Wicking performance comparison from the SWEAT test (continuous flow rate: 50nl/min) on a commercial textured PET single jersey, EASTMAN single jersey knit, and EASTMAN interlock knit fabrics.

5.5. Conclusion

For textile comfort, typical test methods are conducted with either infinite reservoirs or limited, but large amounts of liquid without considering realistic human sweating condition. Wicking behavior tests of textile fabrics are performed with a fabric strip, suspended vertically/horizontally or in integrated three directions (i.e. UHD test) with one end dipped into infinite liquid reservoir. Also, with limited amount of liquid (i.e. a droplet), how fast and how far liquid can move are investigated as a function of time. However, because human sweating is a slow continuous flow generated from each sweat gland, the results from either infinite reservoir or a droplet cannot represent that of human sweating. Furthermore, sometimes the wicking performance comparison results were completely opposite between infinite reservoir test and limited amount of liquid test

due to the quantity of liquid supplied. That means that with the conventional wicking test methods, we still cannot understand the wicking mechanism of textiles thoroughly and we need to develop a better wicking test method to mimic human sweating. If not, we might be obsessed with the meaningless value such as the average effective capillary radius in order to understand liquid transportation of textiles in the wrong way.

In order to mimic realistic human sweating, a new measurement system called the SWEAT test was developed by supplying a continuous microfluidic flow to only a single yarn at a single point within the fabric substrate at a similar flow rate to a single sweat gland. Thanks to the SWEAT test system, we found that liquid movement in yarns in our knit fabrics could not be explained by Lucas-Washburn equation, but it followed the time-wicking length superposition principle: liquid wicked within a single yarn initially, subsequently it spilled over to adjacent yarns, and the initial wicking rate in adjacent yarns was the same as the first course yarn but with a time offset equal to the spill-over time. When liquid spills over to adjacent yarns, transferring occurred only at the connecting point instead of the big void space in-between yarns. If liquid movement along yarns (i.e. within-a-yarn and yarn-to-yarn transfer wicking) can be predicted based on the time-wicking length superposition principle, wicking performance might be controlled depending on various application purpose.

CHAPTER 6. New Textile Wicking Theory

6.1. Wicking Performance in Fabrics

Continuous liquid flow in the SWEAT test allows the yarn-level wicking within a fabric to be investigated through within-a-yarn and yarn-to-yarn transfer wicking. Based on the actual wicking length results, we analyzed them in order to find a principle that can explain liquid movement mechanism in textiles. Consequently, we found that the time-wicking length superposition principle in textile wicking: liquid moves along a single yarn initially, subsequently it spills over to adjacent yarns through their contact points, but the wicking rate in adjacent yarns is identical to the initial yarn. Interestingly, even though the actual wicking length of individual yarn increases in the initial stage, it finally reaches a plateau stage without further increase in wicking length. Therefore, in this chapter, we would try to develop an equational model which explain the experimental results of the wicking phenomenon of knit fabrics by supplying continuous liquid flow.

The capillary pressure to pull liquid through a capillary channel is driving force as reflected in the Laplace equation (eq. 3-9). However, this spontaneous liquid movement is retarded by the dragging force, or back pressure, through a capillary channel by the Poiseuille flow (eq. 3-12) [94]. When continuous liquid flow with the certain pump rate was supplied to the single point of a yarn within a fabric, the liquid movement was started at the first course yarn (i.e. $C(0)$) with which the needle picked. In the case of the SWEAT test, while the capillary pressure is independent of the amount of liquid supplied to the capillary channel (i.e. each course yarn), the back pressure derived from Poiseuille equation increases as the wicking length increases. Because the back pressure gets larger as the wicking length of the first yarn increases, the wicking length of the first course yarn slows or even stops, shown in Fig. 6-1a. However, because the continuous liquid flow

kept supplying liquid through the first course yarn, the liquid must build up within the first yarn, and then, transfer to the adjacent yarns (i.e. C(-1) or/and C(+1)) through the direct contact points. The mean flow in the first course yarn is increased due to transfer to C(-1) or/and C(+1), resulting in increasing wicking length a little bit more in the initial yarn (i.e. C(0)) [95]. Until the back pressure of the integrated capillary channels becomes equal to the capillary pressure in individual yarn, the liquid moves along C(-1) or/and C(+1). Then again, liquid would spill over adjacent yarns, and so forth. However, as the wet area increases, the amount of evaporation also increases until the evaporation rate and feed rate are equal. At this time, the wet area of the fabric does not get any bigger.

6.2. SWEAT Theory of Wicking in Textiles

Due to the complexity of capillary channels in textile, six assumptions could help understanding of textile wicking further: 1) the wetted area ($A(t)$) is linearly proportional to the sum of wicking length of all yarns ($\sum_{i=0}^n L_{C(\pm i)}(t)$), 2) each of the liquid pump rate (k_p) and the evaporation potential rate (E_a) is constant during the experiment, 3) all of the liquid is either stored in the void space of yarns (in-between fibers) or it evaporates, 4) yarn diameter and porosity in a yarn will be constant, 5) each individual yarn in a fabric has the same structure, and 6) the saturation level for all individual yarns will be identical. When liquid moves along each yarn, the liquid in a yarn will be located in the effective space between fibers of arbitrary shape and with arbitrary arrangement instead of making circular channels, as shown in Fig. 5-6. Based on our experimental results, we found the time-wicking length superposition principle, and thus, the wicking rate of each individual course yarn within a fabric is identical, consistent with assumptions 5 and 6.

When continuous liquid flow is supplied to a single point of a yarn within a fabric, the pump rate is constant which represents human sweat rate. Due to a constant liquid pumping rate of the SWEAT test, the instantaneous liquid volume (dV) in time (dt), supplied to a fabric substrate, becomes a constant:

$$\frac{dV_p}{dt} = k_p \quad (6-1)$$

where V_p is the liquid pumping volume, t is time, and k_p is a constant, which is the pumping rate. Total pumped volume until the certain pumping time (t_p) can be obtained as follows:

$$\int_{t=0}^{t_p} \frac{dV_p}{dt} = V_p \quad (6-2)$$

The pumping rate should balance between the stored volume left in a fabric substrate and the lost volume due to evaporation. The stored volume ($V_s(t)$) and the rate of storage (k_s) can be obtained as follows:

$$V_s(t) = s \cdot \sum_{i=0}^n L_{c(\pm i)}(t) \quad (6-3)$$

$$k_s = s \frac{d}{dt} \sum_{i=0}^n L_{c(\pm i)}(t) = \frac{s}{\alpha} \cdot \frac{dA(t)}{dt} \quad (6-4)$$

$$\therefore A(t) = \alpha \sum_{i=0}^n L_{c(\pm i)}(t) \quad (6-5)$$

where the wicking length in a yarn is $l_{c(\pm i)}$ (where $i = 0, 1, \dots$), s is a constant, which relates the wicking length to the cross-sectional void space value of a yarn (i.e. porosity in cross-sectional area), $A(t)$ is the wetted are at time t , and α is a constant relating the wicked length to the wetted area. From eq. 6-5, the sum of the wicking lengths of all yarns (i.e. wetting area, $\sum_{i=0}^n l_{c(\pm i)}$) is

proportional to the wetting area ($A(t)$). The rate of evaporation (k_e) can also be obtained considering the evaporation potential constant (E_a):

$$k_e = E_a \cdot A(t) = E_a \cdot \alpha \sum_{i=0}^n L_{c(\pm i)}(t) \quad (6-6)$$

When evaporation effect is considered, the liquid pumping rate (k_p) is equal to the sum of the stored liquid rate (k_s) in a textile substrate and the lost volume rate derived from evaporation (k_e):

$$k_p = k_s + k_e \quad (6-7)$$

$$\therefore k_p = \frac{s}{\alpha} \cdot \frac{dA(t)}{dt} + E_a \cdot A(t)$$

$$\left| A(t) - \frac{k_p}{E_a} \right| \cong e^{-\frac{\alpha}{s} E_a \cdot t + c_1} = c \cdot e^{-\frac{\alpha}{s} E_a \cdot t} \quad (6-8)$$

For the SWEAT test, when $t=0$, $c = \frac{k_p}{E_a}$ because of $A(t=0) = 0$. However, when a garment already contains sweat (i.e. $A(t=0) \neq 0$), there are two cases as follows:

$$\text{If } A(t=0) < \frac{k_p}{E_a}, c = \left[\frac{k_p}{E_a} - A(t=0) \right] \quad (6-9)$$

$$\text{If } A(t=0) > \frac{k_p}{E_a}, c = \left[A(t=0) - \frac{k_p}{E_a} \right] \quad (6-10)$$

Eq. 6-10 explains the case of drying process when a textile substrate is wet.

For the SWEAT test, where $A(t=0) = 0$, the sum of wicking length of all yarns based on eq. 6-5 and 6-8 becomes as follows:

$$\sum_{i=0}^n L_{c(\pm i)}(t) = \frac{1}{\alpha} \frac{k_p}{E_a} \left(1 - e^{-\frac{\alpha}{s} E_a \cdot t} \right) \quad (6-11)$$

Eq. 6-11 shows that when the sum of the wicking length of all yarns are measured in the SWEAT test, the experimental pump rate (k_p) is a setting value, an evaporation potential constant (E_a) is determined by the environmental conditions. Specifically, the potential rate of evaporation (E_a) was acquired using Dalton-type equation, assuming that evaporation is a function of wind speed and of the difference between the vapor pressure of the liquid surface and the atmosphere [96]. Generally, Dalton-type equation is used to anticipate the rate of evaporation of water from the free water surface over a day (i.e. BPI evaporation pan: 6 ft diameter by 2 ft deep) [97]. Evaporation rate, E (mm reduction of water height in the pan/day), is expressed as:

$$E = f(u) \cdot (e_s - e_a) \cdot A \quad (6-12)$$

where $f(u)$ is a turbulent exchange function which depends on the mixing characteristics of the air above the evaporating surface, e_s is the saturation vapor pressure of liquid at the temperature of the liquid surface, e_a is the liquid vapor pressure of the air in the atmosphere above the liquid surface (mm Hg or kPa) evaporating surface as a function of relative humidity, and A is the surface area of the liquid [98]. Even though the Dalton-type equation is based on the pan evaporation technique for the daily evaporation rate, eq. 6-12 suggests which factors could have an influence on evaporation.

The only adjustable parameters in eq. 6-11 are α and s , which depend on the yarn and the fabric construction. Because E_a , α and s are all constants, we can merge all three to $E_a' = \frac{\alpha}{s} E_a$.

$$\sum_{i=0}^n L_{c(\pm i)}(t) = \frac{1}{s} \frac{k_p}{E_a'} (1 - e^{-E_a' \cdot t}) \quad (6-13)$$

Eq. 6-13 shows that when $t = 0$, $\lim_{t \rightarrow 0} \sum_{i=0}^n L_{c(\pm i)}(t) = 0$, and when $t = \infty$,

$$\lim_{t \rightarrow \infty} \sum_{i=0}^n L_{c(\pm i)}(t) = \frac{1}{s} \frac{k_p}{E_a'} = \frac{1}{\alpha} \frac{k_p}{E_a}$$

6.3. Experimental Analysis Based on the SWEAT Theory of Wicking in Textiles

When the EASTMAN single jersey knit fabric, made of flat filament polyester yarns, was used for the SWEAT test, liquid movement along an individual yarn was observed through within-a-yarn and yarn-to-yarn transfer wicking. Each individual course yarn, $C(n)$, except $C(0)$ has two different yarns symmetrically disposed around $C(0)$ such as $C(+n)$ and $C(-n)$. (i.e. $C(+1)$ is above $C(0)$ and $C(-1)$ is below $C(0)$), shown in Fig 5-5a. Fig 6-1a shows the average actual wicking length of each individual yarn for $C(+n)$ and $C(-n)$, separately. Because $C(0)$ is only a single yarn itself, the total wicking length of all other yarn excluding $C(0)$ became almost a double of the total wicking length of $C(0)$, as shown in Fig 6-1b. Fig 6-1c presents the sum of the actual wicking length of all course yarns at the given time. If eq. 6-13 is an appropriate equation to explain the wicking behavior during the SWEAT test, the fitted model equation from experimental results (i.e. Fig 6-1c) should follow eq. 6-13 with the natural exponential curve. The fitted exponential curve of the sum of wicking length of all yarns is determined with the certain constants' value of E_a , α and s , and it will reach a plateau status at the end.

From three times repeated tests on the identical EASTMAN single jersey fabric on the back side, Table 6-1 shows that the total wicking length of all course yarns has the natural exponential function trendline (eq. 6-13 and Fig. 6-2a). In order to make a better fitted equation model to explain a plateau stage, two data points were added to extend the plateau regions for two and three times from the last data point of the time, since the duration of plateau region is relatively short (~10 min) compared to the whole experimental period (> 80 min) (i.e. the data points of 160 and 240 min were added with the same value of the plateau region, if the last data point of the test #1 in the plateau phrase was 80 min.) In order to compare the value of merged constants in the fitted equations models, a represents $\frac{1}{s} \frac{k_p}{E_a'}$ and b means E_a' . When $F(t) = \sum_{i=0}^n L_{C(\pm i)}(t)$, the range of

a value is from 7.6×10^5 to 8.9×10^5 , while that of b is from 3.2×10^{-2} to 3.1×10^{-2} with an R-squared value of greater than 0.99.

Before reaching to a plateau stage, the trendline of the sum graph of the actual wicking length of all individual yarn increases over time. When evaporation affects the wetting area increase, a considerable evaporation loss relates the wetting-area-related constant (α) and the cross-sectional void space value of a yarn (i.e. porosity in cross-sectional area) (s). During a plateau status, the sum of the total wicking lengths of all yarns of a fabric, $F(t) = \sum_{i=0}^n l_{c(\pm i)}$ can be $\frac{1}{\alpha} \frac{k_p}{E_a} = a$, shown in eq. 6-13. Because the percent error (%) is less than 10 % for all three experiments, the fitted equation model can reflect the experimental data well.

Eq. 6-13 provides a good conceptual model for the observed processes of the SWEAT test, because the sum of wicking length of all yarn will increase following the natural exponential function, and then it will reach to a plateau value. Even though, E_a is related to the environmental factors regardless of fabric substrate properties, eq. 6-13 shows that two merged constants of $\frac{1}{s} \frac{k_p}{E_a'}$ and $-E_a'$ describe the ability of water to evaporate from the wet yarn to the environment. If there is substantial moisture regain, some of the liquid must go into the fibers. This may or may not change the void space in yarns, but it is an additional place for liquid to go and would need to be considered for, both in storage and in evaporation rate.

Table 6-1. The trendline from the three-times repeated wicking performance test of EASTMAN single jersey knit fabric. $f(t)$ is the sum of wicking length function depending on time (unit: micrometer), and [a, b] is the time range from a to b (unit: min).

Modified eq. 6-13	Trendline/ Repeated test	Fitted equation model*		Experimental results of plateau stage	
$F(t) = \frac{1}{s} \frac{k_p}{E_a'} (1 - e^{-E_a' t})$ $= a(1 - e^{-b t})$ $\lim_{t \rightarrow \infty} F(t) = \frac{1}{s} \frac{k_p}{E_a'} = a$	Test #1	[0, 240]	$a = 8.0 \times 10^5$ $b = 3.2 \times 10^{-2}$ $(R^2=0.993)$	[64, ∞]	$F(t)_{exp} = 7.6 \times 10^5$ Percent error= 5.3 (%)
	Test #2	[0, 255]	$a = 8.9 \times 10^5$ $b = 3.1 \times 10^{-2}$ $(R^2=0.994)$	[74, ∞]	$F(t)_{exp} = 8.3 \times 10^5$ Percent error= 7.2 (%)
	Test #3	[0, 327]	$a = 7.6 \times 10^5$ $b = 3.1 \times 10^{-2}$ $(R^2=0.998)$	[99, ∞]	$F(t)_{exp} = 7.5 \times 10^5$ Percent error= 1.3 (%)

*Since the duration of plateau region is relatively short (~10 min) compared to the whole experimental period (> 80 min), two data points were added to extend the plateau regions for two and three times from the last data point of the time in order to have a better fitted model to the actual graph (i.e. the data points of 160 and 240 min were added with the same value of the plateau region, if the last data point of the test #1 in the plateau phase was 80 min.)

In the SWEAT test on the EASTMAN fabric, the wetted area and the individual wet yarn lengths did not change after 1.5 hours, resulting in reaching a plateau stage, as shown in Fig 6-1c. The potential evaporation to estimate evaporation rates may be defined as the maximum rate of evaporation from a pure water surface under given climatic conditions.

Smith et al. developed an evaporation rate equation further in order to investigate the evaporation mass loss rate per unit area based on the experimental data under the certain conditions: water temperature was 28.3°C (83°F) and the air temperature varied from 21.6°C to 27.8°C (71°F to 82.0°F), with relative humidity from 51% to 73% [99]:

$$E_a = \frac{0.76(0.089 + 0.07282 u)(e_s - e_a)}{i_{fg}} \quad (6-14)$$

where E_a is the evaporation rate under actual condition ($\text{kg/m}^2\cdot\text{s}$), u is the air velocity (m/s) and i_{fg} is the latent heat of vaporization of water (2260 J/g). Since the SWEAT test was conducted under the glove bag with negligible air turbulence, the value of E_a calculated from eq. 6-14 became $7.45 \times 10^{-6} \text{ kg/m}^2\cdot\text{s}$ ($=7.45 \times 10^{-9} \text{ g/um}^2\cdot\text{s}$). When we assumed that the supplied liquid evaporates at the same rate ($50 \text{ nl/min} = 8.3 \times 10^{-7} \text{ g/s}$), the calculated value of the wetting surface area at a plateau stage should be $1.11 \times 10^8 \text{ um}^2$. Table 6-2 shows the actual wetting area at the plateau stage from three-times repeated tests (i.e. the range: $0.99 \times 10^8 - 1.03 \times 10^8 \text{ um}^2$) is close to the calculated value, $1.11 \times 10^8 \text{ um}^2$.

Table 6-2. Comparison between the calculated- and the actual-wetting area at a plateau stage from the three-times repeated wicking performance test of EASTMAN single jersey knit fabric. [a, b] is the time range from a to b (unit: min). The calculated wetted area was obtained from equation 6-14.

Repeated test	Actual wetting area at the plateau stage (um^2)		Calculated wetting area at the plateau stage (um^2)
Test #1	[64, ∞]	1.01×10^8	1.11×10^8
Test #2	[74, ∞]	0.99×10^8	
Test #3	[99, ∞]	1.03×10^8	

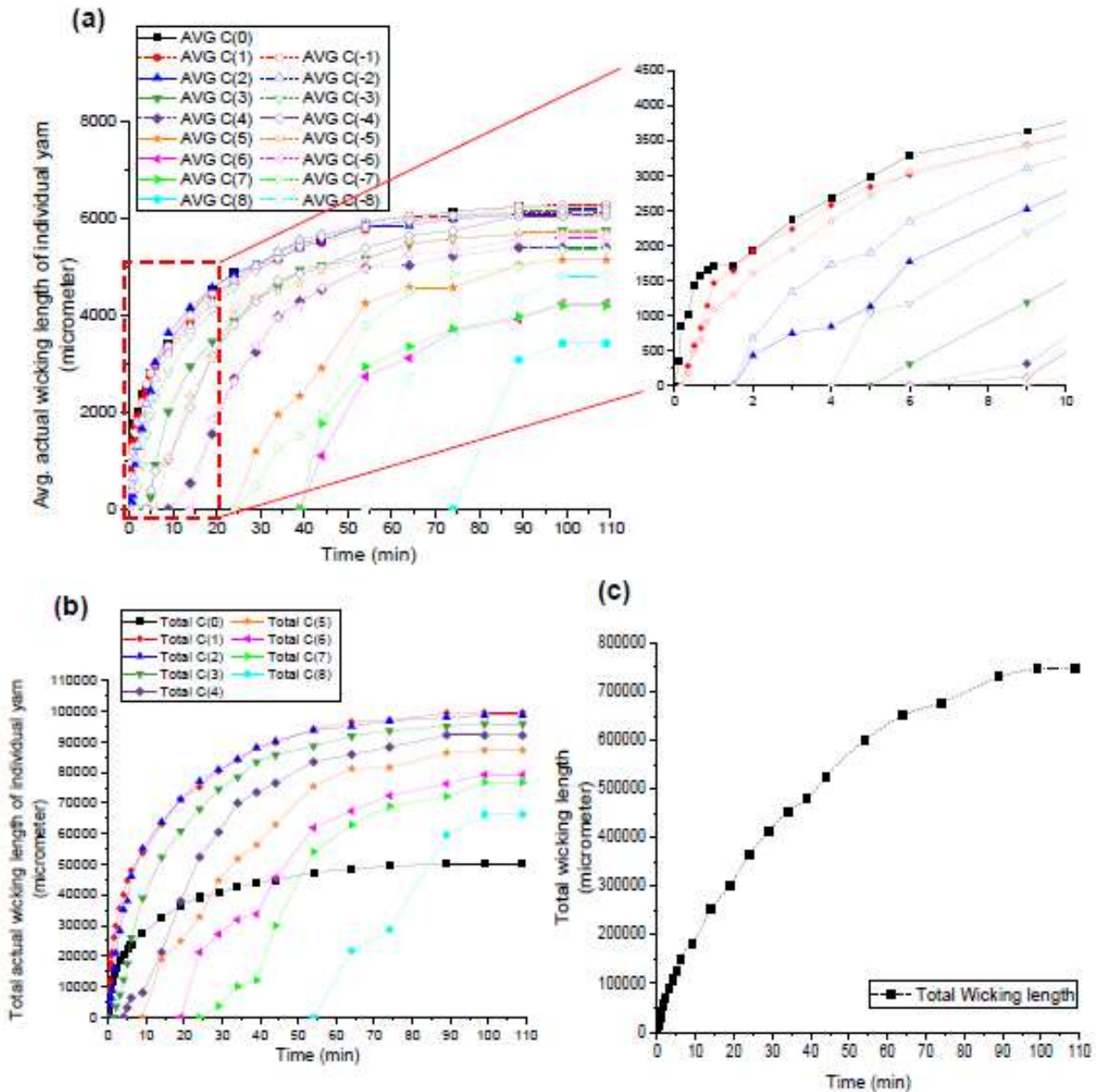


Figure 6-1. (a) Average wicking length of individual yarn, including C(+n) and C(-n), separately, (b) the total actual wicking length of the apparent wicking length of C(n) with C(+n) and C(-n), and (c) the sum of the total wicking length of all yarns at the given time. (Fabric: EASTMAN single jersey knit with multi-filament flat yarn, Test #3 video code: SJK_B_1090)

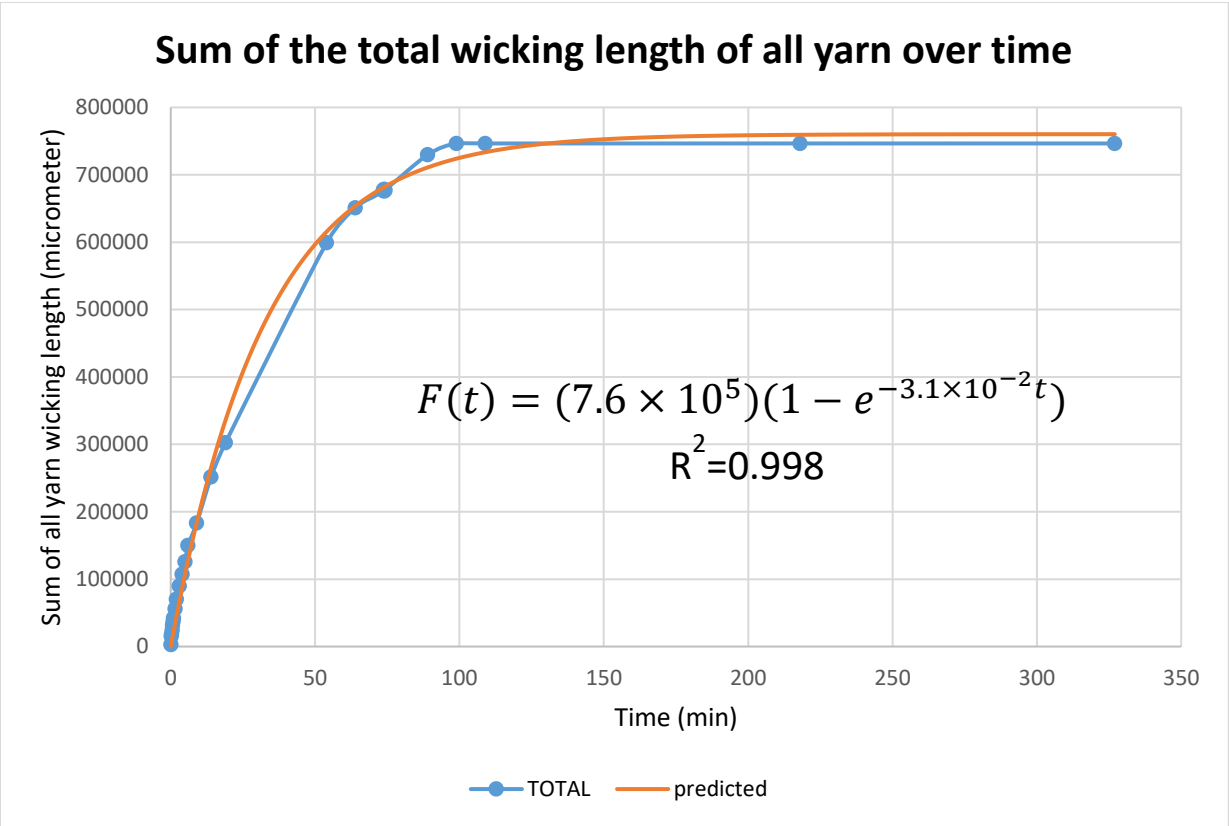


Figure 6-2. Sum of the total wicking length of all yarn over time for the experimental data of the SWEAT test (blue line) and the fitted model (red line). (Fabric: EASTMAN single jersey knit with multi-filament flat yarn, Test #3 video code: SJK_B_1090).

6.4. Supplementary Information

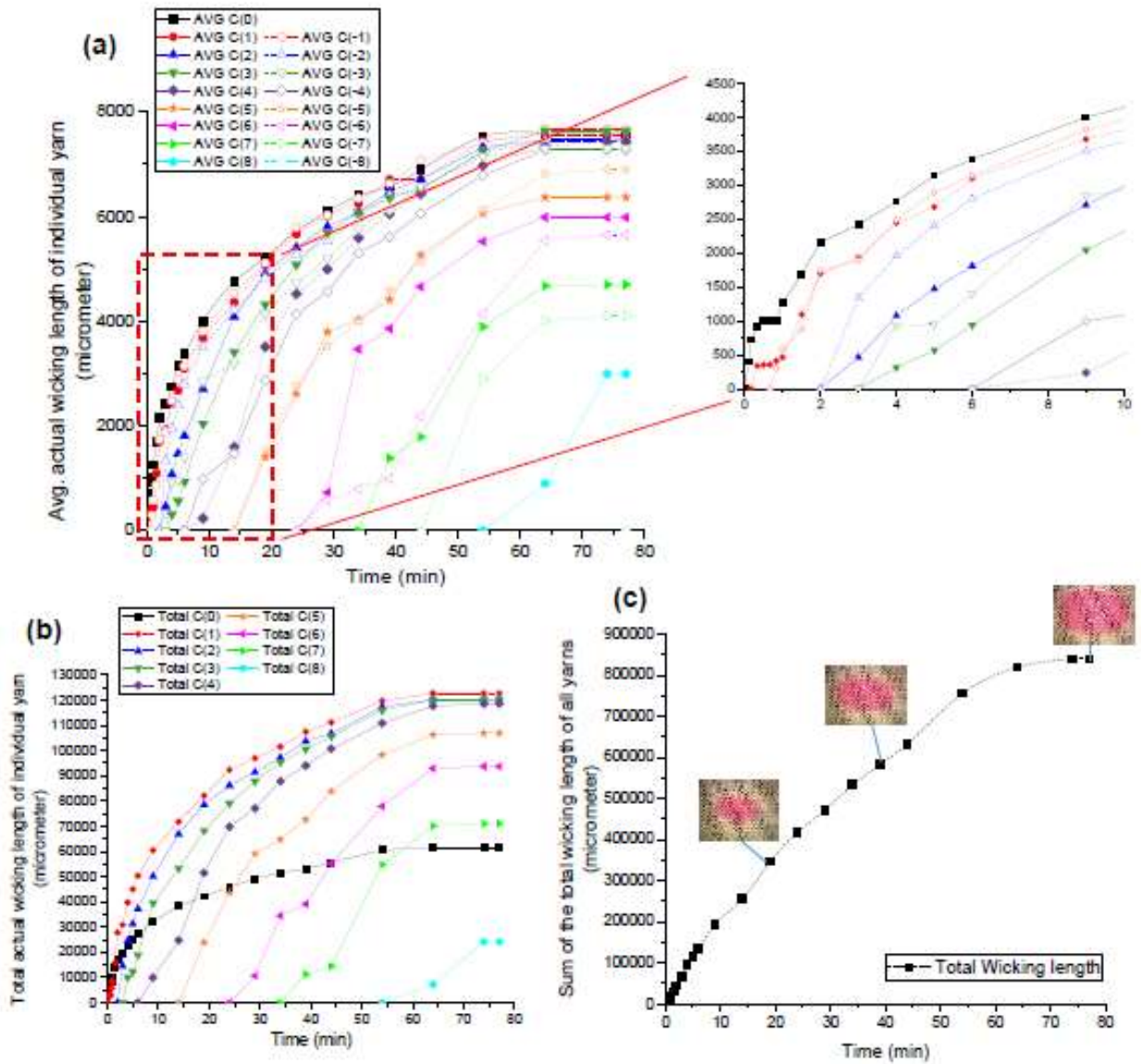


Figure S6-1. (a) Average wicking length of individual yarn, including C(+n) and C(-n), separately, (b) the total actual wicking length of the apparent wicking length of C(n) with C(+n) and C(-n), and (c) the sum of the total wicking length of all yarns at the given time. (Fabric: EASTMAN single jersey knit with multi-filament flat yarn, Test #2 video code: 0425_003)

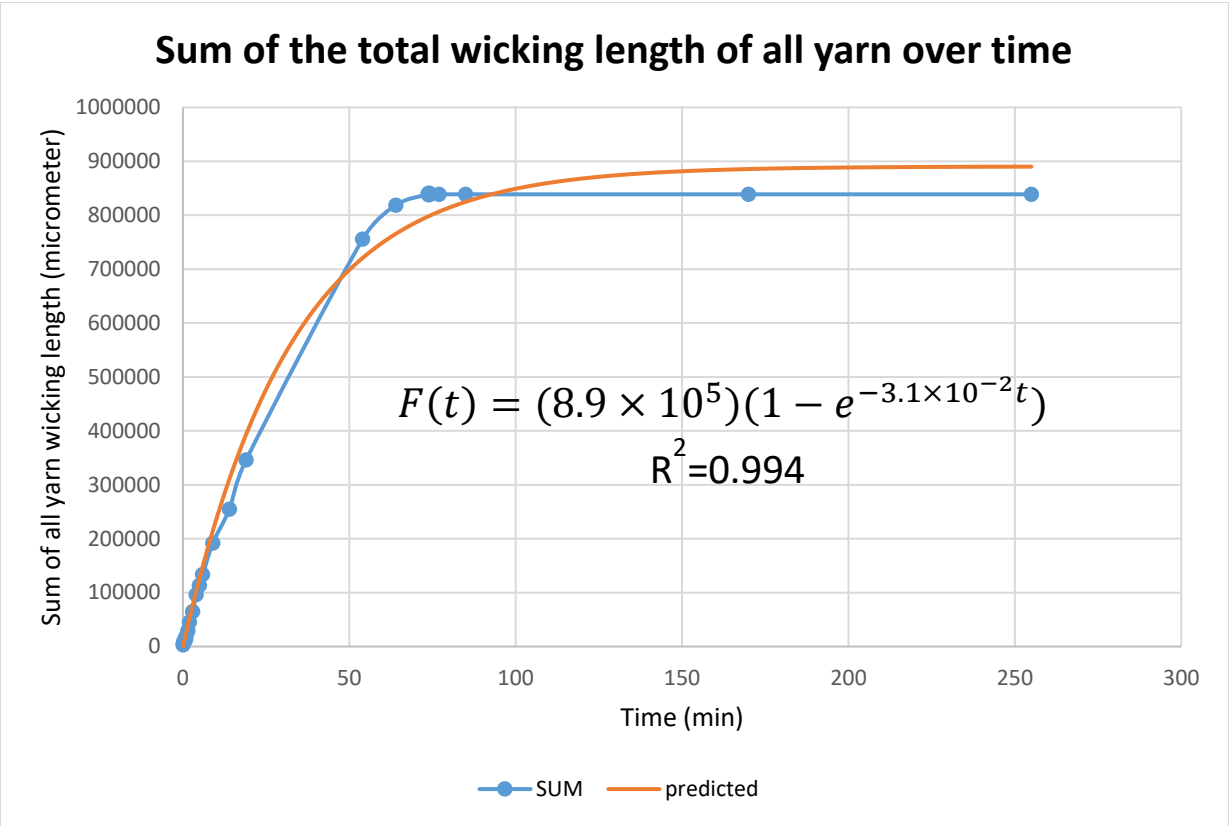


Figure S6-2. Sum of the total wicking length of all yarn over time for the experimental data of the SWEAT test (blue line) and the fitted model (red line). (Fabric: EASTMAN single jersey knit with multi-filament flat yarn, Test #2 video code: 0425_003)

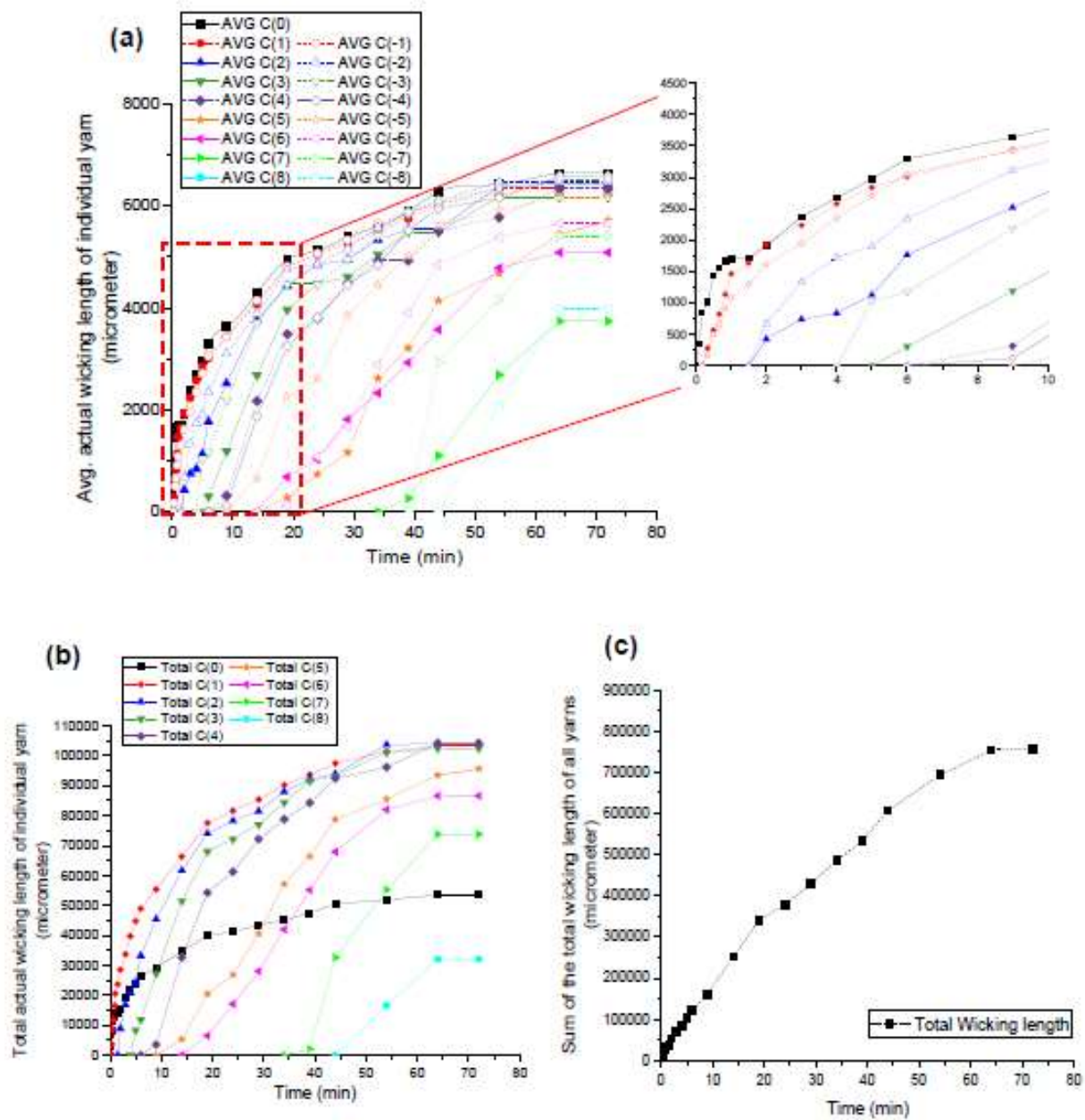


Figure S6-3. (a) Average wicking length of individual yarn, including C(+n) and C(-n), separately, (b) the total actual wicking length of the apparent wicking length of C(n) with C(+n) and C(-n), and (c) the sum of the total wicking length of all yarns at the given time. (Fabric: EASTMAN single jersey knit with multi-filament flat yarn, Test #1 video code: 0425_002)

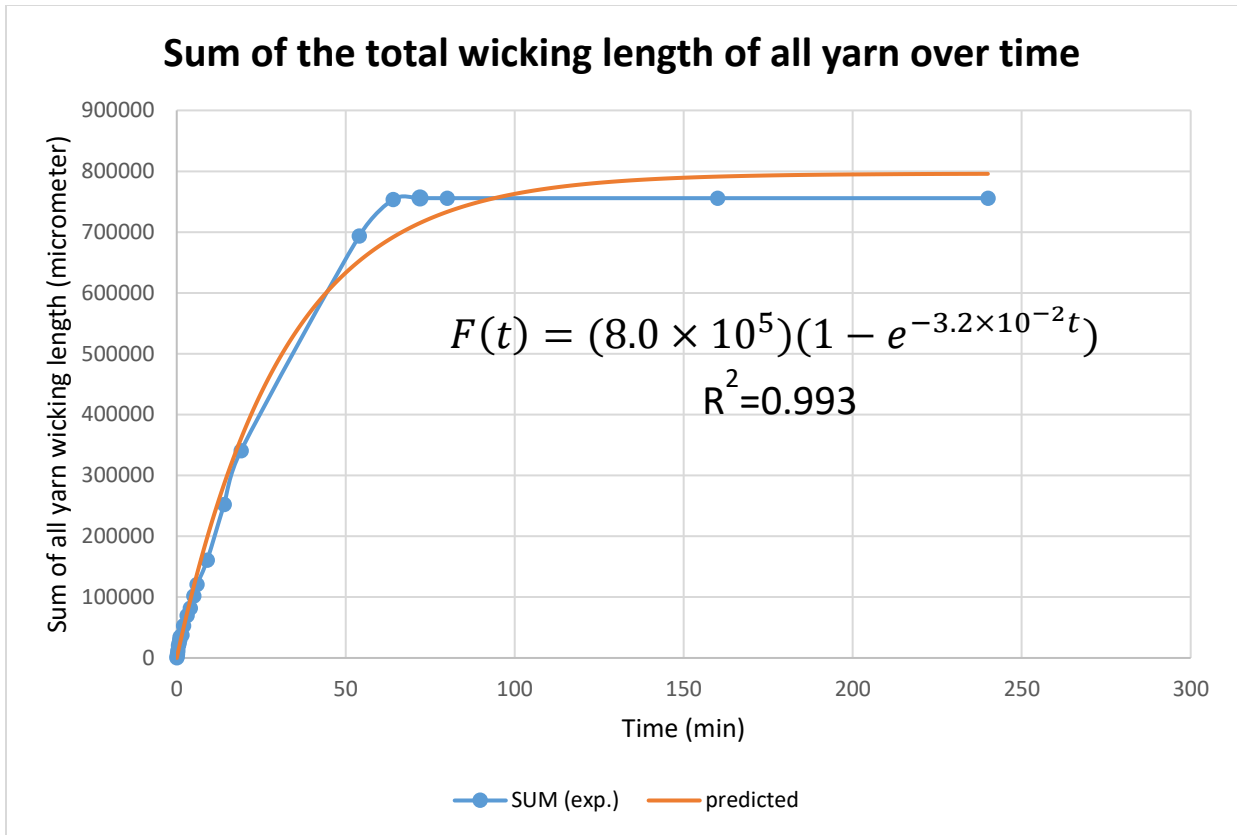


Figure S6-4. Sum of the total wicking length of all yarn over time for the experimental data of the SWEAT test (blue line) and the fitted model (red line). (Fabric: EASTMAN single jersey knit with multi-filament flat yarn, Test #1 video code: 0425_002).

CHAPTER 7. Conclusions and Future Work

In order to understand the wicking phenomenon in textiles, the yarn-level liquid movement within a fabric status should be explained based on fiber properties, yarn structure, and liquid characteristics. Fabric has complicated capillary structures because the twist level and the cross-sectional area of a yarn within a fabric keep changing over the locations within the fabric. However, despite the complex capillary channels in textiles, typical wicking performance test methods such as vertical wicking test (AATCC 197 [6]) and MMT test (AATCC 195 [7]), are too simple to deal with liquid movement through the complicated structures. Those test methods are conducted with either infinite reservoir or limited amount of liquid (i.e. liquid droplet) and do not represent realistic human sweating, which is continuous liquid flow generated from each sweat gland.

We reviewed several previous papers regarding the liquid transport mechanism in porous media for yarn-level and fabric-level, and the liquid movement between two plates to understand wicking mechanism in-between skin and textile. However, any precedent researches cannot explain the yarn-level wicking within a fabric status. If we could find a fundamental principle of wicking phenomenon of textiles based on within-a-yarn and yarn-to-yarn transfer wicking, we might anticipate how liquid transports through the fabric and aim to control the liquid movement mechanism.

To mimic realistic human sweating, the SWEAT test method was developed to supply a continuous microfluidic flow to only a single yarn at a single point within the fabric substrate. This SWEAT test method avoided the flooding liquid stage by controlling flow rate to be similar to a single sweat gland and by choosing a similar diameter of liquid source to sweat gland pore size. With this SWEAT test method, liquid movement along individual yarn within a knit fabric (i.e.

within-a-yarn and yarn-to-yarn transfer wicking) was observed. Furthermore, we found that liquid transferred to adjacent yarns only through the direct contact points with adjacent yarns instead of the relatively big void space in-between yarns. That means that the liquid flow wicks through capillary channels in-between fibers or peripheral region around fibers.

Moreover, the SWEAT test allowed to find the time-wicking length superposition principle when continuous liquid flow was supplied to a single point of a course yarn within a knit fabric. Specifically, the time-wicking length superposition means that liquid wicks within a single yarn initially, subsequently it spills over to adjacent yarns through contact points, but the wicking rate in adjacent yarns is identical to the initiated course yarn. Thanks to this principle, we might anticipate wicking performance and establish a predictive model of wicking performance of textiles in the future.

From the sum graph of the actual wicking length of all individual yarn, we found that the sum of wicking length of all yarns follows a one-minus the exponential function of time model called the SWEAT model, which finally reaches a plateau stage when the wicked area of a substrate does not change over time. The SWEAT model provides a good conceptual idea regarding how to describe the wicking behavior of a textile substrate under human sweating circumstance. However, if we understand two constants' value, the wetting-area-related constant (α) and the cross-sectional void space value of a yarn (i.e. porosity in cross-sectional area) (s), we might anticipate the wicking performance of textiles better considering yarn and fabric structures. Furthermore, if a fabric substrate can absorb the substantial amount of moisture (i.e. moisture regain), we need to consider that some of the liquid must go into the fibers (i.e. moisture regain) in addition to in-between fibers or peripheral region around fibers. According to the evaporation rate equation (Smith, Jones [99]), the calculated value at a plateau stage is similar to the actual

wetted surface area of the EASTMAN single jersey knit fabric with multifilament flat yarns. This required no fitting parameters.

Additionally, the quantitative analysis of wicking video is still a remaining step instead of visual investigation. With the cross-section images of fabrics, even though we can investigate the capillary channel profiles, including intra- and inter-yarn spaces, the cross-sectional 3D image of a fabric through the Nano-CT machine could allow us to understand the accurate open space in yarn over location and the actual liquid location in the cross-sectional area of a yarn. Moreover, if the actual liquid distribution in a yarn can be investigated through the Nano-CT technique, it would help to understand wicking mechanism of textiles much better. Based on the experimental data and profile information, we might calculate the actual value of capillary pressure and backpressure considering yarn properties and various textile structures. If that is possible, we could know how to control liquid movement in textiles for various application purpose.

For further investigation on the yarn-level wicking within fabric, we will simulate adjacent sweat glands' effect with multiple syringes as shown in Figure 7-1a. Moreover, we have a plan to analyze capillary bridge effect between plate and fabric in order to simulate the skin-fabric wicking behavior (Figure 7-1b).

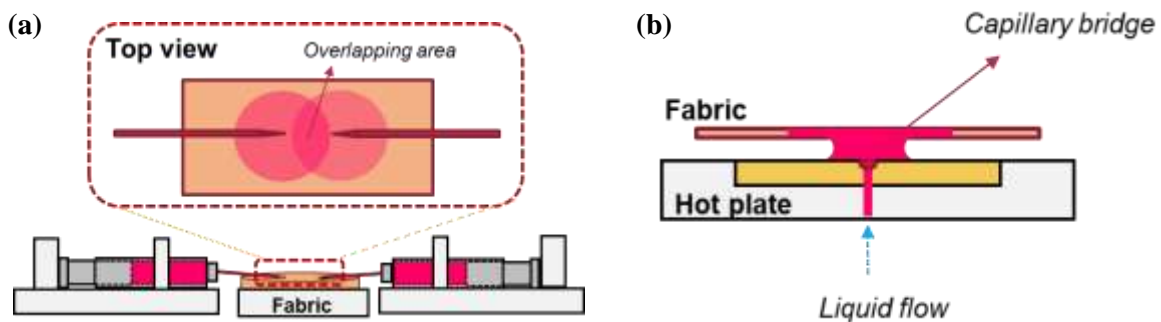


Figure 7-1. (a) Future experimental setup for overlapping effect and (b) future experimental setup for capillary bridge.

REFERENCES

1. Owens, T.L., et al., *Control of microfluidic flow in amphiphilic fabrics*. ACS applied materials & interfaces, 2011. **3**(10): p. 3796-3803.
2. Das, B., et al., *Mathematical model to predict vertical wicking behaviour. Part II: flow through woven fabric*. Journal of the Textile Institute, 2011. **102**(11): p. 971-981.
3. Davis, J.-K. and P.A. Bishop, *Impact of clothing on exercise in the heat*. Sports medicine, 2013. **43**(8): p. 695-706.
4. Berglund, L.G. and R.R. Gonzalez, *Evaporation of sweat from sedentary man in humid environments*. Journal of Applied Physiology, 1977. **42**(5): p. 767-772.
5. Pascoe, D.D., T.A. Bellinger, and B.S. McCluskey, *Clothing and exercise. II. Influence of clothing during exercise/work in environmental extremes*. Sports medicine (Auckland, NZ), 1994. **18**(2): p. 94-108.
6. 197, A.T.M., *Vertical Wicking of Textiles: AATCC technical manual* AATCC Research Triangle Park, NC 2011.
7. AATCC, *TM 195 Liquid Moisture Management Properties of Textile Fabrics*. 2015, AMERICAN ASSOCIATION OF TEXTILE CHEMISTS AND COLORISTS: Research Triangle Park, NC 27709, USA.
8. Kondo, N., et al., *Effects of exercise intensity on the sweating response to a sustained static exercise*. Journal of Applied Physiology, 2000. **88**(5): p. 1590-1596.
9. Kondo, N., et al., *Sweating responses to a sustained static exercise is dependent on thermal load in humans*. Acta physiologica Scandinavica, 2002. **175**(4): p. 289-295.
10. Kissa, E., *Wetting and wicking*. Textile Research Journal, 1996. **66**(10): p. 660-668.
11. Young, T., *An essay on the cohesion of fluids*. Philosophical Transactions of the Royal Society of London, 1805. **95**: p. 65-87.
12. Jasper, W.J. and S. Rasipuram, *Relationship between contact angle and contact line radius for micro to atto [10⁻⁶ to 10⁻¹⁸] liter size oil droplets*. Journal of Molecular Liquids, 2017. **248**: p. 920-926.
13. Letellier, P., A. Mayaffre, and M. Turmine, *Drop size effect on contact angle explained by nonextensive thermodynamics. Young's equation revisited*. Journal of colloid and interface science, 2007. **314**(2): p. 604-614.
14. Jung, Y.C. and B. Bhushan, *Technique to measure contact angle of micro/nanodroplets using atomic force microscopy*. Journal of Vacuum Science & Technology A: Vacuum, Surfaces, and Films, 2008. **26**(4): p. 777-782.
15. Ceylan, M., *Superhydrophobic behavior of electrospun nanofibers with variable additives*. 2009, Wichita State University.
16. Nuraje, N., et al., *Superhydrophobic electrospun nanofibers*. Journal of Materials Chemistry A, 2013. **1**(6): p. 1929-1946.
17. Fournier, R.L., *Basic transport phenomena in biomedical engineering*. 2017: CRC press.
18. Çengel, Y.A. and J.M. Cimbala, *Introduction to Computational Fluid Dynamics*. de Fluid Mechanics: Fundamentals and Applications, First ed., New York, McGraw-Hill, 2006.
19. Oh, D.S., et al., *Effect of capillary action on bone regeneration in micro-channeled ceramic scaffolds*. Ceramics International, 2014. **40**(7): p. 9583-9589.
20. Bruus, H., *Theoretical microfluidics*. Vol. 18. 2008: Oxford university press Oxford.
21. de Gennes, P.-G., F. Brochard-Wyart, and D. Quere, *Capillarity and Wetting Phenomena: Drops, Bubbles, Pearls, Waves*, 2004. **291**.

22. Nemes, I., *Revisiting the applications of drainage capillary pressure curves in water-wet hydrocarbon systems*. Open Geosciences, 2016. **8**(1): p. 22-38.
23. Laplace, P., *Theory of capillary attraction*. Supplements to the 10th book of Celestial Mechanics, 1807.
24. Pujado, P., C. Huh, and L. Scriven, *On the Attribution of an Equation of Capillarity to Young and Laplace*. Journal of Colloid and Interface Science, 1972. **38**(3): p. 662-663.
25. Pasandideh-Fard, M., et al., *The generalized Laplace equation of capillarity I. Thermodynamic and hydrostatic considerations of the fundamental equation for interfaces*. Advances in colloid and interface science, 1996. **63**: p. 151-177.
26. Chen, P., et al., *The generalized Laplace equation of capillarity II. Hydrostatic and thermodynamic derivations of the Laplace equation for high curvatures*. Advances in colloid and interface science, 1996. **63**: p. 179-193.
27. Berthier, J. and P. Silberzan, *Microfluidics for biotechnology*. 2010: Artech House.
28. Marmur, A., *Penetration and displacement in capillary systems of limited size*. Advances in Colloid and interface Science, 1992. **39**: p. 13-33.
29. Kissa, E., *Capillary sorption in fibrous assemblies*. Journal of colloid and interface science, 1981. **83**(1): p. 265-272.
30. Nyoni, A. and D. Brook, *Wicking mechanisms in yarns—the key to fabric wicking performance*. Journal of the textile institute, 2006. **97**(2): p. 119-128.
31. Wang, N., A. Zha, and J. Wang, *Study on the wicking property of polyester filament yarns*. Fibers and Polymers, 2008. **9**(1): p. 97-100.
32. Sengupta, A. and H. Murthy, *Wicking in ring-spun vis-a-vis rotor-spun yarns*. 1985.
33. Sengupta, A., V. Kothari, and R. Rengasamy, *Wicking behaviour of air-jet textured yarns*. 1991.
34. Rajagopalan, D., A.P. Aneja, and J.-M. Marchal, *Modeling capillary flow in complex geometries*. Textile Research Journal, 2001. **71**(9): p. 813-821.
35. Raja, D., et al., *Comparison of different methods to measure the transverse wicking behaviour of fabrics*. Journal of Industrial Textiles, 2014. **43**(3): p. 366-382.
36. Morent, R., et al., *Measuring the wicking behavior of textiles by the combination of a horizontal wicking experiment and image processing*. Review of scientific instruments, 2006. **77**(9): p. 093502.
37. Parada, M., et al., *A review on advanced imaging technologies for the quantification of wicking in textiles*. Textile Research Journal, 2017. **87**(1): p. 110-132.
38. Saville, B., *Physical testing of textiles*. 1999: Elsevier.
39. Miller, B. and I. Tyomkin, *Spontaneous transplanar uptake of liquids by fabrics*. Textile Research Journal, 1984. **54**(11): p. 706-712.
40. Gillespie, T., *The spreading of low vapor pressure liquids in paper*. Journal of Colloid Science, 1958. **13**(1): p. 32-50.
41. Hollies, N.R., M.M. Kaessinger, and H. Bogaty, *Water transport mechanisms in textile materials I Part I: the role of yarn roughness in capillary-type penetration*. Textile Research Journal, 1956. **26**(11): p. 829-835.
42. Lee, K.-J., J.H. Nam, and C.-J. Kim, *Pore-network analysis of two-phase water transport in gas diffusion layers of polymer electrolyte membrane fuel cells*. Electrochimica Acta, 2009. **54**(4): p. 1166-1176.

43. Lou, L., et al., *Simulating adhesion of wet fabrics to water: Gravity of liquid bridge-based theoretical model and experimental verification*. Textile Research Journal, 2017. **87**(7): p. 769-779.
44. Wang, Y., S. Michielsen, and H.J. Lee, *Symmetric and asymmetric capillary bridges between a rough surface and a parallel surface*. Langmuir, 2013. **29**(35): p. 11028-11037.
45. Luo, C., X. Heng, and M. Xiang, *Behavior of a liquid drop between two nonparallel plates*. Langmuir, 2014. **30**(28): p. 8373-8380.
46. Xu, W., et al., *Directional movement of droplets in grooves: suspended or immersed?* Scientific reports, 2016. **6**.
47. Prakash, M., D. Quéré, and J.W. Bush, *Surface tension transport of prey by feeding shorebirds: the capillary ratchet*. science, 2008. **320**(5878): p. 931-934.
48. Washburn, E.W., *The dynamics of capillary flow*. Physical review, 1921. **17**(3): p. 273.
49. Hollies, N.R., et al., *Water transport mechanisms in textile materials: part II: capillary-type penetration in yarns and fabrics*. Textile Research Journal, 1957. **27**(1): p. 8-13.
50. Cummins, B.M., et al., *Time-dependent model for fluid flow in porous materials with multiple pore sizes*. Analytical chemistry, 2017. **89**(8): p. 4377-4381.
51. Tuller, M., D. Or, and L.M. Dudley, *Adsorption and capillary condensation in porous media: Liquid retention and interfacial configurations in angular pores*. Water Resources Research, 1999. **35**(7): p. 1949-1964.
52. Barker, R.L., *From fabric hand to thermal comfort: the evolving role of objective measurements in explaining human comfort response to textiles*. International journal of clothing science and technology, 2002. **14**(3/4): p. 181-200.
53. Fan, J. and L. Hunter, *Physiological comfort of fabrics and garments*. Engineering apparel fabrics and garments, 2009. **1**: p. 201-250.
54. Kayseri, G.Ö., N. Özdil, and G.S. Mengüç, *Sensorial comfort of textile materials*, in *Woven fabrics*. 2012, InTech.
55. Kawabata, S., *Characterization method of the physical property of fabrics and the measuring system for hand-feeling evaluation*. Sen'i Kikai Gakkaishi (Journal of the Textile Machinery Society of Japan), 1973. **26**(10): p. P721-P728.
56. Huang, J., *Sweating guarded hot plate test method*. Polymer testing, 2006. **25**(5): p. 709-716.
57. Huang, J. and X. Qian, *Comparison of test methods for measuring water vapor permeability of fabrics*. Textile Research Journal, 2008. **78**(4): p. 342-352.
58. Horrocks, A.R. and S.C. Anand, *Handbook of Technical Textiles: Technical Textile Applications*. 2016: Woodhead Publishing.
59. Weder, M., et al., *Evaporative cooling and heat transfer in functional underwear*. International Journal of Clothing Science and Technology, 2008. **20**(2): p. 68-78.
60. Waters, N. and M. King, *The unsteady flow of an elastico-viscous liquid in a straight pipe of circular cross section*. Journal of Physics D: Applied Physics, 1971. **4**(2): p. 204.
61. Aguilera, J., M. Michel, and G. Mayor, *Fat migration in chocolate: diffusion or capillary flow in a particulate solid?—a hypothesis paper*. Journal of Food Science, 2004. **69**(7): p. 167-174.
62. Martic, G., J. De Coninck, and T. Blake, *Influence of the dynamic contact angle on the characterization of porous media*. Journal of colloid and interface science, 2003. **263**(1): p. 213-216.

63. Simile, C.B. and H.W. Beckham, *Permeability–saturation–capillary pressure relations in textile fabrics from an integrated upward–horizontal–downward wicking test*. Journal of the Textile Institute, 2012. **103**(9): p. 945-951.
64. Tang, K., et al., *Characterizing the transplanar and in-plane water transport properties of fabrics under different sweat rate: Forced Flow Water Transport Tester*. Scientific reports, 2015. **5**: p. 17012.
65. Zhu, C. and M. Takatera, *A new thermocouple technique for the precise measurement of in-plane capillary water flow within fabrics*. Textile Research Journal, 2014. **84**(5): p. 513-526.
66. Rossi, R.M., et al., *Transplanar and in-plane wicking effects in sock materials under pressure*. Textile research journal, 2011. **81**(15): p. 1549-1558.
67. Zhang, G., et al., *X-ray imaging of transplanar liquid transport mechanisms in single layer textiles*. Langmuir, 2017. **33**(43): p. 12072-12079.
68. Hsieh, Y.-L., *Liquid transport in fabric structures*. Textile Research Journal, 1995. **65**(5): p. 299-307.
69. Li, J., X. Li, and S. Michielsen, *Alternative method for determining the original drop volume of bloodstains on knit fabrics*. Forensic science international, 2016. **263**: p. 194-203.
70. AATCC, *TM 197 Vertical Wicking of Textiles*
2015, AMERICAN ASSOCIATION OF TEXTILE CHEMISTS AND COLORISTS: Research Triangle Park, NC 27709, USA.
71. AATCC, *TM 198 Horizontal Wicking of Textiles*. 2015, AMERICAN ASSOCIATION OF TEXTILE CHEMISTS AND COLORISTS: Research Triangle Park, NC 27709, USA.
72. Francis, J., et al., *Digital nanoliter to milliliter flow rate sensor with in vivo demonstration for continuous sweat rate measurement*. Lab on a Chip, 2019. **19**(1): p. 178-185.
73. Hall, H.J., *Notes on Surgical Gauzes*. The Boston Medical and Surgical Journal, 1897. **137**(21): p. 3.
74. Bogaty, H., and Norman RS Hollies, *The Evaluation of Experimental Fabrics as Alternates for Standard Wool Fabrics*. 1951.
75. Liu, W., *Enhanced Comfort and Faster Drying Textile Finish*. (Doctoral dissertation) 2017(Retrieved from <http://www.lib.ncsu.edu/resolver/1840.20/35001>).
76. Pandiyaraj, K.N. and V. Selvarajan, *Non-thermal plasma treatment for hydrophilicity improvement of grey cotton fabrics*. journal of materials processing technology, 2008. **199**(1-3): p. 130-139.
77. Yu, J., S. Seipel, and V.A. Nierstrasz, *Digital inkjet functionalization of water-repellent textile for smart textile application*. Journal of materials science, 2018. **53**(18): p. 13216-13229.
78. Zaman, M., et al., *Hydrophilic modification of polyester fabric by applying nanocrystalline cellulose containing surface finish*. Carbohydrate polymers, 2013. **91**(2): p. 560-567.
79. Kuno, Y., *Human Perspiration*. Springfield, Illinois: Charles C. Thomas. 1956, Blackwell Scientific Publications: Oxford.
80. Vairo, D., et al., *Towards addressing the body electrolyte environment via sweat analysis: pilocarpine iontophoresis supports assessment of plasma potassium concentration*. Scientific reports, 2017. **7**(1): p. 11801.

81. Baker, L.B., *Sweating rate and sweat sodium concentration in athletes: a review of methodology and intra/interindividual variability*. Sports Medicine, 2017. **47**(1): p. 111-128.
82. Pezron, I., G. Bourgain, and D. Quéré, *Imbibition of a fabric*. Journal of Colloid and Interface Science, 1995. **173**(2): p. 319-327.
83. Van Der Meeren, P., et al., *Quantifying wetting and wicking phenomena in cotton terry as affected by fabric conditioner treatment*. Textile research journal, 2002. **72**(5): p. 423-428.
84. Michel, T., et al., *The hydrodynamics of drop impact onto chemically structured surfaces*. Journal of Physics: Condensed Matter, 2005. **17**(9): p. S607.
85. Stone, H.A. and S. Kim, *Microfluidics: basic issues, applications, and challenges*. AIChE Journal, 2001. **47**(6): p. 1250-1254.
86. Xi, W., et al., *Soft tubular microfluidics for 2D and 3D applications*. Proceedings of the National Academy of Sciences, 2017. **114**(40): p. 10590-10595.
87. Nilghaz, A., D.R. Ballerini, and W. Shen, *Exploration of microfluidic devices based on multi-filament threads and textiles: a review*. Biomicrofluidics, 2013. **7**(5): p. 051501.
88. Simile, C.B., *Critical evaluation of wicking in performance fabrics*. 2004, Georgia Institute of Technology.
89. Owens, T.L., et al., *Validation of the integrated upward–horizontal–downward wicking test for providing intensive properties of textile fabrics*. Journal of The Textile Institute, 2012. **103**(9): p. 952-959.
90. Fukuhara, M., *Innovation in polyester fibers: from silk-like to new polyester*. Textile research journal, 1993. **63**(7): p. 387-391.
91. Kim, S.J., et al., *Wicking and flooding of liquids on vertical porous sheets*. Physics of Fluids, 2015. **27**(3): p. 032105.
92. Kamath, Y., et al., *Wicking of spin finishes and related liquids into continuous filament yarns*. Textile Research Journal, 1994. **64**(1): p. 33-40.
93. Almoughni, H. and H. Gong, *Capillary flow of liquid water through yarns: a theoretical model*. Textile Research Journal, 2015. **85**(7): p. 722-732.
94. Staples, T.L. and D.G. Shaffer, *Wicking flow in irregular capillaries*. Colloids and Surfaces A: Physicochemical and Engineering Aspects, 2002. **204**(1-3): p. 239-250.
95. Johnson, P.C. and H. Wayland, *Regulation of blood flow in single capillaries*. American Journal of Physiology-Legacy Content, 1967. **212**(6): p. 1405-1415.
96. Wilson, G.W., D. Fredlund, and S. Barbour, *Coupled soil-atmosphere modelling for soil evaporation*. Canadian Geotechnical Journal, 1994. **31**(2): p. 151-161.
97. Hover, K.C., *Evaporation of water from concrete surfaces*. ACI materials journal, 2006. **103**(5): p. 384.
98. Gray, D.M., *Handbook on the Principles of Hydrology: with special emphasis directed to Canadian conditions in the discussions, applications and presentation of data*. 1970: Secretariat, Canadian National Committee for the International Hydrological
99. Smith, C., R. Jones, and G. Lof, *Energy requirements and potential savings for heated indoor swimming pools*. ASHRAE Transactions-American Society of Heating Refrigerating Airconditioning Engin, 1993. **99**(2): p. 864-876.